ÅBO AKADEMI

INSTITUTIONEN FÖR KEMITEKNIK

DEPARTMENT OF CHEMICAL ENGINEERING

Processkemiska centret

Process Chemistry Centre

REPORT 12-05

Understanding the *in vitro* dissolution rate of glasses with respect to future clinical applications

Susanne Fagerlund

Academic Dissertation

Laboratory of Inorganic Chemistry

Susanne Fagerlund
MSc in Technology (Chemical Engineering), 2007
Åbo Akademi University
Faculty of Technology
Process Chemistry Centre
Laboratory of Inorganic Chemistry

Understanding the *in vitro* dissolution rate of glasses with respect to future clinical applications

Susanne Fagerlund

Academic Dissertation

Laboratory of Inorganic Chemistry
Åbo Akademi Process Chemistry Centre
Department of Chemical Engineering
Åbo Akademi University

Turku 2012

Supervisors:

Docent Leena Hupa
Laboratory of Inorganic Chemistry
Process Chemistry Centre
Åbo Akademi University
Turku, Finland

and

Professor Mikko Hupa
Laboratory of Inorganic Chemistry
Process Chemistry Centre
Åbo Akademi University
Turku, Finland

Opponent and Reviewer:

Professor Richard Brow
Missouri University of Science & Technology (Missouri S&T)
Department of Materials Science & Engineering
Rolla, MO, USA

Reviewer:
Docent, MD PhD Nina C. Lindfors
University of Helsinki
Department of Orthopedic and Hand Surgery
Institute of Clinical Medicine
Helsinki, Finland

ISSN 159-8205
ISBN 978-952-12-2814-8 (paper version)
ISBN 978-952-12-2815-5 (pdf version)
Painosalama Oy (2012)

"No man is an island"
John Donne (1624)

Preface

The work in this thesis was carried out at the Laboratory of Inorganic Chemistry at Åbo Akademi University during the years 2007-2012 as a part of the activities of the Process Chemistry Centre. The work was mainly funded by the Graduate School in Chemical Engineering (GSCE) and research projects Biowaffle, financed by the Finnish Funding Agency of Technology and Innovations (TEKES), and MoreBags, financed by Academy of Finland. In addition, financial support from Rector of Åbo Akademi University and the Finnish Foundation of Technology Promotion (TES) is gratefully acknowledged.

During my doctoral studies, I have had a privilege to be part of two important groups. Firstly, PCC which is a highly multicultural research group (Centre of Excellence appointed by the Academy of Finland 2000-2005, 2006-2011) founded by the "gang of four grand old men of science". PCC offers an exceptional "hatchery" for tomorrow's scientists. Because a lot of the research activities are done in close collaboration with industrial companies combined with an extensive international collaboration network, possibilities for young scientists are vast. Secondly, GSCE has given me many opportunities to widen my scientific perspective by organizing seminars and courses within the broad field of chemical process engineering. In addition, it is has been valuable to have the possibility to present your own results to an audience which is not only from your narrow field of expertise. Furthermore, all the conference travelling support from GSCE is deeply acknowledged.

This work has been performed under the supervision and with guidance from two inspiring scientists Prof. Mikko Hupa and Docent Leena Hupa. I feel that I have gotten lot of trust to work independently, but at the same time there has always been a safety net available. In addition, I want to thank you both for having given me endless possibilities to attend various courses and conferences, where I have had the opportunity to meet and network with the people behind the faceless journal articles.

I would like to thank firstly Prof. Mikko Hupa for opening his office door to a young inexperienced technology student (without an appointment!) in 2006. This led via summer practice to a master thesis. I am grateful for the possibility to have been able to perform also my doctoral studies at the Laboratory of Inorganic Chemistry. I appreciate deeply your enthusiasm towards my work, and I admire your capability to always ask the right (but at the same time "irritating") questions, which made me every time take one step further. Thank you.

My day-to-day supervisor Docent Leena Hupa is profoundly acknowledged for her never-ending enthusiasm towards and knowledge of glass. You have given me the most important asset for performing this doctoral work, i.e. interest toward glass science. Glass is beautiful, is it not? Your door has always been open, and you have at all times been ready to comment the latest results; to teach to write manuscripts,

rebuttals, and conference presentations, but most importantly encouraged to try, try, and try again after the "not-so-successful-days" in the lab.

No man is an island. When working with my doctoral thesis I have gotten an endless amount of help and support from a vast number of people. A special thank you goes to my co-authors Mr. Paul Ek, Dr. Jonathan Massera, and Dr. Niko Moritz. The collaboration with Dr. Fredrik Ollila from Bonalive Ltd. and Dr. Jukka Tuominen and Mr. Timo Lehtonen from Vivoxid Ltd. is kindly acknowledged. In early 2011, I had the possibility to visit the Nanyang Technological University in Singapore. I wish to extend my thanks to Prof. Subbu S. Venkatraman and Prof. Sam Zhang for giving me this great opportunity to visit the university. During my time in Singapore, I learned to put things in different perspectives and to ask questions beginning with 'why'.

The Laboratory of Inorganic Chemistry (OOK) at Åbo Akademi University has a long background in glass science and has produced many great alumni. I have been privileged to learn from all the bits and pieces of information which you have left behind. Especially, all the priceless practical advice and encouragement from Dr. Hanna Arstila, Dr. Linda Fröberg, Dr. Minna Piispanen, Mr. Erik Vedel, and Dr. Di Zhang are deeply acknowledged. Thank you! I feel like a "kid sister in science".

During my doctoral studies, I have also had a possibility to work with a number of great "junior scientists". Thank you all for all the fun moments and the tricky questions you made! A very warm and humble thank you goes to Ms. Jaana Paananen. You have taught and helped me so much in the lab. You are a true diamond. For the gentlemen from the "other side" of the material group, i.e. electrochemistry, I just want to say thank you for everything! Without you, the mornings would have been much grayer and the number of my fingers would not match ten. Mr. Linus Silvander is acknowledged for operating the SEM and for the "service" with a smile. All the practical help with ICP-OES measurements from Mr. Sten Lindholm is highly appreciated. The gentlemen in the "ion hunt" lab, Mr. Stig-Göran Huldén and Mr. Berndt Södergård, thank you for always been ready to brainstorm and answer my endless questions. Often, though, you created more questions by answering one…

I want to thank all the members of OOK! Warm thanks goes also to all the people in the group for taking care of the "invisible" every day practicalities, making life so care-free at the office and the lab, but especially thank you Eva, Kaj, Maria, Mia, Pettu, and Peter. A warm hug with a smile goes to all the wonderful dear friends from all over the world who I have had opportunity to meet during the course of this thesis. Thank you for sharing all the laughter and tears! Especially, "Pikku-Leena" thank you for making the final stage of writing this thesis so much more fun!

Life is not only about work. A huge hug goes to my all dear friends who have always been around believing in me and encouraged to strive towards my dreams. You

are great, with all of you life is just a bit more sweeter! A special thank you goes to my dear old friends, "Giraffe and Froggy", thank you for being there for me, always!

A warm thank you goes to my entire family. Thanks mum and dad for your never-ending love and trust in my capabilities, for teaching and reminding me about the fundamental values important in life. Finally, I want to thank my mentor, best friend, and "allt-i-allo" Johan. There would be so much to say to you, but I think these three letters says it all: JÄD!

Turku, October 2012

Susanne Fagerlund

Abstract

Glass is a unique material with a long history. Several glass products are used daily in our everyday life, often unnoticed. Glass can be found not only in obvious applications such as tableware, windows, and light bulbs, but also in tennis rackets, windmill turbine blades, optical devices, and medical implants. The glasses used at present as implants are inorganic silica-based melt-derived compositions mainly for hard-tissue repair as bone graft substitute in dentistry and orthopedics. The degree of glass reactivity desired varies according to implantation situation and it is vital that the ion release from any glasses used in medical applications is controlled.

Understanding the *in vitro* dissolution rate of glasses provides a first approximation of their behavior *in vivo*. Specific studies concerning dissolution properties of bioactive glasses have been relatively scarce and mostly concentrated to static condition studies. The motivation behind this work was to develop a simple and accurate method for quantifying the *in vitro* dissolution rate of highly different types of glass compositions with interest for future clinical applications. By combining information from various experimental conditions, a better knowledge of glass dissolution and the suitability of different glasses for different medical applications can be obtained. Thus, two traditional and one novel approach were utilized in this thesis to study glass dissolution.

The chemical durability of silicate glasses was tested in water and TRIS-buffered solution at static and dynamic conditions. The traditional *in vitro* testing with a TRIS-buffered solution under static conditions works well with bioactive or with readily dissolving glasses, and it is easy to follow the ion dissolution reactions. However, in the buffered solution no marked differences between the more durable glasses were observed. The hydrolytic resistance of the glasses was studied using the standard procedure ISO 719. The relative scale given by the standard failed to provide any relevant information when bioactive glasses were studied. However, the clear differences in the hydrolytic resistance values imply that the method could be used as a rapid test to get an overall idea of the biodegradability of glasses. The standard method combined with the ion concentration and pH measurements gives a better estimate of the hydrolytic resistance because of the high silicon amount released from a glass.

A sensitive on-line analysis method utilizing inductively coupled plasma optical emission spectrometer and a flow-through micro-volume pH electrode was developed to study the initial dissolution of biocompatible glasses. This approach was found suitable for compositions within a large range of chemical durability. With this approach, the initial dissolution of all ions could be measured simultaneously and quantitatively, which gave a good overall idea of the initial dissolution rates for the individual ions and the dissolution mechanism. These types of results with glass dissolution were presented for the first time during the course of writing this thesis. Based on the initial dissolution patterns obtained with the novel approach using TRIS,

the experimental glasses could be divided into four distinct categories. The initial dissolution patterns of glasses correlated well with the anticipated bioactivity. Moreover, the normalized surface-specific mass loss rates and the different *in vivo* models and the actual *in vivo* data correlated well. The results suggest that this type of approach can be used for prescreening the suitability of novel glass compositions for future clinical applications. Furthermore, the results shed light on the possible bioactivity of glasses.

An additional goal in this thesis was to gain insight into the phase changes occurring during various heat treatments of glasses with three selected compositions. Engineering-type T-T-T curves for glasses 1-98 and 13-93 were established. The information gained is essential in manufacturing amorphous porous implants or for drawing of continuous fibers of the glasses. Although both glasses can be hot worked to amorphous products at carefully controlled conditions, 1-98 showed one magnitude greater nucleation and crystal growth rate than 13-93. Thus, 13-93 is better suited than 1-98 for working processes which require long residence times at high temperatures.

It was also shown that amorphous and partially crystalline porous implants can be sintered from bioactive glass S53P4. Surface crystallization of S53P4, forming $Na_2O{\cdot}CaO{\cdot}2SiO_2$, was observed to start at 650°C. The secondary crystals of $Na_2Ca_4(PO_4)2SiO_4$, reported for the first time in this thesis, were detected at higher temperatures, from 850°C to 1000°C. The crystal phases formed affected the dissolution behavior of the implants in simulated body fluid. This study opens up new possibilities for using S53P4 to manufacture various structures, while tailoring their bioactivity by controlling the proportions of the different phases.

The results obtained in this thesis give valuable additional information and tools to the state of the art for designing glasses with respect to future clinical applications. With the knowledge gained we can identify different dissolution patters and use this information to improve the tuning of glass compositions. In addition, the novel on-line analysis approach provides an excellent opportunity to further enhance our knowledge of glass behavior in simulated body conditions.

Keywords: glass, *in vitro*, dissolution, continuous measurement, ICP-OES, crystallization

Svensk sammanfattning

Glas är ett unikt material med en lång historia. Produkter av glas används dagligen i ett flertal olika syften, ofta utan att man tänker på det. Glas förekommer således inte enbart i uppenbara föremål som kärl, fönster och lampor, utan även i t.ex. tennisracketar, turbinblad för vindkraftverk, optiska instrument och medicinska implantat. Dagens medicinska glass implantat består av olika oorganiska kiseloxidbaserade smälthärledda sammansättningar och de används huvudsakligen för hårdvävnadsreparationer, dvs. som bentransplantatsubstitut inom tandvård och ortopedi. Beroende på användningsändamål är det nödvändigt att glas av olika reaktivitet tillämpas och det är ytterst viktigt att jonfrisättningen från samtliga glas som används i medicinskt syfte kontrolleras.

Iakttagelser av glasets upplösningshastighet ”in vitro” ger en första approximation av hur glas beter sig ”in vivo”. Forskningen av bioaktiva glas, med särskild fokus på upplösningsegenskaper har hittills varit relativt begränsad och mestadels baserad på undersökningar gjorda i statiska förhållanden. Ett av huvudsyftena med detta arbete är således att utveckla en enkel och exakt metod för att kvantifiera *in vitro*-upplösningshastigheten för glas med mycket olika sammansättningar för eventuella framtida kliniska tillämpningar. Genom att föra samman information från olika experimentella förhållanden har kunskap om olika glas upplösning och deras lämplighet för olika medicinska tillämpningar erhållits. I detta arbete har alltså två traditionella och en ny metod kombinerats för att undersöka lösligheten av olika glas.

Den kemiska hållbarheten hos silikatglas undersöktes i vatten och TRIS-buffrade lösningar i både statiska och dynamiska förhållanden. Den traditionella in vitro-testmetoden som utnyttjar en TRIS-buffrad lösning under statiska förhållanden fungerar bra med bioaktiva och lättupplösliga glastyper, och det är enkelt att följa samtliga jonupplösningsreaktioner. Däremot gick det inte (med hjälp av denna metod) att särskilja mellan glas av mera hållbar natur. Det hydrolytiska motståndet hos olika glas studerades med hjälp av standardförfarandet ISO 719. Det gick inte att erhålla någon relevant information om bioaktiva glas med hjälp av den relativa skalan i standarden, men trots allt skulle de tydliga skillnaderna i de hydrolytiska resistansvärdena kunna innebära att metoden eventuellt kan användas som ett snabbt test för att skapa sig en uppfattning om den biologiska nedbrytbarheten av glaset i fråga. En kombination av standardmetoden tillsammans med jonkoncentrations- och pH-mätningar ger en bättre uppskattning av det hydrolytiska motståndet på grund av den höga mängden kisel som har frigjorts från glaset.

En känslig online-analysmetod som utnyttjar en optisk emissionsspektrometer med induktivt kopplat plasma och en genomströmningsmikrovolymetrisk pH-elektrod har utvecklats för att studera den initiala upplösningen av biokompatibla glas. Detta tillvägagångssätt har visat sig lämpligt för att studera sammansättningar med ett brett spektrum av kemisk hållbarhet. Med denna metod kan den initiala upplösningen av alla

joner mätas samtidigt och kvantitativt, resulterande i en god första uppskattning av de initiala upplösningshastigheterna för de enskilda jonerna och den dominerande upplösningsmekanismen. Dessa slags glasupplösningsresultat presenterades första gången i samband med denna avhandling. Baserat på det initiala upplösningsbeteendet som erhölls med den nya metoden i en TRIS-lösning kunde de experimentella glasen delas in i fyra klasser. Formen på glasens olika initiala upplösningsprofiler korrelerade väl med den förväntade bioaktiviteten. Utöver detta korrelerade även den normaliserade ytspecifika massaförlusthastigheten för de olika *in vivo*-modellerna och faktiska *in vivo*-data väl. Resultaten tyder på att denna typ av tillvägagångssätt med fördel kan användas för preliminär kontroll av lämpligheten hos nya glassammansättningar i framtida kliniska tillämpningar. Dessutom ger metoden intressant information om glasens eventuella bioaktivitet.

Ett ytterligare mål med denna avhandling var att få insikt i de fasförändringar som sker i tre specifika glassammansättningar under varierade värmebehandlingar. För två av dessa, 1-98 och 13-93, kunde praktiska T-T-T-kurvor fastställas. Denna information behövs vid tillverkningen av amorfa porösa implantat och dragandet av kontinuerliga fibrer av glas. Även om båda glasen kan värmebehandlas för att erhålla amorfa produkter under noggrant kontrollerade förhållanden, visade 1-98 en kärnbildning och kristalltillväxthastighet som var en storleksordning större än hos 13-93. Sålunda kan man konstatera att glas av typen 13-93 är bättre lämpad än 1-98 i produktionsprocesser som kräver långa uppehållstider i höga temperaturer.

Det konstaterades också att amorfa och partiellt kristallina porösa implantat kan sintras från bioaktivt glas S53P4. Ytkristalliseringen av S53P4 i form av $Na_2O{\cdot}CaO{\cdot}2SiO_2$ observerades börja vid 650 °C. Sekundära kristaller av $Na_2Ca_4(PO_4)2SiO_4$, som första gången presenteras i denna avhandling, upptäcktes vid högre temperaturer mellan 850 °C och 1 000 °C. De kristallfaser som bildades påverkade upplösningsbeteendet hos implantatens upplösningsbeteende i simulerad kroppsvätska. Denna studie pekar på nya möjligheter att tillverka olika strukturer av S53P4, samtidigt som bioaktiviteten kan skräddarsys genom kontroll av den proportionella mängden av de olika faserna i glaset.

De resultat som erhölls i denna avhandling ger värdefull kompletterande information samt verktyg för den senaste tekniken inom glasdesign när det gäller framtida kliniska tillämpningar. Med hjälp av denna information kan vi identifiera olika upplösningsbeteenden och därmed på ett bättre sätt finjustera glassammansättningen för olika ändamål. Dessutom ger den nya online-analysmetoden oss en utmärkt möjlighet att ytterligare förbättra vår kunskap om hur olika glas beter sig i simulerade kroppsförhållanden.

List of abbreviations and symbols

Abbreviations:

µCT	Micro-computed tomography
AES	Atomic Emission Spectroscopy
ASTM	American Society of Testing Materials
BAG	Bioactive glass
BO	Bonding/bridging oxygen
CaP	Calcium phosphate
CS	Wollastonite, $CaO \cdot SiO_2$
DIN	German Institute for Standardization
DTA	Differential Thermal Analysis
EDXA	Energy Dispersive X-ray Analysis
FDA	U.S. Food and Drug Administration
FTIR	Fourier transform infrared spectroscopy
HA	Hydroxyapatite
HGB	Hydrolytic resistance classification
HSM	Hot stage microscopy
HVG-DGG	Hüttentechnische Vereinigung der Deutschen Glasindustrie e. V - Deutsche Glastechnische Gesellschaft e.V.
ICG	International Commission on Glass
ICP	Inductively coupled plasma
ISO	International Standard Organization
ISO 719/P98	Glass – Hydrolytic resistance of glass grains at 98°C – Method of test and classification
IUPAC	International Union of Pure and Applied Chemistry
JMA	Johnson-Mehl-Avrami exponent
LOD	Limit of detection
LOQ	Limit of quantification
MAS-NMR	Magic-angle spinning nuclear magnetic resonance
NA	Not available
NBO	Non bonding oxygen
NCS	Sodium-calcium-silicate, $xNa_2O \cdot yCaO \cdot zSiO_2$
NCS	Sodium calcium silicate
NL_i	normalized surface-specific mass loss of element i
NR_i	normalized surface-specific mass loss rate of element i
OES	Optical Emission Spectroscopy
p.a.	pro analysi, purity grade. Products with a guarantee certificate and/or suitable for the stated analytical application
PBS	Phosphate buffered solution
PCC	Process Chemistry Centre
PDF	Powder diffraction file
pKa	Logarithmic acid dissociation constant
ppb	Parts per billion (10^9), µg/l
ppm	Parts per million (10^6), mg/l
Q^n	Local configuration around each silicon atom where n is the number of bridging oxygen ranging from 0 to 4
RN	Reaction number
RT	Room temperature
SA	Surface area
SA/V	Surface area volume ratio
SBF	Simulated body fluid
SEM	Scanning electron microscope
Si+CaP	Mixed layer containing both silica and calcium phosphate
SLG	Soda lime glass(es)/float glass(es)

TRIS	tris(hydroxymethyl)aminomethane (IUPAC: 2-Amino-2-hydroxymethyl-propane-1,3-diol) or a solution buffered with it
T-T-T	Time-Temperature-Transformation
TUT	Tampere University of Technology
V_{sol}	Volume of the immersion solution
wt%	weight %
XRD	X-ray diffraction
ÅA	Åbo Akademi University

Symbols:

μ	fluid viscosity
c_i	concentration of element i
D	diffusivity
D_p	average particle diameter
$E_{a,i}$	apparent activation energy for element i (J/mol)
F	flow rate
f_i	mass fraction of element i
G	superficial mass velocity based on the empty chamber cross section
K	constant
M	mol/l
M	mass
N	number of samples
Ø	diameter
R	gas constant 8.314 J/(mol·K)
Re'	modified Reynolds number for backed beds
SA	surface area
T	temperature
T	time
T_g	glass transition temperature
T_l	liquidus temperature
$T_{n\,max}$	temperature of maximum nucleation
$U_{average}$	average crystal growth rate
V	volume
V_{sol}	volume of the immersion solution
X	crystal layer thickness
B	buffer capacity
λ	wavelength

Table of Contents

1. Introduction

1.1. Glass – applications from tableware to medical implants

Glass is a unique material with a long history, and it has even been quoted as an "*indispensable and brilliant material for better life*" [1]. To emphasize this, a few major milestones from the history of glass are presented in the time line in Figure 1, together with some ideas of future glass technologies. Several glass products are used daily in our everyday life, often unnoticed. Glass can be found not only in obvious applications such as tableware, windows, and light bulbs, but also in tennis rackets, windmill turbine blades, optical devices, and medical implants. Because of the high energy demands of glass production, and ever tightening environmental regulations, it is likely that in the future the role of glass will more clearly change from commodity towards high-end technology [1-3].

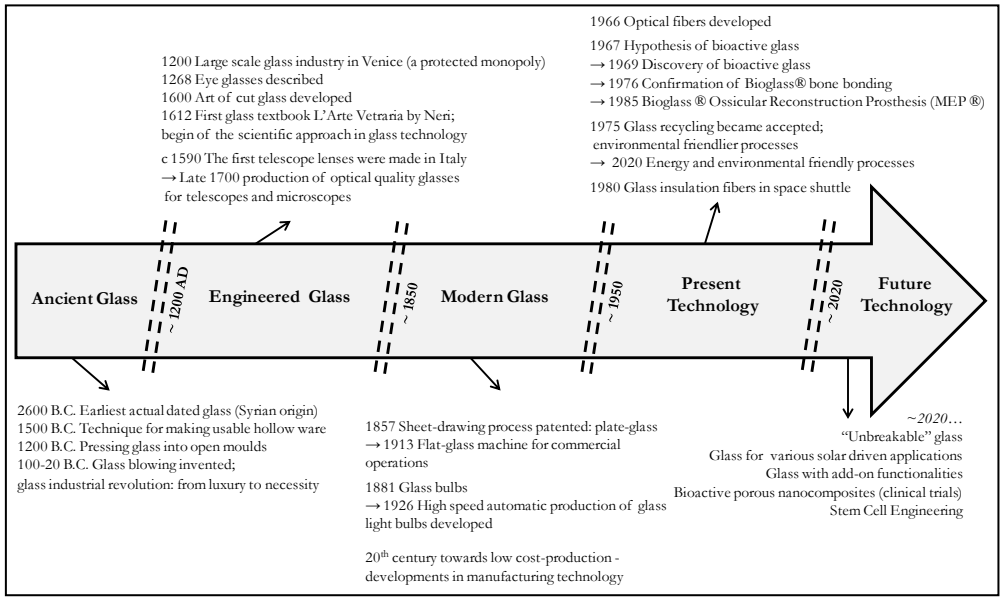

Figure 1. Selected milestones of glass and future targets (data collected from [2-8])

As shown in the timeline, the time for converting glass innovations into production has shortened during the centuries. This is because more resources than ever are invested in innovation and product development, which is also indicated in the growing number of publications. A data search performed using SciFinder (April 11 2012) shows that a vast number of scientific publications including the concept "glass" are produced every year (Inset graph in Figure 2). The height of the columns in Figure 2 indicates the total number of publications per year. Furthermore, as many new applications are based on established glass types, the time from idea to market will likely become even shorter in the future. Still, there are some limitations to how fast a new product can reach the final user.

For example, when glass is intended to be used in medical applications, and especially as an implantable device, there is heavy legislation for protecting the end-user, the patient. The most important single requirement for a glass implant is that it is biocompatible (term discussed further in chapter 2.1), i.e. that it generates the most appropriate beneficial cellular or tissue response in a specific situation [9]. All implantable devices must be proven safe for the intended applications with *in vitro* and *in vivo* experiments, and finally with clinical trials prior to final sales permission [10, 11]. Regulations concerning implantable glass products have been recently summarized by Lindgren et al. [12]. Therefore, we need to accept that even though research steps are advancing rapidly, it will still take time for novel products to enter the clinics.

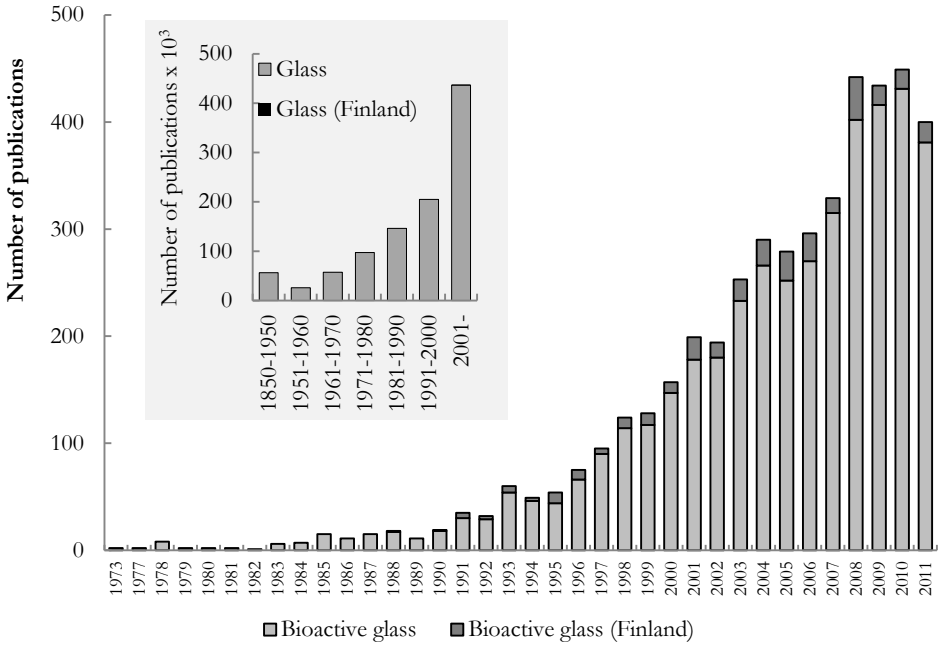

Figure 2. Number of scientific publications containing the term "bioactive glass" published per year, and the corresponding data for the term "glass" in the inset graph (Data search April 11 2012, source SciFinder®)

Today, only a few commercial bioactive glass products are available for clinical use (presented shortly in chapter 1.1.3) even though the concept of using glass as an implant material dates back to the late 1960s [8] and the research around bioactive glasses has become increasingly active (c.f. Figure 2). The glasses used at present as implants are inorganic silica-based melt-derived compositions mainly for hard-tissue repair as bone graft substitute in dentistry and orthopedics. In general, an ideal bone graft substitute is one that promotes bone healing, is replaced by the healing bone, is easy to handle, is inexpensive, and is readily available [13]. The market for all synthetic bone substitutes is around €40 million solely in Europe, and it is expected to increase annually by 12% (original source www.frost.com data adopted from [14]).

The main driving force for the development of bone substitute materials has been to find an alternative for autologous bone harvesting, which is an invasive procedure causing pain, bleeding, and morbidity for the patient [13, 15, 16]. Furthermore, elderly or pediatric patients and patients with malignant disease create limitations for successful bone harvesting [17]. Roughly 2.2 million bone graft operations, with estimated costs of around €2 billion ([18] in [19]), are performed worldwide annually, out of which 90–95% still involve harvesting bone from the patient [17, 19]. The use of frozen allogenic bone, often femoral heads removed during hip replacement [20], is common practice in orthopedics [21]. In Turku, the availability of allograft bones improved when allograft bone banking was started in 1972 for clinical purposes [22, 23]. There are, however, several problems related to allografts and xenografts, such as uncertain availability, viral and bacterial infections, and foreign body reactions [17, 21, 23-25]. When a synthetic substitute is used, the number of invasive procedures is halved, and thus the risk of infection or other complications is reduced. Furthermore, the use of a synthetic substitute usually shortens operation time and reduces the need for a second surgery [13, 19]. Thus, savings for the patient and for society may be noteworthy: the total savings derives not only because of the reduced operational cost but also from the reduced time needed for postoperative rehabilitation.

1.1.1. Bioactive glass

The glasses used in bone repair have a capability to bond to bone because of their special oxide composition. The implanted glass gradually dissolves and promotes new bone growth [26]. The sequence of reactions leading to bone-bonding is more closely presented in chapter 2.2.3. The glasses showing bone-bonding are called bioactive glasses. As commented by Prof. Ylänen from the Department of Biomedical Engineering at Tampere University of Technology (TUT), *"glass is an optimal biomaterial: it does the job and disappears"* [27]. Even though this is not always the case and glass remnants of some compositions have been found after several years of implantation [25, 28], his comment aptly describes the key idea behind bioactive glasses.

Bioactive glasses are in general osteoconductive and have antimicrobial properties [25]. Albeit their physical appearance (cf. Figure 4) resembles that of conventional soda-lime glass, their chemical compositions are highly different, and the same applies to their reactivity in contact with aqueous solutions. A general review of reactions occurring when glasses are in contact with aqueous solutions is given in 2.2.3. Furthermore, the dependence of glass durability and bioactivity on glass compositions is presented in 2.2.4. Bioactive glasses consist of elements that are naturally present in the human body. The first bioactive glasses were based on the Na_2O-CaO-P_2O_5-SiO_2 oxide-system [29], and later, K_2O-MgO-B_2O_3 were added to improve the hot-working properties of the glasses [30]. Other elements, such as Ag [31-33], Al [34], Cu [35], Sr [36, 37], and Zn [38], have also been included either directly to the glass structure or in

coatings on glass to further enhance the antibacterial properties and cell response of the glass [39, 40].

1.1.2. Towards optimal glass composition for each implantation

In addition to the demands presented above, an ideal bone substitute material should be mechanically stable [13]. Glass is a brittle and rigid material and cannot be used as such for load-bearing applications. Furthermore, glass has limitations in terms of shaping and bending.

In our group, significant effort has been placed on developing more versatile product forms (Figure 3), such as sintered glass bodies [41], sol-gel derived structures [42, 43], and thin fibers [44], which could then be used alone or in composite structures. However, the manufacturing of these product forms from bioactive glasses is challenging. The hot-working of glass is dependent on viscosity, which again is dependent on temperature and glass composition. Glass composition further affects devitrification behavior and liquidus temperature [45], which together with viscosity dictate the working range for a certain glass composition. For bioactive glasses 45S5 (Bioglass®) and S53P4 (Bonalive®), the hot-working range is narrow and the forming operations limited. Therefore, these glasses are used clinically only as particulates or monoliths. Today, however, there are glass compositions which are simultaneously bioactive, as shown *in vivo*, and allow hot-working [46-48].

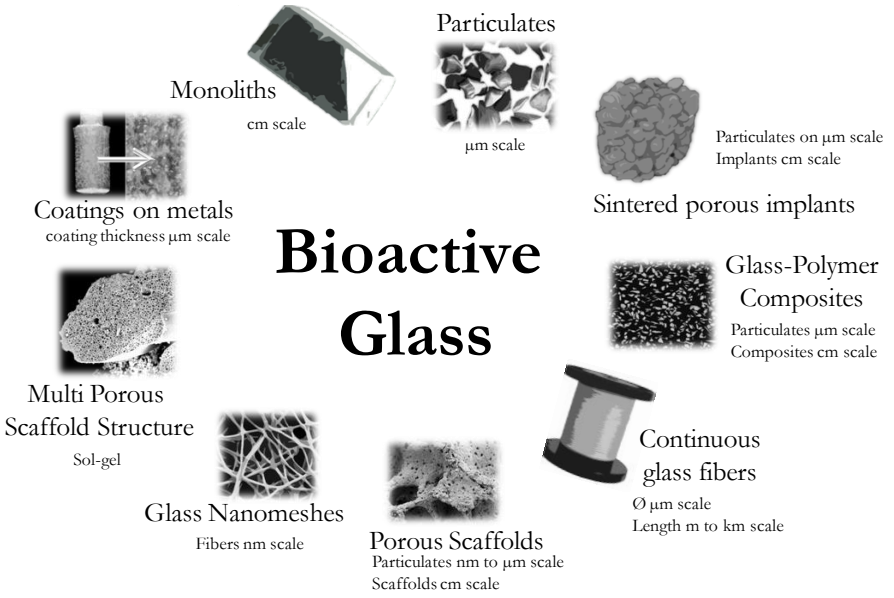

Figure 3. Versatile product forms manufactured from bioactive glasses with various methods ([42, 43, 49-52], publication VI).

The general research aim within our bioactive glass research group has been to improve the understanding of the various physical and chemical properties important for the wide range of applications of bioactive glasses. An essential part of the research has been related to understanding and modeling the different properties as function of

glass composition [41, 44, 53-57]. The work with bioactive glasses started at the Laboratory of Inorganic Chemistry at Åbo Akademi University already at the beginning of the 1980's [58], and the group has been active in publishing since then. When a literature search is conducted with the terms 'bioactive glass', it can be noticed that 5–19% of the annual publications include Finnish contributions (Figure 2), out of which 7–100% include contributions from Åbo Akademi University.

The literature on viscosity, devitrification, and hot-working properties of bioactive glasses has been reviewed and discussed in several theses published by our group [41, 44, 54-56]. In this thesis, the discussion is mainly limited to new findings made in this work, and no separate literature review is given concerning the aforementioned subjects.

Today, not only bioactive glass compositions, but also a range of other glass compositions are of interest to various clinical applications. Hence, the term biocompatible is often used in this thesis instead of the term bioactive. Recent shifts in attitudes and thinking around definitions in biomaterials are discussed in more detail in 2.1, and the different desired glass dissolution behaviors when implanted in the body are described in 2.2. A considerable research effort by our group has been directed towards bioactivity and reactivity of various glass compositions and product forms [41, 44, 53-57]. In this thesis, the relevant concepts concerning bioactivity are revisited, with emphasis on recent literature, in order to help the reader understand the novel findings discussed.

1.1.3. Current trends

One of the leading trends todays for industrial enterprises is to provide solutions to a specific problem rather than merely sell a product. This trend can be observed in companies ranging from the energy sector [59] to the biomaterial business [60]. One good example is shown in Figure 4, where product development has advanced from simply selling loose glass granules to a product combining glass particles with an easy-to-use function (BonAlive® applicator). When the applicator is provided with instructions for surgical procedures, the total solution brings more precision to the user, and finally more safety to the patient.

Most commercial clinical bioactive glass products are based on the U.S. Food and Drug Administration (FDA)-approved compositions 45S5 and S53P4. However, there are new compositions emerging in the market such as Stronbone, which gained CE Marking approval in EU in 2010 [61]. The first clinical bioactive glass products were solid plates (a device for replacing the bones of the middle ear, 1985) and cones (a device designed to support labial and lingual plates in natural tooth roots, 1988), but most current applications are based on particulates [8, 62].

The clinical products and applications of mainly Bioglass® 45S5 have been reviewed by Hench [8, 63, 64] and by Jones [65]. The applications range from non-load

bearing bone grafts to treatment of dentinal hypersensitivity with bioactive glass-containing toothpastes. Recently, also the applications of bioactive glass granules (S53P4) in orthopedics and traumatology, in maxillofacial reconstruction, and dentistry have been summarized by Heikkilä [13] and Peltola and Aitasalo [25]. S53P4 granules have been successfully used in treatment of benign bone tumor, metaphyseal fractures, and osteomyelitis, in posterolateral spinal surgery, in frontal sinus obliteration, and in frontal bone reconstruction, among others.

Figure 4. Bonalive® granules in a pouch package and the BonAlive® applicator with a shovel. Pictures provided by courtesy of BonAlive Biomaterials Ltd., copyright BonAlive Biomaterials Ltd. (2012)

The full potential of bioactive glasses has not been realized yet [66]. There has been interest to broaden the surgical scope of bioactive glasses by developing implantable pastes and putties, which would be more easily moldable during the surgery [67, 68]. In addition, more complicated product forms such as continuous melt derived fibers [69-72] and various types of scaffolds (e.g. [35, 73-77]) have been developed. Thin biocompatible glass fibers have been used in woven porous textile composite structures [78] and in dense biodegradable load-bearing composites [79, 80] together with organic polymers. Different types of scaffold structures for tissue engineering have lately aroused great interest. The goal with the scaffolds is to help the body's own regenerative mechanisms to restore a damaged tissue into its original state. It is possible to design scaffolds with variable degradation rates to match the rate of tissue ingrowth and remodeling [73, 81]. Different methods for manufacturing tissue-engineering scaffolds have been recently reviewed by Gerhardt and Boccaccini [76]. Also the antibacterial properties of bioactive glasses have been of interest [31, 33, 81-86].

A common factor for the function of the above mentioned product forms in the body is the increased need to understand and control ion dissolution from the glasses used to manufacture these. As a consequence, the need for new methods to quantify the ion dissolution has been emphasized.

1.2. Motivation for the work

Knowledge of both dissolution behavior and hot-working properties is of utmost importance when glasses are developed for different clinical applications.

Understanding the *in vitro* dissolution rate of glasses provides a first approximation of their behavior of *in vivo*. Specific studies concerning dissolution properties of bioactive glasses have been relatively scarce and mostly concentrated to static condition studies.

There is no absolute index to provide a measure for chemical durability of glass [4]. Already in 1940, the need for a quantitative approach was recognized by Dooley and Parmelee: *"From the standpoint of a strictly quantitative approach to the problem of measuring chemical durability of glass, there is need for (1) a method to measure the surface area of irregular shaped particles that is independent of their chemical composition and surface condition and (2) methods to measure the actual ions present in extracts from durability tests"* [87].

The motivation behind this work was to develop a simple and accurate method to quantify the *in vitro* dissolution rate of highly different types of glass compositions with interest for future clinical applications. In addition, as information on hot-working properties is required for forming glass, and thus studies concentrating also on these issues were included in this thesis.

1.3. Objective of the work

The objective of this work was to increase the understanding of *in vitro* dissolution behavior of glasses directed towards clinical applications by using different experimental methods. With the gained knowledge we can identify different dissolution patters and use this information to improve the tuning of glass compositions. An additional goal was to shed light on the phase changes occurring during various heat treatments of glasses using three selected compositions.

In short, the thesis aims:

- to work out a reliable method for analyzing the *in vitro* dissolution rate of glasses and to increase knowledge of the dissolution behavior of glasses with a wide range of chemical composition by:
    - comparing the suitability of conventional methods for dissolution studies with bioactive glasses
    - introducing a novel experimental approach to obtain dissolution patterns and rates for dissolution of glasses in the initial stages of fluid contact in a flow environment
    - correlating the initial dissolution with the *in vitro* and *in vivo* bioactivity of the glasses, as suggested by phenomenological models and experimental findings established earlier
- to increase knowledge about the crystallization behavior of selected glasses by:
    - establishing Time-Temperature-Transformation (T-T-T) curves relevant to heat-treatment parameter optimization obtained using differential thermal analysis and conventional heat-treatments

- studying sintering of implants with concurrent crystallization and the effect of phase transformation on *in vitro* reactivity

1.4. List of publications

This thesis is based on the following publications, given as appendices:

I. **Comparison of reactions of bioactive glasses in different aqueous solutions**
S. Fagerlund, L. Hupa, M. Hupa
In: Narayan, R., Singh, M., McKittrick, J., editors, *Advances in Bioceramics and Biotechnologies: Ceramic Transactions Volume 218*, Wiley, 2010, pp.101-113
ISBN: 978-0-470-90548-7

II. **Dissolution kinetics of bioactive glass by continuous measurement**
S. Fagerlund, P. Ek, L. Hupa, M. Hupa
Journal of American Ceramic Society, Vol 95 (2012) 10, pp. 3130-3137
DOI: 10.1111/j.1551-2916.2012.05374.x

III. **On determining chemical durability of glasses**
S. Fagerlund, P. Ek, M. Hupa, L. Hupa
Glass Technology: European Journal of Glass Science and Technology, Part A, Vol. 51 (2010) 6, pp. 235-240

IV. **Dissolution patterns of biocompatible glasses in TRIS buffer**
S. Fagerlund, L. Hupa, M. Hupa
Acta Biomaterialia, in press, corrected proof (2012)
DOI: 10.1016/j.actbio.2012.08.051

V. **T-T-T behavior of bioactive glasses 1-98 and 13-93**
S.Fagerlund, J. Massera, M. Hupa, L. Hupa
Journal of the European Ceramic Society, Vol 32 (2012) 11, pp. 2731-2738
DOI: 10.1016/j.jeurceramsoc.2011.10.040

VI. **Phase composition and *in vitro* bioactivity of porous implants made of bioactive glass S53P4**
S. Fagerlund, J. Massera, N. Moritz, M. Hupa, L. Hupa
Acta Biomaterialia, Vol 8 (2012) 6, pp. 2331-2339
DOI: 10.1016/j.actbio.2012.03.011

In this thesis, the Roman numerals I-VI are used to refer to these original publications. The original publications are reproduced with the kind permission of the respective copyright holders.

1.5. Contribution of the author

The following describes the author's contribution to the papers on which this thesis is based:

I. The author participated in the experimental design of the study and was responsible for all the experimental work. The scanning electron microscope (SEM) analyses were done in collaboration with an SEM specialist. The author evaluated the results, wrote the first draft of the manuscript, and finalized it together with the co-authors.

II. The author was responsible for the experimental design of the study and did the experimental work together with one of the co-authors (excl. BET measurements). The author evaluated the results, wrote the first draft of the manuscript, and finalized it together with the co-authors.

III. The author was responsible for the experimental design of the study as well as for the experimental work. The SEM analyses were done in collaboration with an SEM specialist. The author evaluated the results, wrote the first draft of the manuscript, and finalized it together with the co-authors.

IV. The author was responsible for the experimental design of the study as well as did all the experimental work. The presented hot stage microscopy (HSM) and differential thermal analysis (DTA) data were based on unpublished measurements done at the group. The SEM analyses were carried out in collaboration with an SEM specialist. The author evaluated the results, wrote the first draft of the manuscript, and finalized it together with the co-authors.

V. The author was responsible for the experimental design of the study and for the sample preparation, the isothermal heat-treatments and analysis of the monoliths. The DTA part was performed by one of the co-authors, and all the SEM analyses were done in collaboration with an SEM specialist. The author evaluated the results related to the isothermal heat-treatment, wrote the first draft of the manuscript, and finalized it together with the co-authors.

VI. The author was responsible for the experimental design. The author did all the experimental work. The micro-computed tomography (μCT) and SEM measurements were done in collaboration with specialists. The author evaluated the results, wrote the first draft of the manuscript, and finalized it together with the co-authors.

1.6. List of related contributions

The following list comprises results related to this thesis:

- **Liquidus Temperatures of Bioactive Glasses**
  H. Arstila, M. Tukiainen, S. Taipale, M. Kellomäki, L. Hupa
  Advanced Materials Research, Vols. 39-40 (2008), pp. 287-292

- **Continuous Measurement of the Dissolution Rate of Ions from Glasses**
  S. Taipale, P. Ek, M. Hupa, L. Hupa
  Advanced Materials Research, Vols. 39-40 (2008), pp 341-346

- **Crystallization of 45S5 during isothermal heat treatment**
  S. Fagerlund, L. Hupa
  Materialy Ceramiczne/Ceramic Materials, Vol. 62 (2010) 3, pp. 349-354

- **Surface reactions of bioactive glasses in buffered solution**
  L.Varila, S. Fagerlund, L. Hupa, T. Lehtonen, J. Tuominen
  Journal of the European Ceramic Society, Vol 32 11, pp. 2757-2763
  DOI: 10.1016/j.jeurceramsoc.2012.01.025

- **Crystallization mechanism of the bioactive glasses 45S5 and S53P4**
  J. Massera, S. Fagerlund, L. Hupa, M. Hupa
  Journal of American Ceramic Society, Vol. 95 (2012) 2, pp. 607-613
  DOI: 10.1111/j.1551-2916.2011.05012.x

1.7. Thesis organization

This thesis consists of a summary part and six peer-reviewed publications. In chapter 2 (literature review), the key concepts relevant to this thesis are presented, whereas chapter 3 (materials and methods) shortly summarizes the experimental details. The first four publications concentrate on the dissolution behavior of glasses while the last two have the main focus on the crystallization and sintering of glass. The key findings from each publication are discussed in chapter 4.

Publication I describes the effect of the immersion solution to glass dissolution. Four known glass compositions were tested *in vitro* with three different buffered solutions. Publication II presents in detail the novel experimental approach used in this thesis and introduces the effect of selected experimental parameters on the initial glass dissolution by using one glass composition. In publication III, glass dissolution is studied using three different methods and five glasses with highly different anticipated chemical durability. The dissolution patterns of 16 biocompatible glasses in TRIS were recorded with the novel continuous method presented in publication II, and the results and findings are discussed in publication IV. The results from publications II–IV are dealt with together and discussed as an entity in this thesis. The crystallization behavior

of two bioactive glasses was studied in publication V, and engineering-type T-T-T curves were established. In publication VI, the crystallization and sintering of one bioactive glass composition was studied in detail. Furthermore, the dissolution behavior of the partially crystallized sintered structures was studied.

The conclusions are presented in chapter 5 together with a short outlook for the future. In the appendix, a comprehensive list of definitions is given to clarify the terminology used in this thesis. The definitions in the biomaterial field come from a plethora of sources and are sometimes used in a somewhat "wild-west" manner, which may cause confusion in some cases.

2. Review of the literature

2.1. Biocompatible materials - biomaterials

Biomaterials are designed to improve human health and the quality of life by restoring the function of natural living tissue and organs in the body. Biomaterials can be divided into several subcategories by using material classifications [88], tissue-implant interactions [26], or life-length of the implant in the body [89].

The single most important factor for a biomaterial is that it is able to be in contact with tissues of the human body without causing an unacceptable degree of harm to that body [9], i.e. the material is biocompatible. Biocompatibility has been defined earlier (1986) simply as the *"ability of a material to perform with an appropriate host response in a specific situation"* ([90] in [9]). Even though this definition is valid for long-term implantable devices, it does not cover the ever wider range of different applications of biomaterials. Thus, a more detailed definition encompassing all types of biomaterials was recently given by Williams (2008): *"the ability of a biomaterial to perform its desired function with respect to a medical therapy, without eliciting any undesirable local or systemic effects in the recipient or beneficiary of that therapy, but generating the most appropriate beneficial cellular or tissue response in that specific situation, and optimizing the clinically relevant performance of that therapy"* [9].

The prefix bio- can be defined as 'life or living things', but often it can also refer to something that benefits life, as in the case of the term 'bioceramics' [91]. The challenges with using the prefix bio- was recently (2009) brought up by Williams [91] in his leading opinion journal article in Biomaterials. He reminds us of the need to accept that different disciplines can use the same words for totally different meanings (c.f. automotive company with a biomaterials department). In the same article, the essence of biomaterials is discussed from several viewpoints. Furthermore, the classical definition of biomaterials formulated ten years earlier is challenged, and as a conclusion, William suggests a new definition for biomaterials which takes into account the novel 21st-century biomaterials.

The definition of biomaterial has undergone many revisions and debates, as indicated by the development steps summarized in Table 1. The definitions given in Oxford English Dictionary (1999) [92] and in Larousse dictionary of science and technology (2006) [93] are not in line with the other definitions. These give too simplified a picture of biomaterials and can cause misunderstandings. Otherwise, the definitions reflect shifts in thinking and material development over the years. In the table, examples of emerging biomaterials of each 'era' are given which do not fit the previous definitions and which gave rise to modifications of the definitions. The examples are intentionally limited to materials used to replace, repair, or regenerate parts of the musculoskeletal system of the body. Reviews concerning bone-matrix synthesis and skeletal-function relationships are given in [94-97].

Table 1. Evolution of the definition "biomaterial" and examples of emerging implant materials

Year	Definition	Implant materials emerging
1860s*	Possible to implant materials without infections – first time advantageous to use surgical procedures [89]	Fe, Au, Ag, Pt, Ni, steel [89]
1945**	Causing no or only minimal reactions when inserted in body - lack of toxicity, concerns about biodegradation products from metals, alloys, and polymers [98]	Ceramics [14, 98, 99], PMMA, Ti and its alloys [89]
1974	"A biomaterial is a systemically, pharmacologically inert substance designed for implantation within or incorporation with a living system." ([100] in [89])	Bioactive ceramics [101, 102]
1982	"A biomaterial is any substance, other than drug, or combination of substances, synthetic or natural in origin, which can be used for any period of time, as a whole or as a part of a system which treat, augments or replaces any tissue, organ or function of the body." [103]	Composites [104]
1986	"A non viable material used in a medical device, intended to interact with biological systems." ([90] in [103])	
1991	"A material intended to interface with biological systems to evaluate, treat, augment, or replace any tissue, organ, or function of the body." [103]	Tissue-engineering scaffolds [73]
1999	"An organic substance of biological origin, esp. one forming part of the structure of an organism. Also: a material (typically wholly or partly synthetic) used for prostheses, medical implants, etc.; such materials collectively." [92]	
2006	"A solid material which occurs in and is made by living organisms, such as chitin, fibrin or bone" ([93] in [91])	
2009	"A biomaterial is a substance that has been engineered to take a form which, alone or as part of a complex system, is used to direct, by control of interactions with components of living systems, the course of any therapeutic or diagnostic procedure, in human or veterinary medicine." [91]	"Nanoscale" materials [99, 105, 106], (Non-)viral vectors (such as polymers with embedded DNA, able to introduce DNA into target cells) [91, 107-109]

**time after the aseptic surgical technique developed ** time after Second World War*

Prior to the first aseptic surgical procedures developed by Dr. Lister in the 1860s [89], the usage of biomaterials was trial-and-error-based reconstruction of missing or defective parts of the body [88]. Until the 1970s, the golden rule was that implantable materials should be as inert as possible and only replace a missing function in the body. These nearly inert materials, including metals, ceramics, and polymers, formed the so called first-generation biomaterials [11, 96, 99]. These materials are still widely used today in various applications.

The second-generation materials are aimed to repair tissue. These materials, radically different from their predecessor, the 1st-generation materials, interact with the body and generate reaction products which are beneficial to the host tissue [8, 14, 99]. Materials that are able to have a biological effect or be biologically active, and form a

bond between the tissues and the material, are called bioactive materials [110]. Because of the 40th anniversary (1969-2009) of the invention of the concept of bioactive materials, many review articles concerning the past, present, and future of especially bioactive ceramics have been published recently [8, 14-16, 24, 64-66, 96, 99, 111]. Bioactive materials are considered to have the ability to directly attach to bone without a fibrous capsule, and the bonding strength is typically equivalent or higher than the strength of the implant material or the tissue bonded to the implant [26]. Thus, if a mechanical fracture occurs, it usually starts either in the implant or in the bone but not at the interface.

The first true consensus over the term biomaterial was gained as late as 1986 at the Consensus conference hosted by the European Society for biomaterials [103]. The definition included the term 'interact', taking into account 2nd-generation materials. In the next definition, the term 'interact' is changed to 'interfere', which takes into account materials designed to regenerate tissue instead of only repairing, thus leading into 3rd-generation materials. This generation of materials emphasizes the meaning of bio in the term biomaterials [112, 113]. The latest definition (2009) introduces the engineering aspect to the definition and widens even further the range of possible materials. Materials now being considered include viral vectors, used as DNA carriers to specific cells [91, 107-109], and hybrid sol-gel materials where inorganic and organic materials meet with domain sizes approaching the molecular level enabling engineering of the material nanostructure [114-116].

It may well be that traditional 1st- and 2nd-generation biomaterials will lose some of their previous interest in the research field, but it is undoubtedly clear that they will still, for a long time, serve in clinical applications as such and as substrates and templates for 3rd-generation biomaterials [10, 99]. To gain the best answers for the growing demand of functional biomaterials, highly multidisciplinary approaches are required, which further increases the need for a clear vocabulary. Consequently, the continuous updating of the definitions is vital.

The next chapters concentrate on the principal biomaterial studied in this work, i.e. glass, and the discussion is limited to melt-derived silica-based oxide glasses and glass-ceramics derived from these glasses.

2.2. Biocompatible glasses and glass-ceramics

As is now clear by definition, biocompatible glasses and glass-ceramics are materials desired to generate the most appropriate beneficial cellular or tissue response in a specific situation. However, the definition does not explain what type of glass dissolution behavior is desired in various applications. The non-stable human body environment puts several demands on the implant materials used to replace or augment tissue functions. The degree of glass reactivity desired varies according to implantation situation; the only common factor is the non-toxicity.

In bioresorbable glass applications, such as bone fracture pins and screws, the glass in the composite structure should give mechanical support during the bone fracture healing period and then degrade [67, 79]. The dissolution rate should match the growth rate of the new tissue [73, 81], which in some cases may be slow. In certain applications, such as dentures reinforced with continuous E-glass fibers, glass should be inert and maintain its mechanical properties under several loading cycles and for a long time [117-119].

Today, though, glass is most often designed to act as bioactive bone-grafting material in medical implantations and operations. Glass supports bone formation via dissolution and formation of a hydroxyapatite (HA) surface layer. However, after the discovery that the ion release products from bioactive glasses activate several families of genes [120-123], among others genes that regulate osteogenesis and the production of growth factors, glass research has more and more shifted towards tissue regeneration where glass is desired only to dissolve and offer soluble elements and ions to the genes. The role of the various dissolved ions and ion release kinetics from the glasses on the human cell behavior has recently been reviewed by Hoppe et al. [39].

The reactivity of glass and glass-ceramics in the body environment is highly compositional dependent, but several other factors should also be considered (see 2.2.4). Below, the general structural features of glasses and the reaction mechanisms of glasses in aqueous solutions are reviewed.

2.2.1. Glass and glass-ceramics – structural features

Glass has several characteristics which make it a superior material for medical applications, ranging from fiber optics for endoscopy, thermometers, insoluble porous carriers for antibodies and enzymes to bioactive implants, fillers in bioabsorbable composite structures, and tissue-engineering scaffolds [26, 29, 77, 124, 125]. Glass has a certain compositional freedom allowing a wide variety of characteristics, such as formability, chemical durability, strength, and optical properties. Several of these properties can be smoothly adjusted by the composition within a certain range [126], and this has been exploited in various phenomenological models and optimization routines [34, 46, 127-135]. Glass properties, however, depend not only on the composition but also on the thermal history of the sample, such as cooling rate, annealing time, and hot-working of the glass. The relevant structural and kinetic theories of glass formation have been reviewed in the PhD thesis by Arstila [44], and the viscosity-temperature relationships in the PhD thesis by Vedel [56].

In general, glass can be described as a solid with a liquid-like atomic structure, i.e. atomically disordered solid. Glass, especially melt-derived oxide glass, is often defined by using the following definitions:

- "*an amorphous solid completely lacking in long range, periodic atomic structure, and exhibiting a region of glass transformation behavior*" [5]
- "*an inorganic product of fusion that has cooled to a rigid condition without crystallization*" (ASTM) [136]

The amorphous SiO_4 tetrahedral network forms the backbone structure for silica-based glasses. These SiO_4 tetrahedra are connected at the corners in various orientations to form a continuous 3D network. Each oxygen atom can act as a bridge between neighboring tetrahedra. The local configuration around each silicon atom is expressed with Q^n notation, where n is the number of bridging oxygen (BO) ranging from 0 to 4. The role of alkali and alkaline earth oxides is to modify the network structure, i.e. these oxides reduce the degree of connectivity in the network by replacing BO by non-bridging oxygen (NBO), thus opening up the glass structure. The strength of the individual modifying ion–oxygen bond together with the number of NBOs determines several glass properties, such as viscosity and chemical durability. The role of various glass components and their effect on different physical and chemical properties has been discussed by Paul [137], Shelby [5], and Varshneya [136], among others. The usage of accurate structural analysis techniques, such as MAS-NMR, combined with powerful computational tools has substantially increased the knowledge about the detailed structure of glasses [19], and detailed structural features of silica-based glasses have been widely reported [19, 37, 136, 138-153]. There are also several other glass forming systems than silicate. Especially, phosphate- and borate-based glasses have lately gained increased attention in bioactive glass research [40]. The structural features of phosphate glasses have been discussed by Brow [154] and Kirkpatrick and Brow [155], and the structural features of borate and alkali borosilicate glasses by Hannon et al. [156], Krogh-Moe [157], and Vedishcheva et al. [158].

The strength of glass is defined as the applied stress on failure [136]. Mechanical properties are highly dependent on the surface condition of the glass, i.e. presence of microscopic flaws and cracks, which will propagate under tensile loads. The loading leads to uncontrolled crack growth until the glass physically breaks [136]. The phenomenon is commonly known as fatigue. The theoretical strength of flawless solid silicate glass is ~35 GPa [136, 159], while for instance some steel alloys can reach strengths higher than 1000 GPa. Strength of oxide glasses and the different experimental techniques to measure it have been recently reviewed by Kurkjian [159]. However, the ability of a glass to resist fracture when a crack is present, i.e. fracture toughness, is low. Thus, already small flaws decrease the strength noticeably, and typical strength of common glass products is only around 14-70 MPa [136]. Thus, glasses are brittle and they fail without yielding as indicated by the high Young's modulus of silicate glasses, 45-100 GPa [160]. The corresponding values of cancellous ("spongy") bone and cortical ("compact") bone are .05-0.5 MPa and 7-30 MPa, respectively [13]. The compressive strength of bioactive silica glasses is around 800-1200 MPa [6] and tensile bending strength is 40 to 60 MPa, depending on the

composition of the glass [13]. As a comparison, the compressive strength of cancellous bone is 2-12 MPa and that of cortical bone 100-230 MPa [13].

It has been demonstrated that amorphous porous bioactive glass structures can be sintered from bioactive glasses having a wide hot-working range [35, 161-163]. In general, the compression strength of porous glassy implants is of the same order as that of cancellous bone. A higher sintering temperature usually increases the strength, but it also increases the amount of crystallization and reduces the porosity. If crystallization occurs too rapidly, it interferes with viscous flow sintering. Partial crystallization of the glass particles decreases the viscous flow sintering [164] and produces a residual glassy phase whose viscosity deviates from that of the parent glass. Crystallization of bioactive glasses has been discussed in detail in the PhD thesis of Arstila [44].

The mechanical strength and toughness of glass can in some cases be significantly improved by controlled crystallization. For example lithium disilicate glass-ceramics have been shown to have bending strengths of around 700 MPa while still being translucent [165]. Special shades and various degrees of durability, ranging from highly durable to resorbable, can also be tailored by changing the glass composition [166]. One further advantage with apatite- and mica-based glass-ceramics is that they can be easily processed by drilling [101, 166, 167]. Glass-ceramics, originating from the mid-1950s, are materials that are composed of one or more glassy and crystalline phases formed through controlled nucleation and crystallization of glass [168]. The principles of producing glass-ceramics are well described by Höland [166] and Hill [101]. The applications and developments in the area have been reviewed by Höland [166, 169], Höland et al. [170], Pannhorst [171], and Zanotto [168]. Recently, considerable effort has been directed towards the development of different types of glass-ceramics for tissue-engineering scaffolds and dentistry (e.g. [24, 76, 170, 172, 173]).

The glass-composition and various nucleation agents affect the crystallization mechanism (bulk or surface) [166]. In addition to the glass composition, the glass-ceramic designer can alter the microstructure by controlling the heat-treatment parameters. Glass-ceramics can also be produced by sintering glass powder or granulate (sintering mechanisms are reviewed by Prado [164]). The porosity of the material can be controlled by varying the nominal grain size and heat-treatment parameters. All these parameters give high flexibility for the tailoring of the material properties. However, because glass-ceramics consist of multiple phases and structures, the control of the processing is difficult and the dissolution properties cannot be as easily mathematically modeled as for glasses. Furthermore, the residual internal stresses and mismatches of the different phases may influence the strength and durability of the glass-ceramics [174].

2.2.2. Glass durability

It is vital that the ion release from any glasses used in medical application is controlled. According to Morey [4], producing a glass stable enough to serve its intended purpose places a practical limit on the compositions which may be employed. With knowledge of the reactions and reaction mechanisms taking place in contact with aqueous solutions *in vitro*, the compositions of the glass can be tailored for various implantation conditions.

Glass is in general considered highly durable. In several applications, the chemical durability is well above the product need, and thus it seems to be of less importance [175]. However, all glasses will react under certain conditions with aqueous solutions, only the time scale varies. Glass durability is usually referred to as the resistance to proton-alkali ion exchange between an aqueous solution and a glass surface. Chemical durability or stability is defined as the resistance which glass offers against the chemical attack by water, humidity, and of aqueous solutions of acids, bases and salts. The term hydrolytic resistance describes specifically how well glass withstands reactions with pure water, and can be classed as a subgroup to chemical durability. The term weathering describes the durability against elements in atmosphere, especially, humidity. Durability is measured through several approaches related to the final use of the glasses. However, no absolute measure of chemical durability exists, which is why durability is often determined in a relative scale in which different glasses are compared at similar experimental conditions [137]. Typical durability tests are reviewed in 2.3.

Predictions of glass dissolution in aqueous solutions can be made by a combination of theoretical models and experiments. Traditional modeling techniques used for predicting glass dissolution are based on analytical (kinetics), geochemical (transition state), and thermodynamic (free hydration energy) models [135, 175-182]. Thanks to increased computational power, more sophisticated approaches have become available. Hard and soft computational techniques available for modeling glass dissolution are well described by Aertsens and Ghaleb [135]. Because glass dissolution modeling is outside the scope of this work, this theme is not elaborated further, but it is recognized that the results presented here could be used as a source data for predictive models.

2.2.3. Glass in contact with aqueous solutions

Whereas the corrosion mechanisms of metals or ceramics may be described by fairly simple chemical dissolution, much more complex reactions occur for glasses. According to the definition, corrosion is *"the degradation of a metal by an electrochemical reaction with its environment"* [183]. Despite the contradiction to the original definition, the term corrosion has become well recognized in the literature on glass. It is used more or less as a synonym to dissolution or network breakage of glass. As glasses for medical applications are, however, usually designed to react with the body environment, the negative tone of the term 'glass corrosion' is unsuitable [53]. Hence, in this work, the term 'glass reactions' is used instead.

The glass dissolution reaction mechanisms are well described in the literature [26, 181, 184-195]. Glass can either dissolve congruently, i.e. uniformly, which implies that the ratios of elements in the solution are the same as in the dissolving glass, or incongruently, i.e. to show preferential dissolution/leaching [190]. The reaction mechanisms depend on both glass composition and the environmental conditions such as surface area to volume ratio and pH of the solution. Relevant parameters affecting reaction mechanisms and kinetics of glasses in body environment are reviewed in 2.2.4.

The glass reactions in contact with aqueous solutions are often divided into primary and secondary reactions: (1) ion-exchange, hydration, and hydrolysis, and (2) precipitation. The primary reaction steps for a simple sodium silicate glass are summarized in Figure 5. Each of the reaction steps will be described separately in the following paragraphs, even though in reality the reactions are strongly coupled to each other [185, 191, 195]. The reaction steps reviewed here are restricted to reactions typically taking place at the surface of silicate glasses.

During the first tens of milliseconds when a glass is in contact with aqueous solutions, an electrochemical equilibrium is established at the glass surface ([196-198] in [187]). At pH < 9, a selective leaching process dominates [199, 200] and an ion exchange reaction, i.e. interdiffusion of protons from the surrounding solution and alkali and earth-alkali ions from glass, follows the electrochemical equilibrium (step 2 in Figure 5).

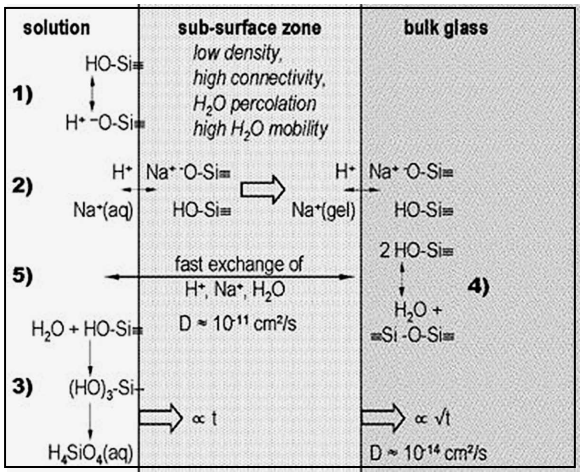

Figure 5. Phenomena observed during the formation of the subsurface zone of a simple sodium silicate glass: (1) instantaneously established electrochemical surface equilibrium; (2) ion exchange; (3) cleavage of silica bonds (network dissolution); (4) condensation of initially formed silanol groups (gel formation reaction); (5) fast exchange of metal ions, protons, and molecular water across the subsurface zone. [187] Reproduced with permission of John Wiley and Sons.

In the ion-exchange reaction, mobile ions are leached out from the glass matrix leaving the matrix material more or less intact, and the charge balance is maintained [190]. The field strength and the radius of the network-modifying ion affect the mobility, i.e. as the charge-to-radius ratio of the cation decreases, the mobility increases. Thus, the alkali ions are the most mobile, and furthermore ions with a larger

ionic radius are more weakly bound to the NBOs and consequently more mobile than ions with a smaller radius. Dissolution of K_2O-containing glasses have been shown to be many orders of magnitude faster than Li_2O-containing glasses [189]. Additionally, water may enter the glass structure as molecular water (hydration).

Example of ion-exchange (1) and hydration (2) reactions are given below [191]:

$$\text{–Si–O}^{-}\text{M}^{+}\text{ (glass)} + \text{H}^{+}\text{ (aq)} \rightarrow \text{–Si–OH (glass)} + \text{M}^{+}\text{ (aq)} \quad (1)$$

$$\text{–Si–O}^{-}\text{M}^{+}\text{ (glass)} + \text{H}_2\text{O (aq)} \rightarrow \text{–Si–OH (glass)} + \text{M}^{+}\text{ (aq)} + \text{OH}^{-}\text{ (aq)} \quad (2)$$

A comprehensive list of water reactions with the glass network is given by Grambow et al. [201]. According to Bunker, alkali leaching is not a reversible reaction because the formed silanol groups react with each other to form Si-O-Si bonds [191], whereas Grambow et al. consider the backward reaction possible [201]. The rate of molecular water diffusion is mainly determined by the structure of the glass, i.e. the size of voids between oxygens [191]. If the voids are too small, the only way for water is to enter the structure via hydrolysis, which is the case for most glasses [191]. Leaching continues inwards to the bulk, and the proton on the silanol group (Si-OH) can change sites with an inner M^+ [136]. Consequently, the phase notation for M^+ could also be 'glass' in reactions 1 and 2 because the M^+ may be trapped in the glass structure [201]. To maintain the charge balance in the glass structure, some internal condensation of molecular water needs to take place. This might explain the observed percolating water phase in the structure [187]. In addition, for soda-lime glasses it has been shown by isotope labeling of water that the ion exchange of Na^+ occurs purely with neither with H^+ nor H_3O^+ [187]. An example of a leached layer is shown in Figure 6. From the cross-sectional SEM image of bioactive glass S53P4 after 1 week of immersion in 10-% lactic acid ($pH_{t=1\ week}$ = 2.9), a typical sharp interface between the leached layer (dark gray) and the bulk glass (light gray) can be observed.

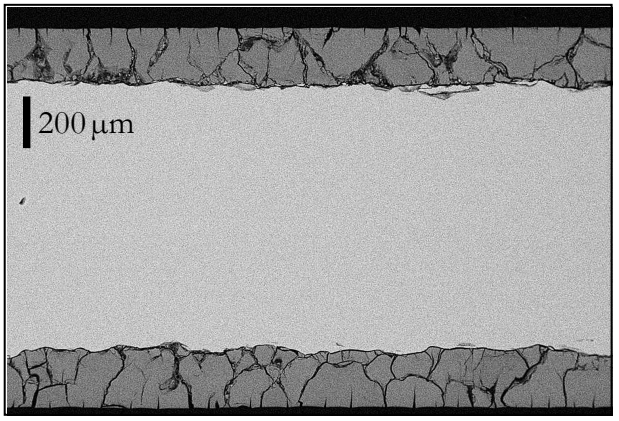

Figure 6. The cross section of bioactive glass S53P4 after 1-week immersion in 10 % lactic acid showing a leached silica rich layer, picture provided with courtesy of Leena Varila, ÅA [202]

The ion-exchange reaction is often described with Fick's law, here given for one dimension (3):

$$\frac{dc}{dt} = \frac{\mathrm{d}}{\mathrm{x}}\left(\mathrm{D}\frac{dc}{dx}\right) \quad (3),$$

where D is the diffusivity of the dissolving ions. For a planar interface with constant surface conditions, the solution of the equation leads to a parabolic rate law [190], and thus the amount of alkali dissolved should be proportional to the square root of time. If sufficient amount of liquid is available, the reaction ends only when the entire glass sample has undergone an ion-exchange reaction [190]. However, as the ion exchange is not the only reaction, the extent and the relative rates of other simultaneous reactions control the glass dissolution process and the kinetics of alkali leaching [195].

The excess hydroxyl (OH) ions in the solution resulting from the cation exchange in the glass with H^+ in the solution act as a catalyst for network dissolution [152]. At the alkaline region (pH >9), the hydrolysis reaction (reaction 4 and reaction step 3 in Figure 5) starts to dominate, causing depolymerisation of the glass structure. A silicon bridge is opened in the hydrolysis reaction. The reaction is caused by the nucleophilic attack by OH^- and leads to a more open glass structure. As shown in Figure 5, the -Si-OH groups may react further, which gradually leads to the dissolution of the glass network (soluble silica). The simultaneous condensation reaction (reaction 5 and reaction step 4 in Figure 5), where the formed silanol groups are polymerized again to Si-O-Si bonds, may take place. This leads to enrichment of surface SiO_2 and to formation of a gel-like layer.

$$\text{–Si–O–Si (glass)} + \text{OH}^- \text{(aq)} \rightleftharpoons \text{–Si–OH (glass)} + \text{Si–O}^- \text{(glass)} \quad (4)$$

$$\text{–Si–OH (glass)} + \text{OH–Si– (glass)} \rightleftharpoons \text{–Si–O–Si (glass)} + \text{H}_2\text{O (aq)} \quad (5)$$

Molecular water is released by the condensation reaction, and it can react further, increasing the rate of network dissolution. The condensation reaction may lead to a structure with enhanced connectivity ([203] in [187]), increasing the diffusion of water, but simultaneously many of the ion exchange sites are eliminated in the process [191]. Also, a structural compaction of the outermost layer and closure of the formed pores has been reported ([184, 186], [204] in [187]), which would further retard dissolution.

When the solubility limit of the dissolved ions is exceeded, a secondary reaction, i.e. precipitation, occurs. The precipitation may take place on suitable nucleation sites either on the glass surface or inside the leached layer. The precipitated layer may act as a diffusion barrier and protect the glass from further dissolution [188]. The precipitate layer also acts as a substrate for further adsorption [190], and several secondary layers may form. Given enough time an initially amorphous precipitated layer can crystallize.

An example of a secondary reaction layer, calcium phosphate (CaP), formed on top of a leached layer is given in Figure 7 (unpublished image from data set published in [205]). Bioglass® 45S5 was immersed in simulated body fluid (SBF) for one week. SBF resembles the inorganic part of human extracellular fluid [206].

The CaP layer is formed by migration of Ca^{2+} and PO_4^{3-} groups to the surface through the SiO_2-rich layer by incorporation of soluble calcium ions and phosphates from the solution [26, 207] or simply by precipitating from appropriate solutions. With time, the CaP layer crystallizes into HA. Also other anions, such as F^-, OH^-, and CO_3^{2-}, may be incorporated into the crystalline structure [26, 207]. This crystallized HA is similar to that in natural bone. The biological HA acts as reinforcement in hard tissue being responsible for the stiffness of bone, dentin, and enamel [89]. The formed HA layer is able to form a chemical bond with natural bone via a series of biological reactions. The formation of an HA layer on the leached silica-rich layer may act as a diffusion barrier, depending on the density of the layer. This decreases the driving force for further dissolution and might partially help explain why, with some bioactive glass compositions, intact core glass is still found after several years of implantation as reported by Lindfors et al. [28].

To summarize, the reaction sequences leading to bone bonding in the body environment follow the same reaction steps as presented above [26, 207]. These reactions may partly occur also for conventional soda-lime glasses (SLG). However, rates for the primary reactions are slow for SLG, and thus they are encapsulated in the body [26]. These primary stages are followed by the formation of a CaP layer on bioactive glasses. The additional steps include adsorption of biological moieties, such as proteins, to the reaction layers, followed by the action of macrophages and stem cell attachment, among others [26, 113]. The reaction sequence leading to bone bonding can up to HA formation be simulated *in vitro* with various aqueous inorganic solutions, and they occur during the first hours for Bioglass® 45S5 [26].

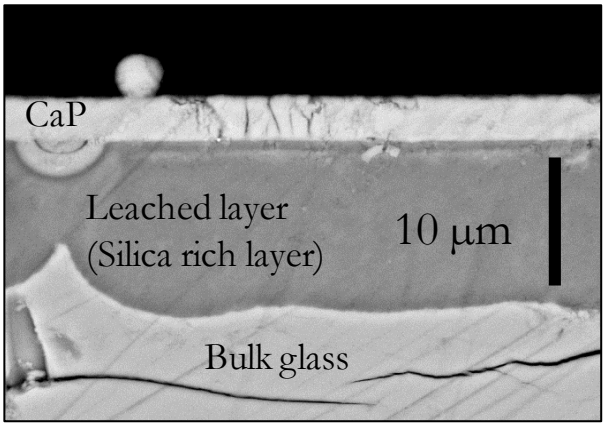

Figure 7. The precipitated CaP layer on top of the leached silica-rich layer on 45S5 after one-week immersion in SBF (unpublished image from data set published in [205])

2.2.4. Reactivity - bioactive to bioinert and vice versa

The reactivity of glass and glass-ceramics in a body environment is highly composition dependent, but several other factors affect as well. Sample form, surface morphology, dosage, and implantation site all play an important role. Figure 8 shows parameters which affect glass durability, and thereby also the reactivity. Naturally, when the glass is implanted in the human body the solvent and the environmental parameters, apart from the surface area to volume ratio (SA/V), cannot be affected. Thus, the variables that can be affected, i.e. glass composition and sample parameters, should be determined by the glass engineer prior to clinical implementation.

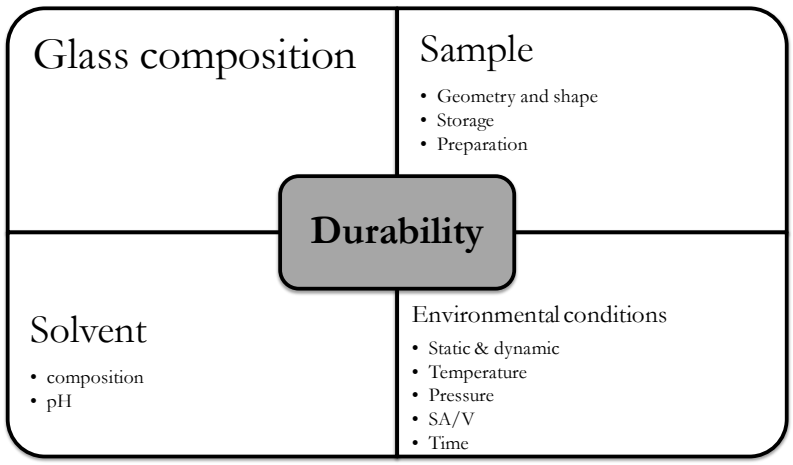

Figure 8. Various parameters affecting glass durability

As mentioned in the introduction, the first bioactive glasses were based on the Na_2O-CaO-P_2O_5-SiO_2 oxide-system [29]. The first composition, 45S5, that was shown to form a bond with bone consisted of (wt %) 24.5 Na_2O, 24.5 CaO, 6.0 P_2O_5. 45.0 SiO_2. 45S5 is still today the most bioactive glass composition available, and most of the research is concentrated around this composition. In the Na_2O-CaO-SiO_2 ternary phase diagram, the compositional dependency of bone bonding and reactivity according to Hench is shown (Figure 9) [8]. Class A bioactivity (region S in the figure) implies that the glasses bond both to bone and to soft tissue, while class B (green region) bonds only to bone [29]. The glasses in blue area are not bioactive and react only slowly. The composition of these glasses is close to traditional soda-lime glasses (SLG). However, it needs to be kept in mind that SLG are multi component glasses containing also several other oxides. The blue region might be of interest when glass is wanted to give only temporary support to bone healing, while the yellow region might be suitable to drug delivery applications.

The atomic structure of glass is directly related to composition, and therefore to the dissolution rate. Already seemingly small changes in glass composition affect bioactivity. For example, an addition of 1-1.5 wt% Al_2O_3 has been shown to significantly reduce bioactivity [34]. Often the connectivity of the silica network is related to bioactivity [208-213]. It was recently reported by Hill and Brauer [212] that

the phosphate content and the network polymerization (Q^n structure) strongly influence glass dissolution and subsequent apatite formation. The authors showed that different network models may be useful in predicting bioactivity in simple SiO_2–P_2O_5–CaO–Na_2O glasses. However, when more components are added to the glass systems, care should be taken when using network based models.

Typically, the compositional effect studies have been limited to the substitution of one or two components in a certain glass composition [57]. However, *in vitro* and *in vivo* behavior have also been reported [34, 46, 48, 130, 214] for multi-component systems with five to seven oxides in order to study the compositional dependency of the dissolution rate. The compositional effects on the reactivity of bioactive glasses have been reviewed recently by Hupa [126]. In addition, reviews on the effect of various elements to the bioactivity are also given in PhD theses by Zhang (2008) [57], Ylänen (2000) [41], and Brink (1997) [55]. Recently, the effect of the addition of elements like Ag, Cu, F, K, Mg, Sr, and Zn to the bioactivity of the glasses have been reported [31, 32, 35-38, 144, 146, 147, 215-218]. Despite extensive research efforts, the effect of composition on the properties of bioactive and biodegradable glasses is far from fully understood [126].

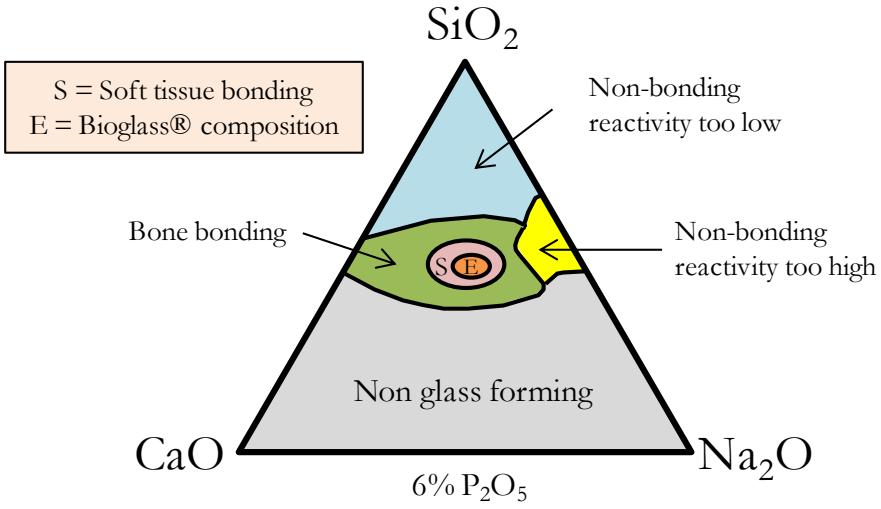

Figure 9. Compositional diagram for bone-bonding. Region S is a region where bioactive glasses bond to both bone and soft tissues and are gene activating. [8] Redrawn according to L. Hench (2006) [8].

It has been shown that glass composition alone does not determine bioactivity. Glass which in one physical form is bioactive may fail to show bioactivity in another form [219]. In a study of Alm et al. [219], the bioactive glass composition 1-98 failed to demonstrate a positive effect on osteogenesis in the form of thin fibers in a composite structure. Earlier, though, a positive effect was observed with the same glass in the form of solid discs and sintered microspheres [47, 220]. The large surface area given by the thin fibers together with the fluid flow around the fibers caused rapid resorption of the glass. Particle size has also been shown to play a role in the *in vivo* and clinical

behavior of bioactive glass [221-227]. In general, better bone formation has been observed with large granules and/or with a broad particle size range (typical size > 500 μm or size range 90-710 μm) than with smaller particles (typical ~20 or 100-300 μm). No clear difference in the bone formation has been reported for the large granules of different sizes.

The effect of glass dosage on dissolution behavior and cell cytoxicity has been reported [228, 229]. The results indicate that the rate of HA formation on bioactive glass powders *in vitro* depends on the concentration of the powders in solution [229]. In a study where submicron bioactive glass particles were used, the cell activity decreased with increasing dosage [228].

2.3. Glass dissolution measurements

When glasses are placed in aqueous solutions, changes occur both in the glass and in the solution [193]. Thus, a wide variety of analysis methods and experimental setups are needed to characterize the dissolution process. Typical analysis methods utilized to characterize glass dissolution are listed in Table 2 together with example references to bioactive glass studies where these analysis methods have been used.

Table 2. Typical analysis methods used to characterize glass dissolution

	Analysis Method	**Utilized in**
Surface	Fourier transform infrared spectroscopy (FTIR)	[35, 230, 231]
	(Solid state) Nuclear magnetic resonance spectroscopy (NMR)	[144, 147, 153, 232]
	Raman spectroscopy	[218, 232]
	Scanning electron microscopy with Energy-dispersive X-ray spectroscopy (SEM-EDX)	[43, 130, 233, 234]
	Surface area measurements	[231]
	X-Ray Diffraction (XRD)	[231]
	X-ray microtomography (μCT)	[75]
Solution	Inductively coupled plasma optical emission spectroscopy (ICP-OES)*	[84, 235]
	pH measurements	[84, 130, 144]
	Spectrophotometry (SPM)**	[130]
	Titration	[236, 237]

** Synonym: Inductively coupled plasma atomic emission spectroscopy (ICP-AES), **Nowadays usually replaced by ICP based measurements*

Unlike in a body environment, several parameters are available to be adjusted when an *in vitro* dissolution experiment is designed. The characteristics of the solvent, both initial pH and ionic composition, are the most decisive factors for the outcome of the experiment [238]. The pH effect on glass dissolution has been already well established [192, 200], but solution movement is less recognized. It affects the environment around the glass sample, and consequently also the reaction mechanisms and rates. Dissolution studies are often conducted under static conditions, which may lead to increased pH values and local saturation [239]. In this thesis, these are defined as conventional dissolution measurements. Studies where only mixing or agitation of the solution is used are also placed in the same category. Measurements where some kind

of movement of the solution occurs are called dynamic in the literature. Thus, in this thesis the term 'continuous' was chosen instead of 'dynamic' to describe all studies where the solution is continuously flowing with respect to the sample. When flow tests are used, the solution composition and the pH can be more easily controlled than in static tests [238].

Many of the traditional glass dissolution studies are performed under accelerated conditions. Such conditions can be obtained by using elevated temperatures and high glass surface area to solution volume ratios (SA/V) [238]. These types of accelerated experiments are crucial when glasses used for long-term storage of nuclear waste are studied [201, 240]. Not unexpectedly, the increase of temperature has been shown to have a significant effect on the glass dissolution rate (as a rule of thumb, glass dissolution rate is roughly doubled per every 8 to 15°C increase [137]), and it is found to follow the Arrhenian type of behavior [137, 192, 241, 242]. A high SA/V can be obtained for example by using powdered glass or thin fibers. However, the specification of the surface area of the particles may be difficult because of the crushing and sieving procedure needed to make the particles. There are always fine particles attached to the surface of the larger particles, and the particle shape and size fraction may vary considerably.

2.3.1. Conventional glass dissolution studies

Because the chemical resistance or durability of glass is not as easily defined as properties such as viscosity or thermal expansion, several standardized test methods have been developed. The need for standardized testing originates mainly from the container and float glass industry where it is necessary to evaluate how the product will withstand the intended consumption and wearing [190]. However, nowadays also the bioactive glass research community moves towards standardized test procedures to be able to compare the reactivity of various glass compositions.

One of the commonly used methods to test the durability is the ISO 719 standard, which measures the hydrolytic resistance of glass grains at 98°C [243]. The ISO 719 test is cheap, easy, and fast for industrial quality control. The scale of hydrolytic resistance ranging from one (durable) to five (non durable) is often used to compare soda-lime glasses. Other similar standards include leaching in water at 121°C (ISO 720), acid resistance test (DIN 12116), and alkali resistance test (ISO 695). These are, however, not of great interest in designing glasses for biological applications because they are designed mainly for highly durable glasses (e.g. borosilicate glasses for laboratory ware use). The ISO 719 test has also been utilized for studying the reactivity of bioactive glasses [55, 244]. However, no real correlation between bioactivity and durability has been reported. Andersson et al. reported a phenomenological model for chemical durability of bioactive glasses, suggesting that the first hour of corrosion may correlate with the biological behavior [244]. However, no real conclusions were made based on the hydrolytic resistance experiments. Most of the glasses studied by Brink

[55] exceeded the upper limit of the standard, and the pH of water after the test rose to values above 9. This implied that network dissolution was also occurring and the dissolved silica affected the result. Therefore, she suggested that the standard should be modified so as to be applicable to bioactive glasses as well. The durability results obtained by Brink [55] were, however, suggested to correlate with the *in vitro* chemiluminescence activity of human polymorphonuclear leukocytes [245]. Based on the findings of Andersson et al. [244] and Lindfors et al. [245], it seems that the ISO 719 test gives a good preliminary estimate of the reactivity of the glass. Thus, this method was also included in this thesis. In addition to the standard measurements, also the dissolved ions were measured in this work.

In vitro reactions of bioactive glasses are commonly studied in buffered inorganic solutions under static conditions to evaluate whether CaP precipitates on the sample. CaP precipitation has been used as an indication of *in vivo* bioactivity [246]. Some studies have been performed under mixing or agitating conditions [229, 247]. The studies are usually performed in TRIS [248] or SBF [206]. The bioactive glass reactions in TRIS and SBF are well reported, and studies comparing bioactive glass reactions in these solutions are also available [218, 249]. In addition, purely phosphate buffered solutions (PBS) [250] and simple pure water [188, 249] have been used to study the glass reactions. However, PBS is normally used to evaluate hydrolysis of polymer/bioactive glass composites [251-254] and to produce HA from glasses for drug delivery applications [255]. According to the SciFinder Scholar library program, a total of more than 500 scientific papers dealing with SBF and glass have been published by June 2012. The corresponding numbers for TRIS and PBS are 70 and 40, respectively.

There have been studies where the effect of TRIS-buffer on the dissolution behavior of glass has been evaluated [74, 256]. The presence of TRIS buffer has been reported to increase the glass dissolution. In thermodynamic calculations by Bastos et al. [257], the protonation and alkaline earth ion complexation with TRIS are reported. The authors state that the amount of free calcium and magnesium is reduced in a TRIS-containing solution because of the formation of complexed species. In TRIS, the amino group acts as a ligand for metal ions able to form complexed species. The formation of TRIS-complexed species could thus explain why the observed extent of dissolution was higher in TRIS than in water.

It has been shown with thermodynamic calculations that SBF is a metastable solution and supersaturated towards apatite crystals [258]. Thus, if a material is immersed for a time longer than the induction time, i.e. the time for the metastable solution to become thermodynamically stable by precipitating apatite crystals, apatite precipitation will occur [259]. However, studies can be found where the authors are convinced about the bioactivity only by analyzing HA formation of the samples which have been immersed in SBF for several weeks (e.g [260]). Normally, though, multiple

analysis methods are used to evaluate dissolution behavior and the layer formation. There also exists a standardized method for detecting the apatite formed on a surface of a material in SBF (ISO 23317:2007), but this has been criticized, and a need for a new standard has been acknowledged [7].

2.3.2. Continuous glass dissolution measurements

To better imitate the reality, different continuous testing methods have been developed. The continuous approach to glass dissolution has been mainly used in nuclear waste glass studies [261-263], but it has been also adopted in bioactive glass research [75, 264-267]. The characterizing parameter for these types of experiments is the ratio between transport and dissolution rates [190]. This ratio determines the dissolution type. Often, the same solution is circulated in the system causing changes to the original solution composition, and the sampling is performed at predetermined time intervals [75, 264, 266, 267]. In continuous measurements, the CaP precipitation process has been reported to be slower, and the flow rate has been reported to affect the layer formation [266].

By connecting a dynamic measurement method directly into a fast analysis method, such as pH or ion measurement, on-line data can be collected. This provides the possibility to estimate the reaction kinetics of glass dissolution. The idea of analyzing the outcoming solution and to gain a complete analysis of the extracted solution has been introduced already by Cross in 1959 ([268] in [194]). However, at the time, the trace element analysis techniques were not sensitive enough to allow successful analysis. Today, though, sensitive solution analysis techniques are available.

Inductively coupled plasma optical emission spectroscopy (ICP-OES) offers a sensitive method, which has been in wide use for routine elemental analysis in the laboratories since the 1980s [269]. ICP-OES is based on atom emission spectroscopy, and the functional principles and instrumental details are well described by Dean [270]. ICP is an efficient atomization source with high tolerance for high salt concentrations [269]. The ICP-OES instrument consist of a high power radio frequency generator, a pneumatic nebulizer associated with a spray chamber, a torch, a dispersive system, a detector, and a computer [269, 270]. The advantage with atom emission spectrometry, dating back to the 1800s, is that photons can easily travel and be collected with simple optics [269]. Furthermore, the photons do not have a memory effect, and they do not degrade the detectors.

ICP-OES enables qualitative and quantitative determination of metals and certain non-metals in solution. Furthermore, it is a multi-element technique with a wide analytical range. The detection limits offered by ICP-OES operated with simple sample matrices are in range of the parts per billion (ppb) in solution for many elements. Two main types of spectral interferences for ICP-OES can be categorized [270]: spectral overlap and matrix effects. The source of possible interferences needs to be carefully considered and evaluated when the experimental parameters and wavelengths for the

analysis are chosen. In addition, when modifications to the sample injection setup are made the sensitivity may decrease.

ICP-OES can also be used for sensitive on-line analysis as discussed in this thesis. This approach has also been used in automatic dynamic chemical fractionation for advanced characterization of solid biofuels [271] and to do online dialysis to estimate bioavailability of minerals in nutrients [272]. The strength of the online approach for the solid biofuel analysis was that the overall extractable pools of ash-forming elements were quantified in merely 3 h versus 7 days in normal batchwise leaching tests. Similarly, the dialysis study the nutrients were digested and fully analyzed during the first 30 min.

3. Materials and methods

The nominal oxide compositions of the glasses and the different experimental methods used in this thesis are collected in this chapter. The motivation for the choices of the glass compositions used in the dissolution part tasks was to study the chemical durability of glasses with various oxide compositions. In addition, already established compositions were chosen so that it would be possible to compare the obtained novel data to the available *in vitro* and *in vivo* literature [48, 128-131, 273, 274]. The glass compositions for the crystallization and sintering studies were chosen because of the general interest towards these glass compositions in the bioactive glass field. Furthermore, the experimental techniques for characterization of the changes in immersion solutions and glasses are summarized. The publications in which the experimental techniques are implemented are given in parenthesis after each section heading.

3.1. Nominal oxide compositions of the glasses

The nominal oxide compositions (weight %) of the glasses studied are summarized in Table 3 together with the corresponding publications. The glasses above the dashed line were prepared in-house, and the other glass compositions were of commercial quality.

The nominal, i.e. theoretical, oxide composition of 45S5 was compared with the oxide composition of the actually melted glass by using data from energy dispersive X-ray analysis (EDXA). In addition, a standard glass (from HVG-DGG), a commercial composition with strict quality requirements and specifications [275], was analyzed. Both glasses were analyzed as plates and particulates. Furthermore, 45S5 was also analyzed as cones (as used in [48]). The results from the comparison are given in Table 4. The relative standard deviation gives the difference between the analyzed points, and the Δ-value gives the difference between the nominal and measured oxide content. The results are intentionally given with extra digits to better emphasize the variations.

Systematically higher Na_2O and lower SiO_2 contents were found for the analysis results. A larger deviation from the nominal composition for Na_2O and SiO_2 was observed when the sample was analyzed as particulates, as is clearly seen with the standard glass where the exactly same glass batch is analyzed in two sample forms. The deviation from the nominal composition is partly dependent on the fact that the oxide values are calculated, while a somewhat better agreement with the nominal values is obtained using the atom-% basis (Table 5). To gain a more accurate total compositional analysis, wet-chemical methods should be utilized. However, the results show that our melting procedure does not give any significant alkali losses due to volatilization because the Δ-values for standard glass and 45S5 are very similar.

Table 3. Nominal oxide compositions (wt%) of the glasses

Glass code	Na_2O	K_2O	MgO	CaO	B_2O_3	P_2O_5	SiO_2	Reference
45S5	24.5			24.5		6.0	45.0	I , III, IV
S53P4	23.0			20.0		4.0	53.0	I , IV, VI
1-98	6.0	11.0	5.0	22.0	1.0	2.0	53.0	I, II, IV, V
13-93	6.0	12.0	5.0	20.0		4.0	53.0	I, IV,V
0106	5.9	12.0	5.3	22.6	0.2	4.0	50.0	IV
0206	12.1	14.0		19.8	1.6	2.5	50.0	IV
0306	24.6			21.6	1.3	2.5	50.0	IV
0906	5.0	9.0	6.0	23.2		0.8	56.0	IV
1106	5.0	15.0		20.6		1.1	58.3	IV
1306	22.1		1.9	15.0	1.2	0.5	59.3	IV
1406	5.5	11.2	3.4	16.3	2.0	0.7	60.9	IV
1606	5.0	10.2		15.0	2.0	4.0	63.8	IV
1806	18.4		0.1	15.0	1.5		65.0	IV
Tableware*, **	14	7		3	NA		64	III
E-glass*	0.1	0.7	0.7	23.5	6.4		53.9	III, IV
Standard glass (DGG-1)*	15.0	0.3	4.2	6.7			71.7	III, IV
Float*	15.2		3.6	4.6			72.6	III, IV

** Contains also Al_2O_3: E-glass 14.1, Standard glass 1.2, Float 1.7, Tableware 1*
*** According to EDX analysis, contains additionally BaO 8.2 and ZnO 3.3, NA not possible to analyze with EDX*

Table 4. Average oxide compositions for 45S5 and Standard glass analyzed in different sample forms using EDX

Sample		Na_2O	K_2O	MgO	CaO	P_2O_5	SiO_2	Al_2O_3
45S5 plate (N = 9)	EDX (wt%)	25.65	0	0	25.05	5.90	43.27	0.11
	RSD (%)	3	-	-	4	2	1	78
	Δ (wt% points)	-1.15	0	0	-0.55	-0.10	1.73	-0.11
45S5 particles (N = 6)	EDX (wt%)	26.09	0	0	25.36	5.77	42.10	0.19
	RSD (%)	14	-	-	15	2	3	23
	Δ (wt%)	-1.59	0	0	0.86	0.23	2.91	-0.19
45S5 cones (N = 16)	EDX (wt%)	26.52	0	0	24.23	6.05	43.10	0.09
	RSD (%)	1	-	-	1	2	1	107
	Δ (wt% points)	-2.02	0	0	0.27	-0.05	1.90	-0.09
Standard glass plate	EDX (wt%)	16.40	0.62	3.09	7.37	0	70.77	0.97
(N = 3)	Δ (wt% points)	-1.40	-0.32	1.1	-0.67	0	0.93	0.23
Standard glass particles	EDX	18.12	0.32	3.53	6.53	0	70.47	1.02
(N = 6)	RSD (%)	4	15	5	2	0	1	9
	Δ (wt% points)	-3.12	-0.04	0.67	0.17	0	1.24	0.18

RSD calculated with all the samples, Δ (wt%) = Nominal – EDX

Table 5. Difference between nominal atom weight-% and analyzed atom weight-% for the same plate samples as in table above

Sample		Na	K	Mg	Ca	P	Si	Al
45S5 plate (N = 9)	Δ (wt% points)	-0.86	0	0	-0.40	0.04	0.81	0.06
Standard glass plate (N = 3)	Δ (wt% points)	-1.08	-0.08	0.66	-0.46	0	0.45	0.12

⊿ (wt%) = Nominal – EDX

3.1.1. Sample preparation

All the glass batches were prepared using the same protocol. The batches consisted of Belgian quartz sand (glass quality) together with analytical grade reagents listed in Table 6. They were melted in an uncovered platinum crucible for 3 h at 1360°C, cast, annealed, crushed, and remelted to ensure homogeneity. For glasses 1406, 1606, and 1806 higher final melting temperature (≥ 1400°C) was needed to adjust the viscosity suitable for casting.

Table 6. Chemicals, CAS numbers and producers

Chemical	CAS	Producer
Na_2CO_3	497-19-8	Sigma-Aldrich
K_2CO_3	584-08-7	Sigma-Aldrich
MgO	1309-48-4	Fluka
$CaCO_3$	471-34-1	Sigma-Aldrich
H_3BO_3	10043-35-3	Merck
$CaHPO_4{\cdot}2H_2O$	7789-77-7	Sigma-Aldrich
SiO_2 (Quartz sand)		origin Belgium

In all publications, glass particles were used. Annealed glass blocks were crushed and sieved to give a desired size range fraction. No additional annealing of the glass particles was performed after crushing. To minimize fine-grained powder on their surfaces, the particles were rinsed with acetone in an ultrasound bath at least five times, or until the rinse solution was clear. After rinsing, acetone was evaporated, and the particles were dried at 120°C. An example of the glass particles (300-500 μm) before and after acetone rinsing is given in Figure 10.

In publication I, the glass particles and glass fibers were studied. The 1–98 fibers were downdrawn semiautomatically from melt using laboratory scale fiber equipment with the same parameters as Arstila et al. [276]. The 13–93 fibers were kindly provided by Vivoxid Ltd. In publication V, monolithic samples, cut from the annealed glass blocks with a low-speed saw to dimensions 20 mm x 10 mm x 5 mm, were utilized to study the crystallization behavior of 1–98 and 13–93.

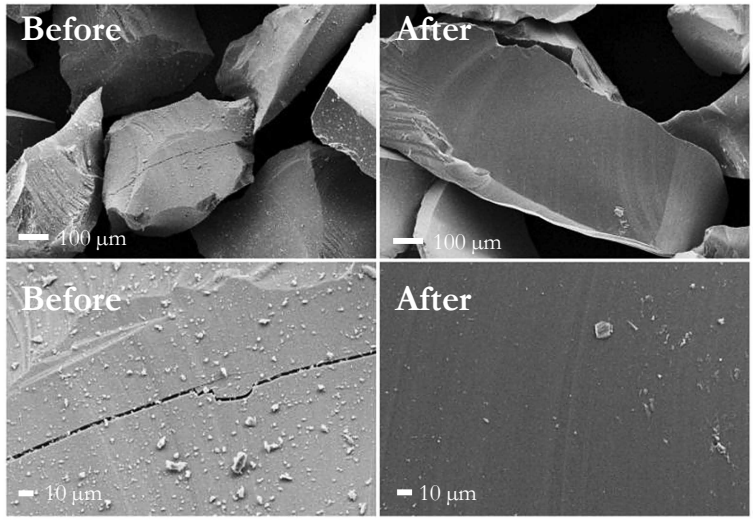

Figure 10. Glass particles (300-500 µm) before and after rinsing procedure with acetone

3.2. Experimental techniques

3.2.1. Inductively coupled plasma-optical emission spectrometry, ICP-OES (publications I-IV and VI)

The ion concentrations in the solutions were measured using an inductively coupled plasma-atomic emission spectrometer, ICP-OES (Optima 5300 DV, Perkin Elmer). The instrumental conditions for Optima 5300 DV are summarized in Table 7. In addition, the detected wavelengths, limits of detection (LOD) according to the used software (WinLab32, Perkin Elmer), and estimated limits of quantification (LOQ) for the normal and the continuous measurements are shown in Table 8.

Additionally, another ICP-OES instrument was utilized for ion concentration measurements in publications I and III (Thermo Jarrell Ash AtomScan™ 25, software ThermoSPEC 6.20). The elements and corresponding emission lines were the same as when using Optima 5300 DV.

Table 7. ICP-OES Optima 5300 DV instrumental conditions

Parameter	Setting	Parameter	Setting
RF power	1300 W	Read delay**	60 s
Nebulizer flow	0.8 l/min	Back-ground correction	2 points
Auxiliary flow	0.2 l/min	Auto integration	1 s min – 5 s max
Sample pump flow	1.5 ml/min	Rinse**	30 s
Plasma viewing*	axial	Replicates**	3
Viewing distance	15 cm (axial and radial)	Spray Chamber	Scott-type
Processing mode	peak area, 3 points	Nebulizer	cross-flow

** Na and K additionally analyzed using radial viewing during non-continuous mode*

*** Continuous mode read delay 2 s, rinse never, 1replicate*

Table 8. Detected wavelengths, limit of detection (LOD) given by WinLab 32 software (Perkin Elmer), and the estimated limit of quantification (LOQ) values for conventional (publications I,III,VI) and continuous measurements (publications II and IV)

Element	Wavelength (nm)	Ionization state I = neutral atom II= + 1 ion	LOD (mg/l)	~ LOQ (mg/l)	~ LOQ_{cont} (mg/l)
Si	251.611	I	0.0120	0.1	0.3
Na	589.592	I	0.0690	0.5	1
K	766.49	I	NA	0.3	0.3
Ca	317.933	II	0.0100	0.1	0.2
Mg*	285.213, 279.077	II	0.0016	0.02	0.05
P**	213.617	I	0.0760	0.1	0.3

** Thermo Jarrell Ash 279.553 nm*

*** Possible interference: Cu II 213.597 (relative sensitivity: Cu II 35000, P 5400)*

3.2.2. Scanning electron microscopy, SEM (publications I, III, V, and VI)

The overall appearances and oxide compositions of the glass samples were studied by SEM-EDXA (Scanning Electron Microscope with Energy Dispersive X-ray Analysis, SEM, LEO 1530 from Zeiss, EDXA Ultra Dry by Thermo Scientific). All the samples were sputtered with carbon prior to the analysis. Furthermore, formation and thickness of different reaction layers was followed with SEM-EDXA from the cross-section of the samples. To establish the cross-section, the samples were embedded into epoxy, cut, and polished. The NSS 3.0.116 (Thermo Electron Corporation) software was utilized in the data analysis.

3.2.3. X-Ray powder diffraction, XRD (publications V and VI)

The phase composition of heat-treated samples was analyzed using X-ray diffraction (X'pert by Philips, Cu α radiation, 40 kV, 30 mA). The measuring range was 5–60° 2θ and the scan speed was 0.8° 2θ /min. The phase identification was done using the Philip X'Pert HighScore program equipped with Powder Diffraction File database Data Sets 1-49 plus 70-86 (ICDD 1999).

3.2.4. Differential thermal analysis, DTA (publications IV and V)

In publication IV, the glass transition temperature T_g was determined by Differential Thermal Analysis (Mettler Toledo TGA/SDTA851^e). The experimental parameters were the same as used by Arstila [129]. The measurements were performed on 15 mg samples with the particle size < 45 μm in platinum pans in an N_2 atmosphere with a heating rate of 20°C/min. The T_g was taken from the onset of the endothermic peak as in [129].

In publication V, the glass transition temperature T_g and the crystallization temperature T_p were determined by the same instrument as above at various heating rates (10, 15, 20, and 30°C/min). The measurements were performed on 50 mg samples with the particle size range 300–500 μm (Pt pans, N_2 atmosphere). In this

study, the T_g was taken at the inflection point of the endotherm, obtained by taking the first derivative of the DTA curve and the T_p was taken at the maximum of the exothermic peak. The equations and procedures for the calculation the activation energy associated with the crystallization temperature, Johnson-Mehl-Avrami (JMA) exponent, and the nucleation-like curves are presented in detail in publication V.

3.2.5. Hot stage microscopy, HSM (publication VI)

The sintering behavior of S53P4 (size fraction < 45 μm) was studied using hot stage microscopy (HSM, Misura 3.0, Expert System). The heating rate was 40°C/min to 480°C and then 5°C/min to 1200°C. A cylindrical sample (height 3 mm, diameter 2 mm) pressed from the powdered glass was imaged after every 5°C increase in temperature. Based on these images, a sintering curve was plotted showing the height of the sample as a function of temperature.

3.2.6. Micro-computed tomography, μCT (publication VI)

The porosity of cylindrical implants sintered in publication VI was measured using micro-computed tomography, μCT (Skyscan 1072 micro-CT, Skyscan n.n.). The implants were cut into four sectors so that they would fit in the sample holder. Each sample was imaged with a step angle of 0.45° over a full range of 180°. The source voltage was 61 kV, the source current was 163 μA, and no filter was used. During image acquisition, a single 16 bit grayscale shadow projection image was obtained for each step angle without frame averaging.

3.2.7. Standard crushing device (publication VI)

The compression strength σ of sintered structures was measured with a standard crushing device (L&W Crush Tester, Lorentzen & Wettre). The rate of compression was 10 mm/min. The exact size of each implant was measured to calculate the compression strength per mm^2.

3.3. Conventional dissolution studies (publications I-IV, V)

The glass dissolution in static, i.e. no flow, conditions was studied using two different methods. The first method was the conventional chemical durability test, ISO 719, designed for assessing chemical durability of commercial, rather durable, glasses. In the second method the glasses were immersed in buffered solutions at ambient temperatures, which is suitable for bioactive glass studies. Both of these methods are briefly described below.

In addition to the concentrations values, normalized mass loss values were used in this work calculated according to equation 6:

$$NL_i = \frac{c_i}{f_i(SA/V)}, \qquad (6),$$

where c_i is the concentration of the cation i in solution and f_i is its mass fraction in the original glass, SA is the calculated surface area, and V volume of the solution [238, 242]. The surface area was calculated assuming spherical particles with an average diameter of 400 μm and a density of 2.4 g cm^{-3}. The specific surface area for the 300-500 μm size range particles was calculated to be 62 $cm^2\,g^{-1}$. The normalized mass loss values facilitate the comparison of the dissolution of the different elements from one glass to another, and also to some extent to compare experiments made in different conditions.

3.3.1. ISO 719 (Publications II and III)

The hydrolytic resistance according to ISO 719 is measured by the volume of HCl required for titration of the alkali extracted from 2 g of glass particles (300-500 μm). The particles were kept for 60 min in 50 ml de-ionized water at 98°C, and thereafter, 25 ml aliquot of the obtained solution was titrated against 0.01 M HCl solution using methyl red as an indicator solution [243]. In addition to the standard, the pH of the solution was measured at room temperature (Mettler Toledo) before titration and an aliquot (10 ml) was saved for ion concentration analysis with ICP-OES. Hydrolytic resistance classification (HGB) is based on the acid consumption in the titration and given on a relative scale 1–5 (Table 9). The lower the HGB class is the better is the hydrolytic resistance of the glass. The sodium oxide equivalent is obtained from the following relationship: 1 ml of HCl with concentration 0.01 mol/l corresponds to 310 μg of sodium oxide.

To evaluate the temperature effect on the hydrolytic resistance, the same test procedure was repeated at 40, 60, and 80°C. The hydrochloric acid consumption values at different temperatures were fitted into the Arrhenius equation and the same equation was also used to determine the activation energy values for the initial dissolution rate for different elements NR_{i0} (Equation 7):

$$\mathrm{NR_{i0}} = Ke^{-\frac{E_{a,i}}{RT}} \qquad (7),$$

where: NR_{i0} = initial dissolution rate for element i, K = constant, $E_{a,i}$ = apparent activation energy for element i in J/mol , R = gas constant 8.314 J/(mol·K), T = absolute temperature in K [242]. NL_i calculated with equation 6 was converted to initial normalized rate (NR_{i0}) by dividing with the duration of the experiment, one hour.

Table 9. Hydrolytic resistance classes according to ISO 719 [243]

V(HCl), [ml]	HGB	V(HCl), [ml]	HGB
≤ 0.10	1	0.85–2.0	4
0.10–0.20	2	2.0–3.5	5
0.20–0.85	3	>3.5	>5

3.3.2. In vitro test (publications I, III, and VI)

The *in vitro* behavior of the glasses was studied using different immersion solutions which are summarized in Table 10. The source chemicals used in solution preparation together with their CAS numbers and producers are given in Table 11.

Table 10. Inorganic ion concentrations of the human blood plasma and of the immersion solutions used in this thesis (mmol/l). In addition, the concentration of organic buffering agent (TRIS) is given.

	c [mmol/l]			
Ion	**Blood plasma [206]**	**SBF [246]**	**Na-PBS**	**Tris**
Na^+	142	142	156.2	
K^+	5	5		
Mg^{2+}	1.5	1.5		
Ca^{2+}	2.5	2.5		
Cl^-	103	147.8	100.9	45
HCO_3^-	27	4.2		
HPO_4^{2-}	1	1	24.9	
SO_4^{2-}	0.5	0.5		
$H_2PO_4^-$			5.5	
Tris		50		50
Used in publication		**I, VI**	**I**	**I, II, III, IV**

Table 11. Chemicals (p.a. grade), CAS numbers and producers

Chemical	**CAS**	**Producer**
$C_4H_{11}NO_3$ (Trizma Base)	83147-39-1	Sigma-Aldrich
$CaCl_2 \cdot 2H_2O$	10035-04-8	Merck
HCl (Titrisol 1M)	7647-01-0	Merck
$K_2HPO_4 \cdot 3H_2O$	16788-57-1	Merck
KCl	7447-40-7	Merck
$MgCl_2 \cdot 6H_2O$	7791-18-6	Merck
Na_2HPO_4	7632-05-5	Merck
Na_2SO_4	7757-82-6	Merck
NaCl	7647-14-5	Merck
NaH_2PO_4	7558-80-7	Merck
$NaHCO_3$	144-55-8	J.T. Baker

The experimental parameters for the *in vitro* test used are summarized in Table 12. The common features of the procedure used in all the conventional *in vitro* experiments are listed below:

- The glass samples were carefully weighed in polypropylene beakers and the pre-heated immersion solution (37°C) was added on the glass sample
- Beakers were kept in a thermostat at 37°C
- pH of the solutions was measured periodically during the immersion (Mettler Toledo)
- After immersion, the solution and the sample were separated
- The samples were rinsed with ultra-pure water (Millipore) to remove residual salts, with ethanol/acetone to terminate the reactions
- The final pH of each immersion solution was recorded after the separation
- The immersion solutions were analyzed with ICP-OES
- The solid samples were analyzed with SEM-EDXA

Table 12. The parameters used in the conventional in vitro tests

Sample	m_{glass} (mg)	V_{sol} (ml)	immersion time (h)	Static/ shaker	Repeated samples	Reference
Particles (500–800μm)	$1.5 \cdot 10^3$	15	1–336	static	3–6	I
Fibers (Ø 20–140μm, length 2-3 cm)	15	16	1-336	static	3–6	I
Particles (315–500μm)	200	25	4 and 24	static	3–6	III
Sintered porous implants (from particles 500–800μm)	600	25	24 and 48	shaker	3–6	VI

3.4. Continuous ion dissolution studies (publications II–IV)

The early-stage chemical durability of the glasses was measured with a novel *in vitro* experimental setup developed in this work. In the setup, a flow-trough cell was connected directly to ICP-OES (Optima 5300 DV, Perkin Elmer). The ions dissolved from the glasses were recorded continuously. The duration of the experiments applying the continuous mode varied from 15 to 60 minutes.

The schematic flow sheet of the system and the sample cell are shown in Figure 11. The cylindrical sample cell was filled with irregular glass particles, and a random packing of the particles was assumed. The solvent was fed with a peristaltic pump through a bed of glass particles so that it travelled upwards vertically through the bed. The flow rates were gravimetrically determined and were shown to be in the laminar region (Re' <1 in all cases in Table 14). The ion concentrations were measured on-line every 12 seconds (one replicate per measurement). Furthermore, the pH values of the dissolution medium were recorded every 10 seconds with an otherwise similar setup except that the ICP-OES was replaced by a flow-through micro volume pH electrode (Konelab, Thermo Scientific).

The calibration was performed with ultra-pure water (Elga), and multi-element standards (diluted from Ultra Scientific RI) with concentrations of 1 ppm (K 10 ppm; Si 0.5 ppm) and 10 ppm (K 100 ppm; Si 5 ppm). It was always performed with the same flow parameters as those used in the sample concentration measurements. The stability of the calibration was controlled by measuring a standard solution sample between runs. The background level was recorded before each sample run, and all reported ion concentrations were background corrected.

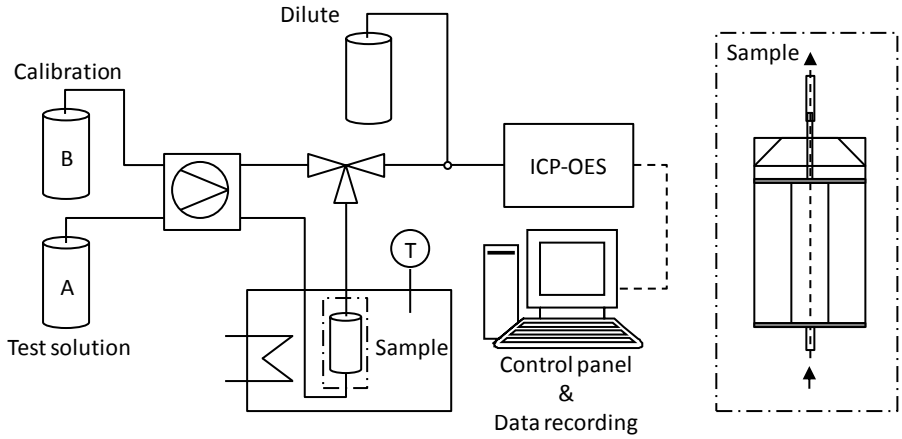

Figure 11. Schematic flow sheet of the continuous ion measurement system and the sample cell (II,III, and IV)

The calibration of the pH meter was performed using the same experimental parameters as those for the ion concentration measurements, with two pH standards (pH 7 and 9). The stability of the pH standards was checked regularly with a static conventional pH meter (Mettler Toledo).

The experimental parameters for the continuous measurements are collected in Table 13, where F is the flow rate and T the temperature. In one series 3 different sample size dimensions were tested (short, long, medium). Otherwise, a sample cell with the dimensions length 10 mm and diameter 5 mm was used (noted normal in the table) in the measurements. The sample mass normally used was 280 ± 5 mg with few exceptions (cf. Publication II).

Table 13. Parameters used in the different experimental series using continuous in vitro test

Experiment series	F (ml/min)	Solvent	T (°C)	Sample cell	Reference
1	0.2	H_2O	40	s, m, l*	II
2	0.08–0.8**	H_2O	40	normal	II
3	0.2	H_2O	40, 60, 70, and 80	normal	II
4	0.2	H_2O	40 and 80	normal	III
5	0.2	TRIS	40	normal	II, IV

** Short (dimensions), medium (dimensions), long (dimensions) **Listed separately in Table 14*

Table 14 shows the superficial mass velocity based on the empty chamber cross section (G) and the modified Reynolds number for backed beds (Re'). The Re' was calculated using the Equation 8:

$$Re' = D_p G/\mu \quad (8)$$

where D_p is average particle diameter (m), defined as sphere, G fluid superficial mass velocity based on the empty chamber cross section (m/s), and μ fluid viscosity (m^2/s) [277]. The fluid dynamic viscosity of water at 40°C is $6.59 \cdot 10^{-7}$ m^2/s.

Table 14. Flow rate (F), fluid superficial mass velocity (G), and the modified Reynolds number (Re') calculated according to Equation 1 (II)

F (ml/min)	G (cm/min)	Re'
0.08	0.4	0.04
0.12	0.6	0.06
0.2	1.0	0.10
0.4	2.0	0.21
0.8	4.1	0.41

As in the case of conventional dissolution studies, the concentrations were converted into the normalized mass loss rates similarly to equation 6. Only, the volume of the solution (V) is changed to flow rate of solution in m^3/s (*F*).

3.5. Crystallization and sintering (publications V and VI)

Crystallization and sintering behavior were studied using 1-98, 13-93, and S53P4 to gain more information regarding the suitability of these compositions for hot working.

A preheated electric furnace was used both in crystallization (publication V) and sintering (publication VI) studies. Monolithic samples (20x10x5 mm^3, publication V) of glasses 1-98 and 13-93 were heat treated in a graphite mould isothermally in the 600°–1000°C temperature range for 10 min to 8 h. Porous implants were produced for publication VI by sintering irregular particles (500 to 800μm) of glass S53P4 at the same temperature interval for 1 h. The particles were put into cylindrical holes of different sizes in two graphite molds: i) Ø10 mm, height 5 mm; and ii) Ø 5 mm, height 5 mm.

All the samples were pushed into a preheated furnace with a nitrogen atmosphere. Recording of the time began when the temperature reached 95% of the target value; usually, this took around 15 min. The target temperature was maintained for the desired time, and then the samples were cooled rapidly in nitrogen flow to room temperature. The samples were stored in a desiccator prior to the analysis.

4. Results and discussion

4.1. Conventional dissolution studies

Below, the key results obtained using the traditional static *in vitro* testing (publication I) and the hydrolytic resistance values measured with ISO 719 (mainly publications II and III) are discussed.

4.1.1. Glass reactions in different immersion solutions

When a buffer solution is chosen for *in vitro* experiments, the objective and the nature of the tested materials need to be considered closely. Therefore, in publication I, glass reactions in three immersion solutions TRIS, SBF, and Na-PBS were studied and compared. The main driving force behind this study lies with the findings of a previous research project (Biowaffle, Tekes Finland) that was done in cooperation with TUT. During this project, bioactive glass fibers (1-98) embedded in a polymer matrix (P(L/D)LA and P(L/DL)LA) were found to dissolve completely and interestingly produce hollow HA tubes (Figure 12) [278]. Similar hollow structures in PBS have been reported earlier and are discussed by Rahaman et al. [40] in a review article.

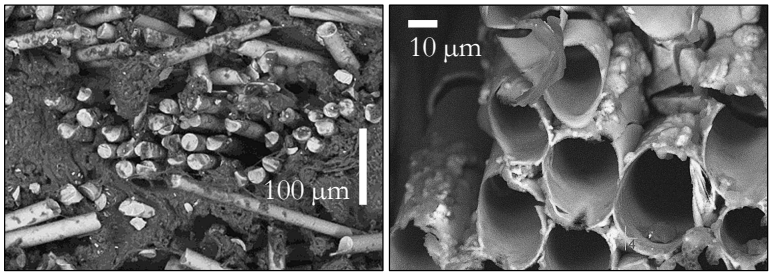

Figure 12. Bioactive glass polymer composite prior to immersion (right) and after two weeks of immersion in 50 ml Na-PBS [278] (Samples for SEM analysis were kindly provided by Mikko Tukiainen, TUT)

The buffering systems available in the three immersion solutions together with pKa values are given in Table 15. In addition, logarithmic diagrams for the acid base equilibriums as a function of pH for the different systems at 25 °C, calculated using principles demonstrated by Hägg [279] and Sillén [280], are given in Figure 13-Figure 15. The preparation of SBF (composition is given in Table 10) is the most complicated of these three solutions and includes a high risk of precipitation during the preparation stage and storage. As can be observed from the table and Figure 15, in SBF different buffering systems are present whereas the two other solutions have only one system. The carbonate system, because of the atmospheric carbon dioxide, is excluded here from TRIS and Na-PBS. Na-PBS can be easily prepared by dissolving sodium chloride, monosodium phosphate, and its conjugate base disodium phosphate into ultra-pure water to generate pH values around 7 (pKa_2=7.2). The effective buffering range of PBS is between 6.2 and 8.2. The pH of the solution is not sensitive to temperature changes in contrary to TRIS-buffered solutions. In comparison, the effective buffering range of TRIS (pKa=7.8 at 37°C) is between 6.8 and 8.8, which is the dominant

buffering system both in SBF and TRIS. It has been shown by titration that the buffering capacity of TRIS and SBF are similar [57]. This was verified by calculating theoretical titration curves with all the three solutions with CurTiPot software (version 3.6.1 for MS-Excel 2007-2010) using 0.1 M strong base as a titrator. The buffering capacity of the initial solutions was also evaluated with the same program. The buffer capacity for an aqueous solution defines how much acid or base must be added to the solution to influence the pH. The buffer capacity can be calculated using eq. 9:

$$B = \frac{dC_b}{d(pH)} = -\frac{dC_a}{d(pH)} \quad (9)$$

,where C_b gives the concentration of the added base and C_a the concentration of the added acid [281]. The buffer capacity is an additive property and all the active components contribute to the buffer capacity [281]. The titration curves together with the calculated buffer capacity of the initial solutions are shown in Figure 16.

Table 15. Available buffering systems in the immersion solutions together with the acid dissociation constants , pKa (values from [282, 283])

Buffering system	**pKa (25°C)**	**Solution**
$(HOCH_2)_3CN^+H_3$ (aq) ⇌ H^+(aq) + $(HOCH_2)_3CNH_2$ (aq)	8.06 #	SBF, TRIS
H_3PO_4 (aq) ⇌ H^+(aq) + $H_2PO_4^-$(aq) $H_2PO_4^-$(aq) ⇌ H^+(aq) + HPO_4^{2-}(aq) HPO_4^{2-}(aq) ⇌ H^+(aq)+ PO_4^{3-}(aq)	2.16 7.21 (pKa_2) 12.37 (pKa_3)	SBF, Na-PBS
H_2CO_3*(aq) ⇌ H^+(aq) + HCO_3^-(aq) HCO_3^- (aq) ⇌ H^+ (aq) + CO_3^{2-} (aq)	6.37 10.32 (pKa_2)	SBF

Δ *Ka/°C = -0.027, H_2CO_3* is used here to represent both dissolved CO_2 and H_2CO_3*

The high initial phosphate concentration of Na-PBS gives a fast precipitation when calcium species are added to the solution and is likely to increase the dissolution rate of bioactive glasses. This questions the suitability of studying bioactivity in Na-PBS. In this study, *in vitro* reactions of four bioactive glasses were followed. Glasses 45S5 and S53P4 were tested as granulates (500-800 μm), whereas glasses 13-93 and 1-98 were tested as fibers (d_{fiber} 20-140 μm).

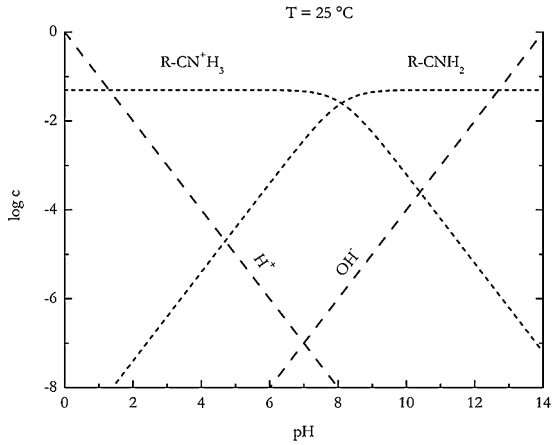

Figure 13. Logarithmic diagram for the acid base equilibrium as a function of pH for TRIS-buffer system at 25°C, calculated using principles demonstrated by Hägg [279] and Sillén [280] and using 50 mM as the total concentration [R-CN+H3]+[R-CNH2].

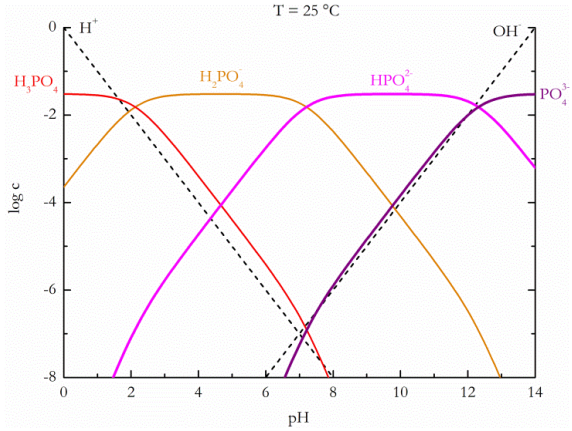

Figure 14. Logarithmic diagram for the acid base equilibrium as a function of pH for H3PO4 system at 25°C, calculated using principles demonstrated by Hägg [279] and Sillén [280] and using 30.4 mM as the total concentration of [H3PO4]+ [H2PO4-]+[HPO42-]+[PO43-].

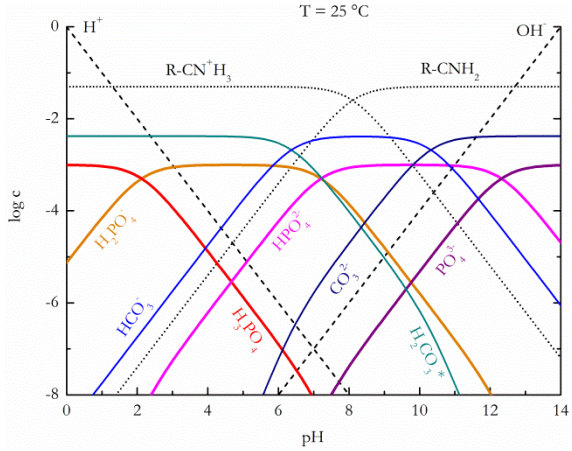

Figure 15. Logarithmic diagram for the acid base equilibriums as a function of pH for TRIS, H3PO4, and H2CO3* system at 25°C, calculated using principles demonstrated by Hägg [279] and Sillén [280] (the total concentrations: [R-CN+H3]+[R-CNH2] = 50 mM, [H3PO4]+ [H2PO4-]+[HPO42-]+[PO43-] = 1 mM, and [H2CO3*]+ [HCO3-]+[CO32-] = 4.2 mM).

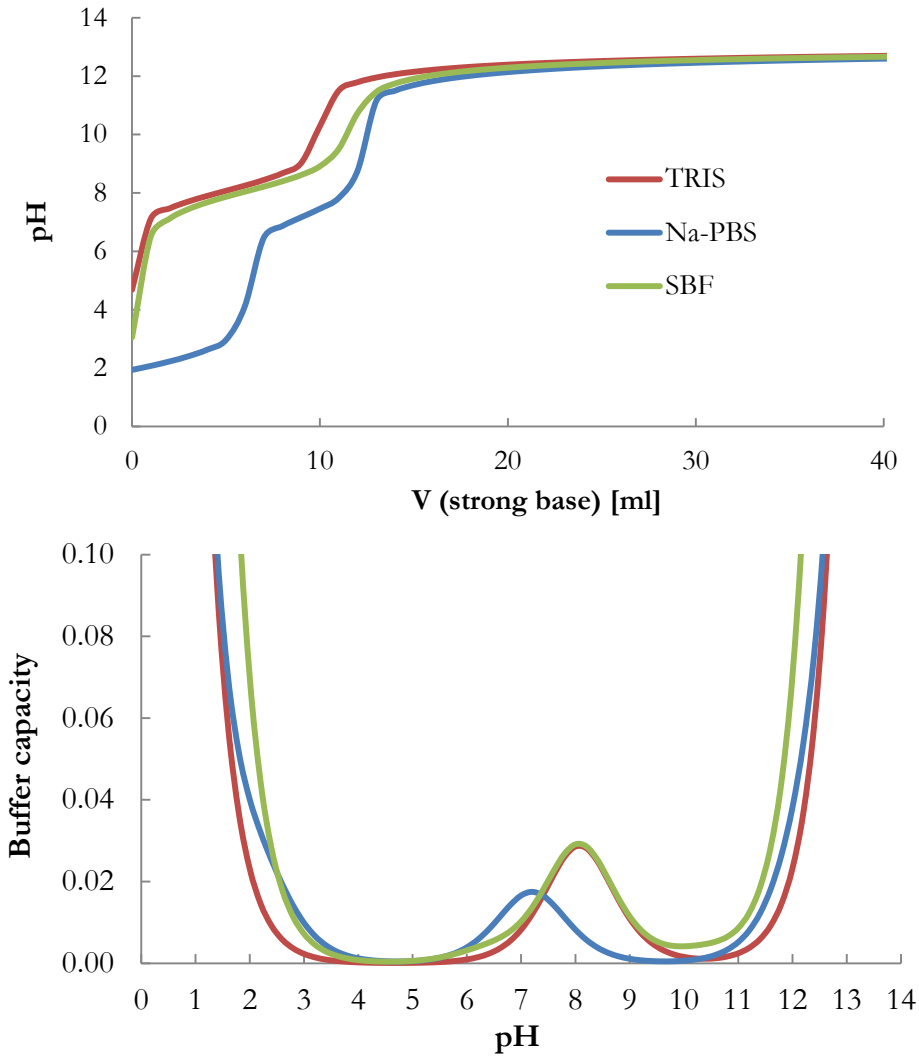

Figure 16. Theoretical titration curves for the three solutions used in publication I calculated with 0.1 M strong base as a titrator and the buffer capacity of the solutions using CurTiPot software

Figure 17 shows the pH increase of the three immersion solutions for the four glasses. 45S5 and S53P4 undergo a rapid ion-exchange reaction, and already after four hours of immersion the effective buffering range of Na-PBS has been passed. After this point, pH continues to increase to similar levels as with the unbuffered solution, water (data given in publication I). The pH increase stabilizes to values near the pKa_3 for H_3PO_4. The overall increase of pH was lower with the fiber samples as with granulates; this was also expected because of two reasons: the different SA/V relationship, and the different reported reactivity of the glass compositions [130]. Both fiber compositions follow the same trends, even though the actual values of 1-98 and 13-93 cannot be directly compared because of the 13-93 fibers were coated. It could be concluded from the pH results both with granulates and fibers that SBF could maintain pH close to the original for a much longer time than Na-PBS.

The high pH in Na-PBS gave partly increased glass dissolution, but also faster CaP formation as was verified with both ion concentration and SEM measurements. However, under these experimental conditions no hollow structures were obtained with any glasses. Figure 18 shows the oxide composition of 13-93 fiber surfaces at different time points. Clear differences in the different solutions in the layer formation can be observed. The time scale of layer formation differed, and the composition of the formed layers showed differences.

This study verified that the choice of immersion solution and conditions at the immersion are highly important. In TRIS and SBF, the initial ion dissolution was found to be similar. For 45S5 and S53P4, a three layered structure, consisting of silica rich, mixed (Si+CaP), and CaP layers, was observed in both solutions. However, differences in the layer formation in these two solutions were observed with 1-98 and 13-93. In TRIS, no or only sporadic CaP layer formation was noticed. This was probably because of the low amount of phosphorus present in the original glass compositions. In SBF the three layered structure was observed. Depending on experimental conditions, Na-PBS led to faster glass dissolution or CaP layer formation due to the initial high phosphorus content in the solution and the lower buffer capacity than TRIS and SBF. Hence Na-PBS testing can give misleading information on the bioactivity of the glass.

The trends observed in the reactivity of the glasses in the different solutions can be used when comparing experimental results in one of the solutions with reported observations of the same glass in the other solutions. However, care should be taken when such comparisons are made because also other experimental parameters affect the *in vitro* test outcome.

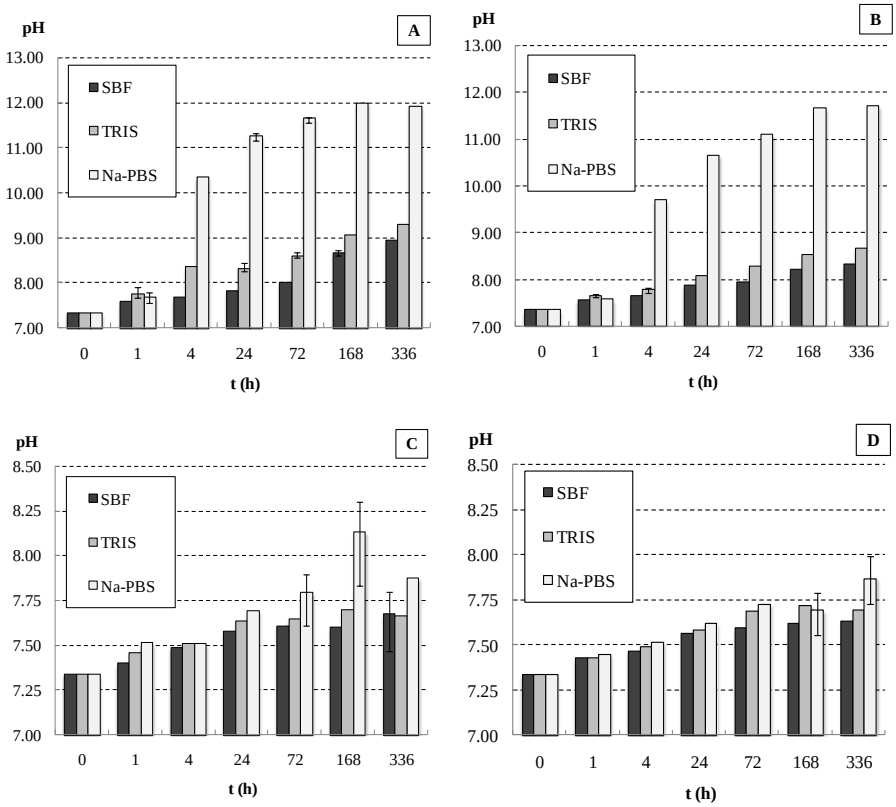

Figure 17. pH change in SBF, TRIS, and Na-PBS, ΔpH <0.05 pH unit if error bars not presented (A: 45S5, B: S53P4, C: 1-98, D: 13-93) [publication I]

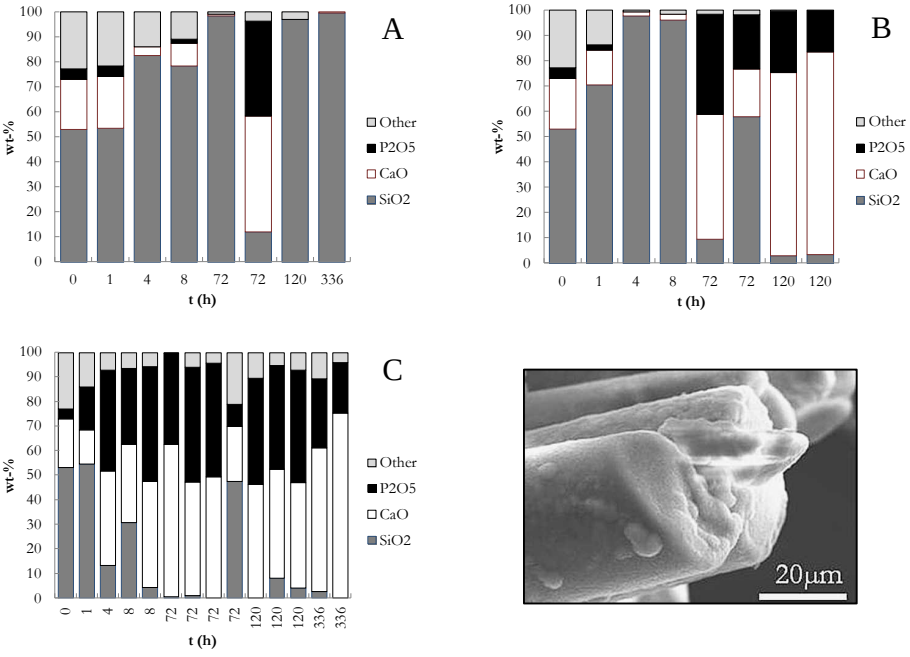

Figure 18. EDXA of the oxide composition on the 13-93 fiber surfaces. (A: TRIS, B: SBF, and C: Na-PBS). The SEM-image (1.5kx) shows the surface after 120 h in Na-PBS. [publication I]

4.1.2. Hydrolytic resistance

One of the objectives of this thesis was to test the suitability of different methods for obtaining fundamental information on glass dissolution at different experimental conditions. As discussed in chapter 2.3.1, hydrolytic resistance correlates with the reactivity of glasses, and eventually also with their bioactivity. Thus, hydrolytic resistance was also considered. Bioactive glasses have earlier been found to dissolve readily, potentially exceeding the relative scale given in the standard [55, 284]. Nevertheless, hydrolytic resistance might give relevant data when testing slowly dissolving glasses for biomedical applications which are closer to typical SLG than bioactive glasses.

The ISO 719 standard method does not take into account the pH of the solution before the titration. However, pH has been shown to increase to values above 9 with several tested glass compositions [55, 284]. This implies that the acid consumption does not depend only on the alkali extraction but is also affected by dissolution of the glass network, typically taking place for silicate glasses above pH 9 [200]. Thus, pH measurements together with ion concentration measurements were added to the standard procedure. The hydrolytic resistance results are mainly discussed in publication III, but also in publication II. The hydrolytic resistance of the glasses used in publication IV has only been discussed previously in an oral presentation given by the author (2012) [285], but the data is also included here to allow correlations to be made with the results presented in publication IV.

Table 16 summarizes the hydrolytic resistance values of all the glasses. The hydrolytic resistance is given as the consumption of hydrochloric acid according to ISO 719 together with the pH values of non-titrated solutions measured at room temperature. In addition, hydrolytic resistance values measured at different temperatures, but otherwise following the standard, are also given.

E-glass showed a medium resistance, glass 45S5 a very low resistance, while the other glasses had values in between. Similar results for float glass can be found in the literature [286, 287]. Also hydrolytic resistance of 13-93 is of the same order as reported by Brink [55]. The average pH values of the solutions at room temperature were all higher than 9, except for E-glass at lower temperatures. The decomposition of the glass network and the ion-exchange reaction were verified by the concentration of the ions dissolved from the glasses (Table 17). The ion concentrations in the solutions were converted to normalized surface-specific mass loss. At 98°C the ion-exchange reaction was dominating for all compositions.

The relative scale fails to give any relevant information when bioactive glasses are studied. However, the differences in the hydrolytic resistance values imply that the method could be used as a rapid test to get an overall idea of the biodegradability of the glasses. As can be seen from the table, the high silicon concentrations released from the glasses decrease the volume needed in the titrations. Thus, the ion

concentration measurement together with the pH values gives a better estimate of hydrolytic resistance.

Both hydrolytic resistance and T_g are dependent on the mobility of the modifying ions. Interestingly, when these two values for glasses are plotted against each other, a preliminary correlation can be seen (Figure 19). In addition, it seems that all the glasses forming wollastonite (CS) as a primary crystal phase have higher hydrolytic resistance than glasses forming sodium calcium silicate (NCS) crystals. It would be of interest to elaborate on this further to see whether a true correlation can be obtained.

Table 16. Hydrolytic resistance (ISO 719) given as consumption of HCl [ml] per gram of glass grains at different temperatures, %RSD given for glasses with number of titrated samples ≥ 6.

Glass code	**T** [°C]	**V (HCl)** [ml/ g glass]	**% RSD**	**pH (RT)**	**Ref.**	**Glass code**	**T** [°C]	**V (HCl)** [ml/ g glass]	**% RSD**	**pH (RT)**	**Ref.**
E-glass	40	0.04		8.3	III	45S5	25	1.1		10.2	III
	60	0.1		8.4			40	2.1	2	10.3	
	80	0.2		9.0			60	2.3	8	10.5	
	98	0.3	3	9.2			98	5.3	4	10.8	
Table ware	40	0.1	21	9.4	III	1-98	40	0.5		10.1	II
	60	0.3	4	9.4			60	0.8		10.0	
	80	0.5		9.8			98	2.3	4	10.2	
	98	0.8	4	9.8							
Float	40	0.2	4	9.5	III	DGG1	98	1.0	1	9.9	III
	60	0.2	8	9.5							
	80	0.5	10	9.8							
	98	1.0	4	9.8							
0106	98	2.1		10.0	[285]	1306	98	2.7	9	10.4	[285]
0206	98	2.7	12	10.3	[285]	1406	98	1.4		9.8	[285]
0306	98	3.9		10.6	[285]	1606	98	1.2	20	9.7	[285]
0906	98	1.5		10.1	[285]	1806	98	2.3		10.1	[285]
1106	98	1.7	8	9.9	[285]	13-93	98	2.7		10.7	[285]
						S53P4	98	3.4		10.7	[285]

Table 17. Average ion concentrations in solution after one hour at 98°C (ISO 719), the same references apply as given in Table 16. For selected glasses error given as %RSD

	Na (mg/l)	**K (mg/l)**	**Mg (mg/l)**	**Ca (mg/l)**	**Si (mg/l)**
Hydrolytic resistance class 3:					
E-glass	0.4	0.5	0.1	3.1	4.3
%RSD	*13*	*15*	*20*	*7*	*6*
Tableware	6.0	2.8		0.4	10.4
%RSD	*2*	*5*		*33*	*2*
Hydrolytic resistance class 4:					
DGG 1	7.9	1.0	0.2	1.5	12.0
%RSD	*1*	*43*	*2*	*4*	*4*
1606	2.0	6.7	0.0	4.0	20.7
1406	2.4	7.8	0.2	8.6	18.9
Float	10.2	0.2	0.1	4.3	29.3
%RSD	*6*	*20*	*7*	*9*	*5*
0906	6.1	15.7	4.1	26.5	43.2
1106	3.2	13.3	0.0	10.8	27.0
Hydrolytic resistance class 5:					
0106	7.8	23.9	2.8	21.6	35.7
1-98	6.2	11.0	0.3	12.8	28.3
1806	13.3	1.7	0.0	5.1	23.4
1306	19.3	3.3	0.1	4.6	21.6
0206	11.8	16.8	0.1	8.9	25.2
13-93	6.5	13.2	0.3	11.1	29.1
S53P4	30.9	0.3	0.0	4.2	18.7
Hydrolytic resistance class > 5 i.e above the scale:					
0306	26.3	2.9	0.1	4.3	18.2
45S5	41.9	0.3	0.0	8.0	27.5
%RSD	*9*	*16*	*31*	*10*	*4*

** The missing value clearly under LOD*

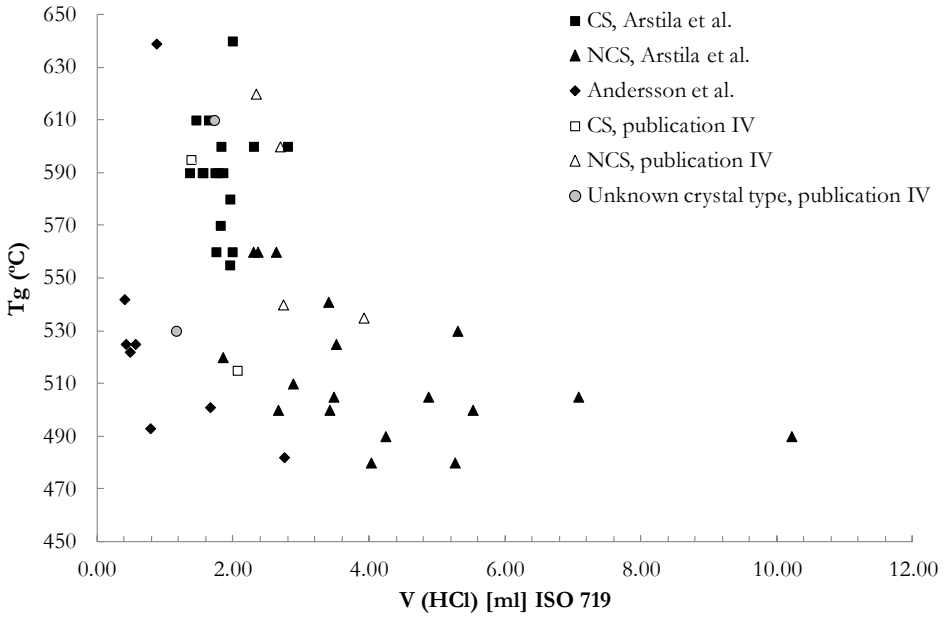

Figure 19. Correlation between Tg and V(HCl), data collected from [129, 131, 244] and publication IV, CS = wollastonite, NCS = sodium calcium silicate. For Andersson et al. no primary crystal data available.

The ISO 719 test procedure was applied at lower temperatures to determine the temperature effect on glass corrosion: as expected the lower the temperature the lower was the dissolution tendency (Table 16). At static conditions, the dissolution rate increased according to the Arrhenian behavior (discussed both in publication II and III). Arrhenius plots, i.e. the volume of HCl (ml) as a function of the inverse of temperature are shown in Figure 20. The plots are linear with similar slopes.

Apparent activation energy can be used to determine the dissolution control mechanism. Diffusion controlled processes have commonly been assigned a low energy barrier with Ea in the range of a few kJ/mol, while surface reactions give rise to an higher barrier of around 80 kJ/mol [190]. The apparent activation energy, based on hydrochloric acid consumption, was between 21 kJ/mol (45S5) and 33 kJ/mol (E-glass). This suggests that the dissolution was diffusion controlled for all the glasses. Also, the apparent activation energy values for the release of sodium (13-26 kJ/mol) and calcium (11-27 kJ/mol) would suggest the same. However, the apparent activation energy values for silicon dissolution from E-glass and float glass are high. This implies that for these glasses, the reaction mechanism is surface controlled. For the non-durable bioactive glasses the apparent activation energy values for silicon dissolution suggested diffusion control. The ISO 719 method performed at different temperatures and combined with pH and ion concentration measurements gave also a possibility to estimate the reaction mechanisms.

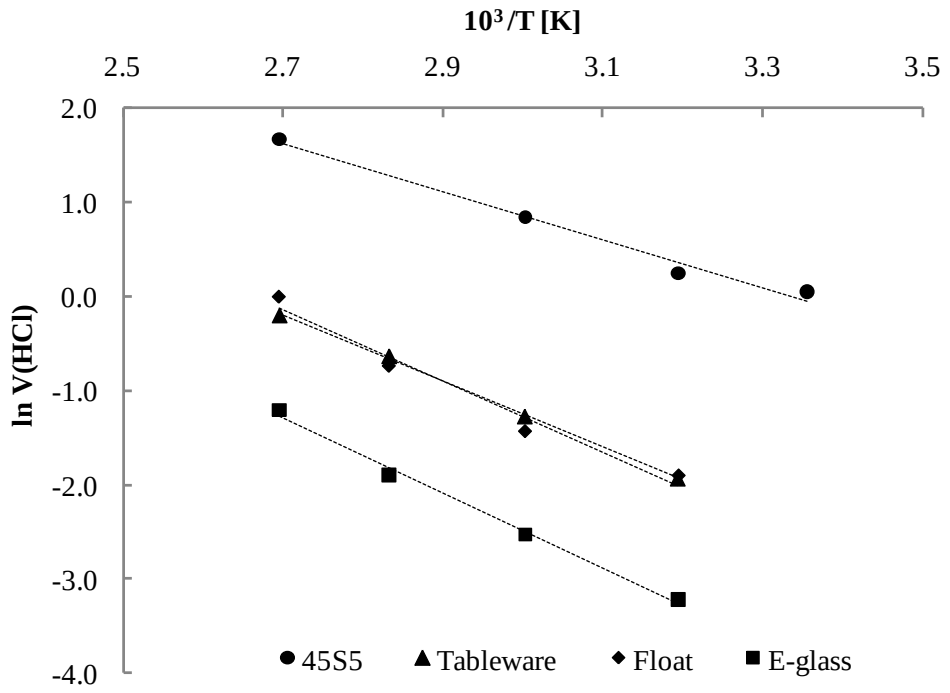

Figure 20. Arrhenius plot of the volume of hydrochloric acid, V(HCl), consumed in titration after one hour. (publication III)

4.2. Continuous dissolution studies

In publication II, a sensitive on-line analysis method utilizing an inductively coupled plasma optical emission spectrometer and a flow-through micro-volume pH electrode was developed to study the initial dissolution of bioactive glasses. The developed method was utilized to study the initial dissolution reactions of highly different types of glass composition in publications III–IV and [284].

The novelty and strength of this method is that all the ions can be measured immediately after the reaction and followed simultaneously both qualitatively and quantitatively. To the best of the author's knowledge, this type of approach has not been applied for studying glass dissolution reactions. In addition, in many studies the solution is circulated and thus the composition of the solution changes. In our approach, fresh solution with constant initial composition is continuously fed to the sample cell.

The impulse response of the system was studied using yttrium. No significant impulse broadening because of the glass particle bed was observed and the ion release from the glass started as soon as the solution came into contact with the sample (publication II). One example of the initial ion dissolution graph obtained with the method is shown in Figure 21 for glass 1–98 in contact with ultra-pure water. The time-lag before the solution flow from the sample cell reached the ICP detector was around 140-180 s depending on the tubing length. The concentration peaks around

this time indicated high initial dissolution of alkalis. The smooth increase of silicon concentration in the beginning of the measurement suggests that the alkali ion peaks were not caused by uniform dissolution of glass, but depended on the ion exchange reaction with hydrogen in the solution. Usually, the derivatives of the curves approached zero around 400 s, suggesting that steady-state leaching conditions were reached.

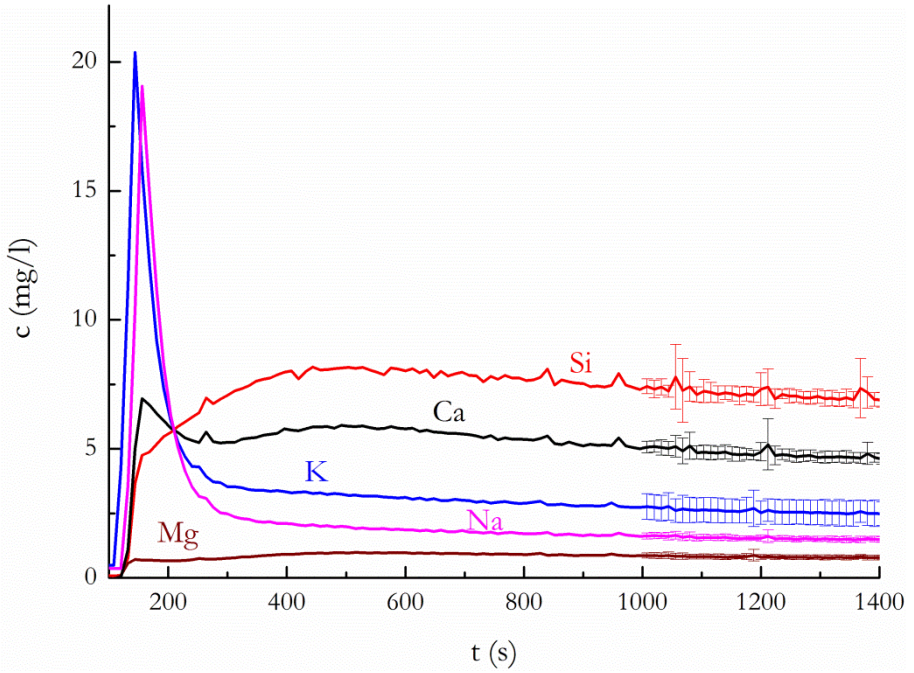

Figure 21. An example initial dissolution profile of 1-98 in contact with ultra-pure water, the error bars give the representative simple standard deviation for the measurements (publication II)

4.2.1. Effect of various parameters on the initial dissolution profile

The novel method was tested by measuring the effect of flow rate, temperature, and solution composition, among others, on the initial dissolution behavior of bioactive glass 1-98 consisting of several oxides (publication II). This study was performed to validate whether similar trends are gained with this method as with conventional studies. In addition, this study was important for choosing suitable parameters for the following studies. The key observations from the effect of the different parameters on the initial glass reaction are listed in Table 18.

Table 18.Effect of various parameters on the initial reactions of glass in contact with aqueous solutions (publication II)

Parameter	Key observations
Surface area and sample mass	• Studied using two particle size fractions. • For the size fraction 315–500 μm the initial top peak concentrations of potassium and sodium correlated almost linearly with the sample mass but for size fraction 62-125 μm no clear correlation with the sample mass and initial top peak height was observed o Several parameters affected the available effective surface area: fine powder attached to the glass particles, variations in the particle shape, size distribution of the particles, and packing of the particles in the sample cell. These may cause a large difference between initial real and calculated surface areas. Detailed attempts at correlating different size fractions were not included in this work • Results suggest that surface area was not the dominating parameter that controls the dissolution. The most important single parameter is probably the solution pH. • Changes in the effective surface area with proceeding dissolution may also have contributed to the observed non-linear dissolution trend between the samples with different masses.
Particle bed dimension	• Studied using three length and diameter combinations (L/Ø in mm 18.0/3.2, 11.8/4.0, and 6.3/5.0), constant flow, temperature, and sample mass. • Induced no significant differences in the initial ion dissolution profiles. • Conditions inside the sample cell were assumed to remain constant, regardless of the bed height, for a certain flow and temperature
Flow rate	• Studied using five different flow rates between 0.08-0.8 ml/min and constant temperature 40°C. • Flow was laminar with all the tested flow rates • Over the whole flow rate range studied, the initial profiles did not change their overall form • Dissolution was uniform, within the experimental accuracy at all the measured flow rates • When using the highest flow rates of water, the dissolution rate changed from a diffusion-controlled towards a surface-controlled mechanism.

Temperature	• Studied using 40°, 60°, 70° and 80°C and constant flow rate (0.2 mL/min).
	• As a result of the temperature increase, the overall dissolution increased according to Arrhenian behavior (24-36 kJ/mol) and led more rapidly to steady state dissolution.
	• A clear decreasing trend in magnesium and phosphorus concentrations at higher temperatures was observed.
	  o Back-precipitation (solubility of $Mg(OH)_2$ decreases with temperature)
	  o Complexation to silica gel is considered possible [288]

Table 18 continues on the next page.

Parameter	Key observations
Solvent composition	• The change of solution from unbuffered (ultra-pure water) to TRIS-buffered solution changed the dissolution mechanism from uniform to preferential (example graph shown in Figure 22). • Higher concentrations of all ions were measured in TRIS than in pure water.

All the obtained trends and results were in agreement with results obtained with conventional dissolution studies. Thus, the results indicate that the method enables on-line qualitative and quantitative analysis of the ions dissolving from glasses. The method developed is sensitive and promising for rapid screening of the dissolution mechanism of glasses in different experimental conditions. Even though only silica-based glasses were studied within this thesis work, the method would also be suitable for studying the dissolution of other glass systems. In the future it would be interesting to compare the results obtained with this continuous method with results obtained with different type of simulation tools such as Monte Carlo models. Recently, Monte Carlo simulations have been successfully used to predict glass dissolution reaction mechanisms in near-equilibrium conditions in a flow environment for borosilicate glasses [289].

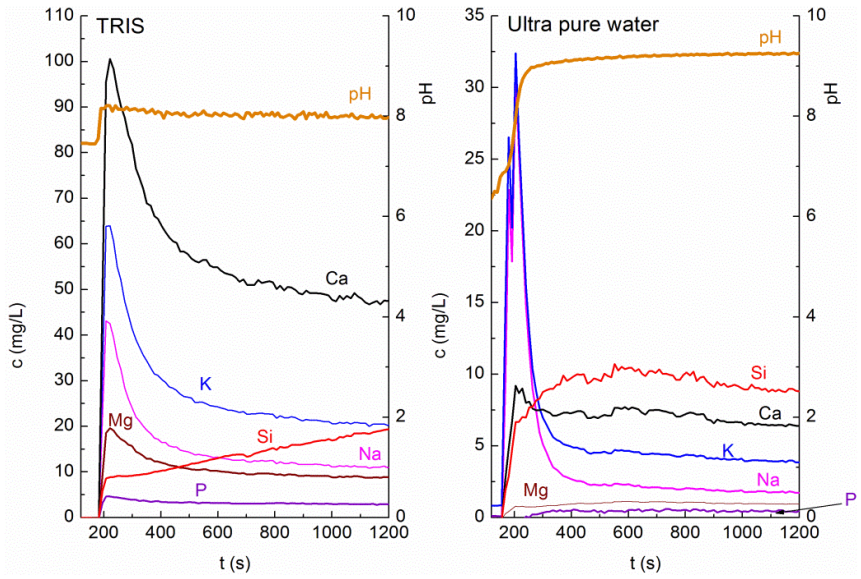

Figure 22. Initial dissolution profile of 1-98 (0.2 mL/min, 40°C) in TRIS and in ultra-pure water (publication II)

4.2.2. Dissolution patterns of biocompatible glasses in TRIS

In publication IV, the initial dissolution of 16 glasses in TRIS was recorded in a flow environment to give time-dependent dissolution profiles. TRIS was selected as the immersion solution because it has a suitable buffering range and does not contain any ions that may interfere with the ICP-OES measurement of ions dissolved from the glasses. Furthermore, as was observed in publication I, the initial dissolution behavior

in SBF and TRIS is highly similar. The same sample cell as used in publication II was utilized, and flow rate (0.2 ml/min) and temperature (40°C) were kept constant during all the measurements. In addition, the sample mass was kept constant because no accurate surface area measurements were available. Still, it is noted that the dissolution reactions are surface area-dependent, and that the estimation to use the same calculated surface area for all the glasses is a possible source of error in the normalization procedure. For more accurate analysis of the data, the density of each glass as well as the real initial surface area should be used in the future. When assuming a constant glass density, a roughly 10-% error is inflected on the results through the surface area calculations.

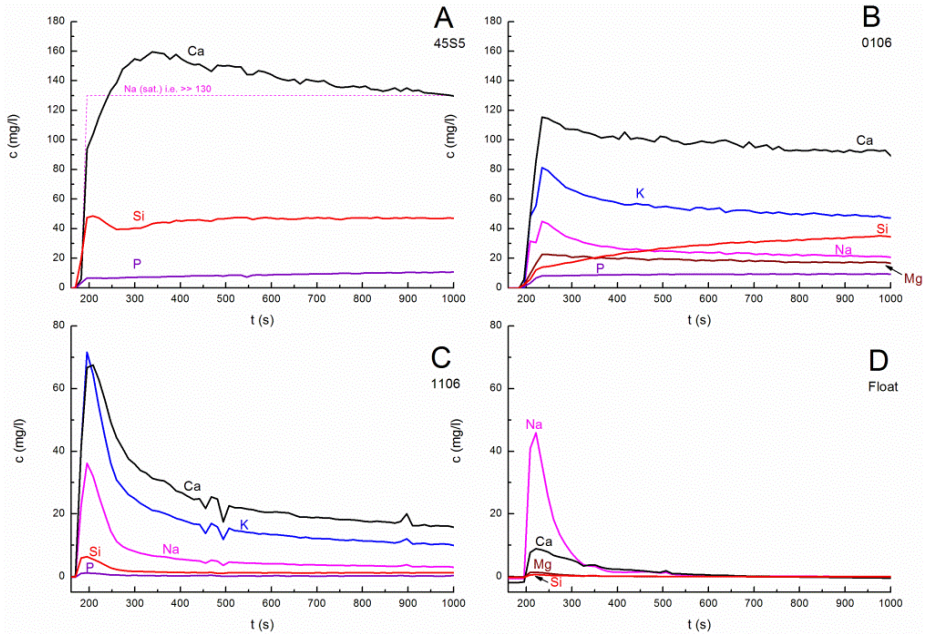

Figure 23. Four typical initial profiles for the experimental glasses (publication IV)

The dissolution behavior of the glasses could be fitted into four profiles (A-D), which cover all the dissolution patterns obtained in this work (Figure 23). The detailed description of each patter is given in publication IV.

The ion dissolution rates of the glasses were compared using the normalized surface-specific mass loss rate NR_i ($gm^{-2}s^{-1}$). Based on the NR_i values, all the glasses show preferential alkaline and alkaline earth ion dissolution in TRIS. The dissolution rates for these elements are of the same order, even though the values for alkaline earths are slightly higher than those for the alkalis. This may be due to rapid alkaline earth ion complexation with TRIS [257], which favors further dissolution.

The role of phosphorus in the structure of silica-based glass has been studied by Lockyer et al., Elgayar et al., Tilocca et al., O'Donnell et al., and Pedone et al. [138, 142, 145, 147, 150, 153], who suggested that P_2O_5 is present as an orthophosphate species rather than as a component in the silica network. In the presence of

orthophosphate, cations such as Na^+ and Ca^{2+} are needed to maintain the charge balance [147]. It is likely that the high initial dissolution rate of phosphorus is due to the solubility of orthophosphate species. Specifically, sodium orthophosphate is highly soluble when exposed to water [147]. Thus, during the initial dissolution, orthophosphate species may have an important influence on the rate at which calcium phosphate (CaP) forms on the glasses. Although NR_P values based on phosphorus concentrations close to LOQ must be treated with some caution, the phosphorus dissolution rate for most of the glasses is of the same order as the alkaline earth dissolution rate. As a clear exception, for 45S5, the NR_P is of the same order as the NR_{Si}. However, because it has been shown that in 45S5 P_2O_5 is present as orthophosphate species [145, 153], this discrepancy needs to be investigated in future studies.

The normalized surface-specific mass loss rates and the steady-state concentrations were compared with reported *in vitro* and *in vivo* behavior of the glasses [30, 34, 48, 131, 273, 274]. In addition, the hydrolytic resistance of the glasses, given in Table 16, was compared with the results obtained with the continuous measurements. The key observations and similarities of each pattern have been collected in Table 19, and in addition one of the *in vivo* model correlations is shown in Figure 24.

Table 19. Key observations of the different patterns A-D

Pattern	Key observations
A = bioactive glasses	• high initial dissolution • poor hydrolytic resistance • rapid Si and CaP layer *in vitro* • bond to bone • crystallize easily
B = ”medium” bioactive	o noticeable but clearly lower ion dissolution o poor hydrolytic resistance o medium Si and CaP layer *in vitro* o bond to bone but slower o allow hot working
C = biodegrable	• Slow release of ions • medium to poor hydrolytic resistance • no distinct layers after 72 h *in vitro* • no bone bonding • variable hot working properties
D = “inert”	o sharp alkali dissolution peak o good to medium hydrolytic resistance o no distinct layers after 72 h *in vitro* o no bone bonding o good hot working properties

In Figure 24, the normalized mass loss rate and the calcium and silicon concentrations are compared with the *in vivo* reaction number (RN) calculated using the model by Andersson et al. [34]. This model gives a relative value that can be

correlated with the reactivity of the glass *in vivo*: an RN of 1 implies that the glass is nearly inert; glasses with RN > 5 exhibit bone bonding and CaP formation; and intermediate values correspond to limited layer formation and no bone bonding. The model excludes the oxides of potassium and magnesium, and thus approximations are required to calculate the RN for the experimental glasses. In this work, we used the same approximations as those suggested by Brink [30], who replaced the amount of Na_2O in the RN model with the total amount of alkali (Na_2O+K_2O), and the amount of CaO with the total amount of alkaline earths (CaO+MgO) [30].

The dissolution rate in the continuous flow-through reactor was consistent with the *in vitro* and *in vivo* reactivities of the glasses studied. Glasses that bond to bone, but crystallize easily under hot-working conditions show high initial dissolution of Na, Ca, and Si. The compositions that allow hot working and bone bonding exhibit noticeable, but clearly lower, ion dissolution profiles. However, ion dissolution can also be measured for glasses that are likely to dissolve slowly in buffered solutions, and low initial concentrations were recorded for glasses that are nearly inert in the body environment.

Initial ion dissolution behavior in continuous fluid flow seems to provide an innovative and fast approach for pre-screening the suitability of different glass compositions as materials for bioactive, biodegrading, and bioinert medical devices.

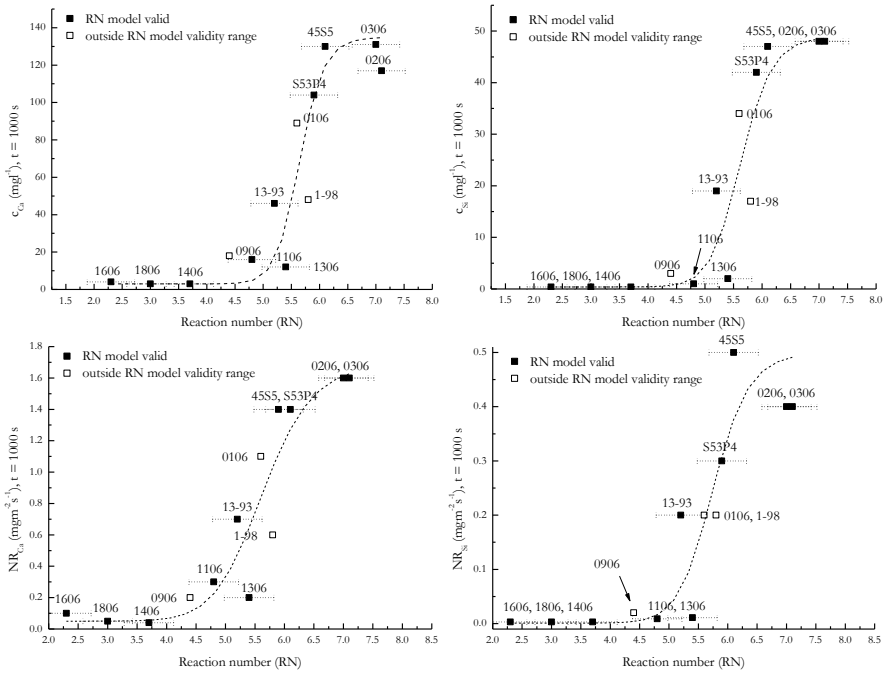

Figure 24. $c(Ca)_{t=1000s}$, $c(Si)_{t=1000s}$, normalized mass loss rate for calcium (NR_{Ca}), and normalized mass loss rate for silicon (NR_{Si}), plotted as functions of *in vivo* reaction number (RN). The RN model and its standard deviation are taken from [34]**. The same approximations to the RN model were used as suggested by Brink** [30]**. The lines are drawn to guide the eye. (publication IV)**

4.3. Combining information from conventional and continuous studies

By combining information from various experimental conditions, a better picture of glass dissolution and the suitability of the glasses for different medical applications can be obtained. Chemical durability of silicate glasses was tested in water and TRIS-buffered solution at static and dynamic conditions at different temperatures. In all experimental conditions, the dissolution order of the glasses was the same.

At dynamic conditions in water at 80°C, the soda-lime glasses dissolved uniformly while preferential dissolution was observed with E-glass. For the compositions studied in publication III, steady state dissolution conditions were approached after fifteen minutes. Measuring simultaneously all the ions released from the glasses gave a possibility to quantify the dissolution rate. This method was found suitable for compositions within a large range of chemical durability.

In the static TRIS-buffered solution, only the bioactive glasses have been observed to dissolve readily (publication III). Thus, in the buffered solution no marked differences between the more durable glasses were observed. However, at the dynamic conditions with TRIS a sharp initial dissolution peak for alkali metals was observed, after which all measured concentrations decreased to near or under the limits of quantification. This suggests preferential alkali extraction during the first minutes of dissolution. However, the extent of extraction was too low to cause any essential changes in the solution pH. The low pH does not favor additional network dissolution. However, clear differences in the hydrolytic resistance of these glasses could be obtained.

4.4. Crystallization and T-T-T for 1-98 and 13-93

Publication V reports the crystallization characteristics of bioactive glasses 1–98 and 13–93, and gives information on the T-T-T behavior in thermal treatments. The working ranges of both glasses are close to or partly within the temperature region in which they show high tendency to crystallize [45, 128]. The number and size of the crystals in heat treatment depend on the degree of overlapping of the nucleation and crystal growth domains. Both of these regions were estimated with DTA.

The obtained results are presented together with the measured viscosity values for the glasses by Vedel et al. [128] in Figure 25. The calculated nucleation domain for 1–98 was broader and possessed a higher amplitude than 13–93. The temperature of maximum nucleation ($T_{n\,max}$) was measured for glass 1-98 at 725°C and for 13–93 at 700°C. The differences in the $T_{n\,max}$ suggest that the nucleation rate for 1–98 is one order of magnitude higher than for 13-93. Even though the nucleation-like curves do not give the actual nucleation rates, these can be used as a good estimate of the actual ones. According to both DTA and isothermal heat-treatments, the crystallization of 1–98 and 13–93 was found to commence around 800°C and it started from all surfaces, as confirmed by the optical microscope images. At this temperature, the thermal

properties clearly changed and the samples shape deformed (publication V). The upper limit for the crystallization range is characterized by the liquidus temperature where the formed crystals start to melt. This was estimated with DTA to take place around 1150-1250°C confirming the results obtained by Arstila et al. [49].

The JMA parameter "*n*", which is related to the growth dimensionality in crystallization, was close to 1 for both glasses in agreement with the observed surface crystallization. In addition, the activation energy for the crystallization of both glasses was of the same order (280 kJ/mol). This suggests that the primary crystalline phase is identical for both compositions, as was also verified by XRD and SEM analyses. The identified primary crystalline phase was wollastonite ($CaSiO_3$) as reported earlier by Arstila et al. [129].

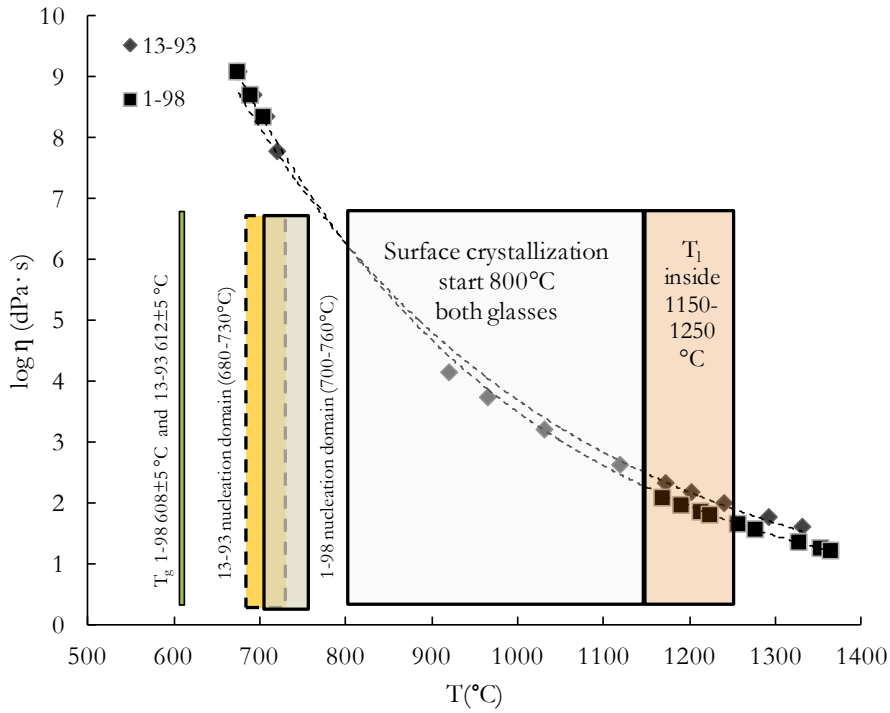

Figure 25. Nucleation and crystallization domain for the glasses obtained using DTA (Data publication V). In addition, the measured viscosity values for the glasses are given [128].

The typical viscosity values utilized in sintering and fiber drawing of glasses are 10^8–$5{\cdot}10^8$ dPa·s and 10^3–$5{\cdot}10^3$ dPa·s, respectively. The fiber drawing values coincide with the crystallization range (Figure 25). However, in practice if the crystal growth rate below the liquidus temperature is low enough, limited glass processing can still be performed. To estimate the average crystal growth rate ($U_{average}$) for the glasses isothermal heat-treatments were performed. Albeit being a laborious approach it gave valuable information about the differences in the crystallization rates. In the studied temperature interval, the crystal layer thickness as a function of time was found to be highly linear. The average crystal growth rate was estimated by plotting the slopes from

the time dependent curves versus temperature. The dependency was found to be exponential as a function of temperature. The values are given as arithmetical means with error bars indicating the minimum and maximum values.

Equation 10 for glass 1-98 and Equation 11 for glass 13-93 were formulated based on the experimental results:

$$X(\mu m) = \left(\frac{t}{s}\right) \cdot 3 \cdot 10^{-11} \cdot e^{0.0257 \cdot T(°C)} \quad (10)$$

$$X(\mu m) = \left(\frac{t}{s}\right) \cdot 2 \cdot 10^{-11} \cdot e^{0.0241 \cdot T(°C)} \quad (11)$$

where X is the crystal layer thickness, t time, and T temperature. The equations can be used to estimate the crystal layer thickness as a function of the heat treatment time and temperature. It should be observed that they are valid only in the studied temperature interval; at higher temperatures, a decrease in the crystal growth is expected. The crystal layer thicknesses calculated with Equations 10 and 11 are drawn as functions of both heat treatment time and temperature in a 3D plot in Figure 26. The figure clearly illustrates the large difference in the crystal growth rate for the two glasses.

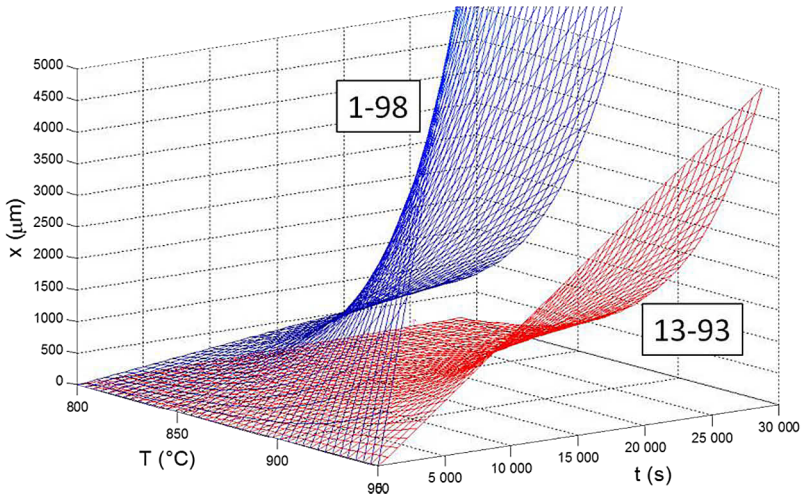

Figure 26. Crystal growth as a function of time and temperature using the Equations 10 and 11 (publication V)

According to the SEM images, it appears that the crystal layer thickness should be around 100 µm to cover the entire sample surface. This value was used as a boundary between conditions for crystalline and amorphous phases when drawing the approximate T-T-T curves in Figure 27. Thus, at conditions below the lines, the glasses do not crystallize, while at conditions above the lines, crystallization is expected to take

place. In the same figure, the experimental values from Arstila et al. [290] for crystallization of particles (500-800 μm) of glass 1-98 are given.

A good correlation can be found between the values reported for crystallization of the particles and the obtained T-T-T curve for 1-98 [290]. The T-T-T curve suggests that monolithic samples or large particles of 1-98 can be heat-treated below 800°C for several hours and below 850°C for at least 20 min before they start to crystallize. Within 800-850°C, the viscosity of the melt is low enough to allow viscous flow sintering into porous bodies [45]. However, in the temperature range from 850 to 1000°C, the melt crystallizes easily. The T-T-T curves suggested can be used estimate to the parameters for glass processing within the temperature range from glass transition up to liquidus.

The information gained is essential in manufacturing amorphous porous implants or drawing of continuous fibers of the glasses. Although both glasses can be hot-worked to amorphous products at carefully controlled conditions, 1-98 showed one magnitude greater crystal growth rate than 13-93. Thus, 13-93 is suited better than 1-98 for working processes which require long residence times at high temperatures. The more rapid crystal growth rate in 1-98 than 13-93 explains partly the reported differences in the fiber drawing properties of the glasses with preforms [49]. When fibers were drawn below the liquidus, 1-98 crystallized faster than the 13-93. The slow growth rate in 13-93 allowed for manufacture of continuous fibers, while crystallization faster prohibited the fiber drawing from 1-98 In addition, when the fiber drawing is done with a preform, the glass passes through the nucleation range affecting the fiber drawing success.

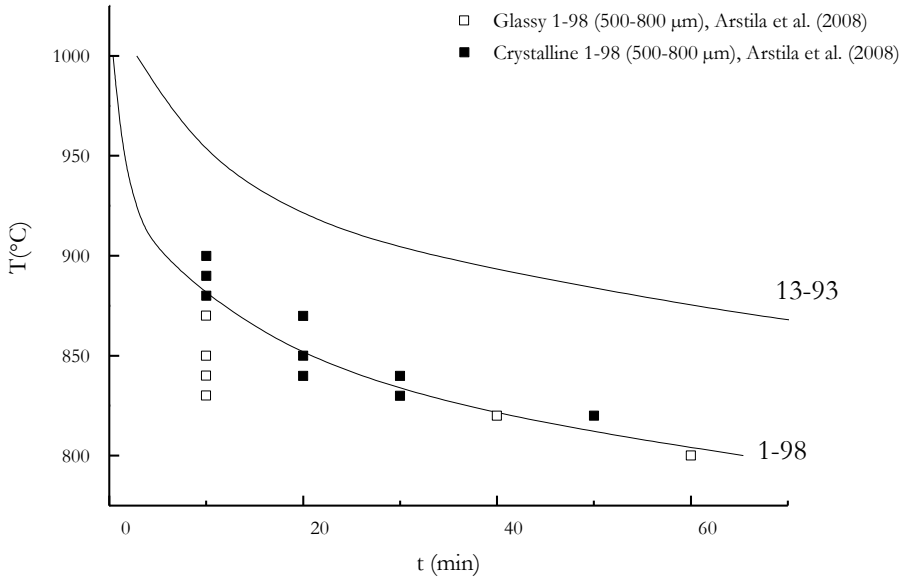

Figure 27. T-T-T graph calculated using the Equations 10 and 11. Threshold between glass and crystal layer in the T-T-T graph assumed 100 μm (publication V)

4.5. Sintering of porous implants of S53P4

In publication VI the influence of sintering temperature on the *in vitro* reactivity and mechanical strength of porous implants made of S53P4 was investigated. In general, the mechanical strength of the porous glassy implants is poor, although it improves with higher sintering temperature. Unfortunately, higher sintering temperature also increases the amount of crystallization, and if crystallization occurs too rapidly, it interferes with viscous flow sintering. Accordingly, to be able to sinter scaffolds from powdered fractions of bioactive glasses, it is essential to acquire a detailed understanding of the high temperature properties and crystallization mechanisms of the glasses. Then, a convenient heat treatment with suitable time and temperature parameters can be designed. The crystallization behavior of S53P4 has been studied earlier [129, 163, 217, 291], and the results relevant for heat treatments are collected in Figure 28.

As suggested by the figure, amorphous implants could be sintered below 650°C. But, below this temperature the viscosity was too high to allow proper strengthening of the implants during the 1 h sintering time (c.f. Figure 28). Furthermore, in accordance with the literature [129, 291], surface crystallization of S53P4 was observed to start at 650°C by formation of $Na_2O{\cdot}CaO{\cdot}2SiO_2$ crystals (PDF 01-077-2189). Rapid heating to temperatures higher than 800ºC produced fewer but larger primary crystals and a greater amount of residual glassy phase. The highest volume fraction of crystals in the surface layer formed at 800°C. Thus, nucleation and the number of crystals were highest at around 800ºC, while crystal growth dominated at the higher temperatures.

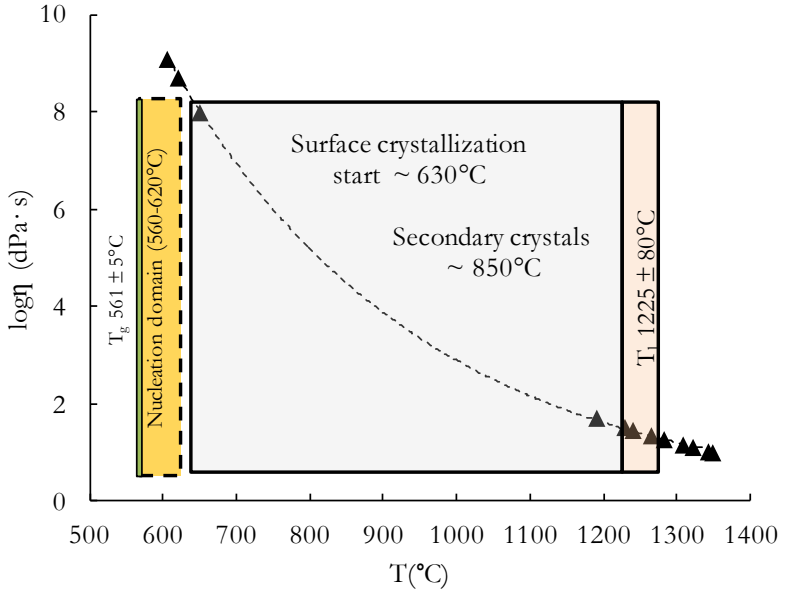

Figure 28. Nucleation [217] and crystallization domain for S53P4 obtained using DTA and isothermal heat treatments (publication VI). In addition, the measured viscosity values for the glasses are given [128].

As a novel finding, secondary crystals of $Na_2Ca_4(PO_4)2SiO_4$ (PDF 00-032-1053) were detected at higher temperatures, from 850°C to 1000°C. In the thermal treatment of 45S5, the phosphate-rich glassy phase that forms around larger crystallites of primary $Na_2CaSi_2O_6$ is thought to catalyze the formation of secondary $Na_2Ca_4(PO_4)_2SiO_4$ crystals [292]. In this work, most of the secondary crystals were found in the vicinity of the primary crystals, suggesting that secondary nucleation occurs close to the interface between the primary crystals and the residual glassy phase.

It was shown in this work that the bioactive glass S53P4 can be sintered into amorphous and partially crystalline porous implants within a broad temperature interval (620°C to 1000°C). Consolidation of the S53P4 particles occurred via viscous flow sintering, as indicated by the substantial amount of residual glassy phase and the rounded particle shapes and neck formation seen throughout the whole temperature range studied. This implies that the sintering kinetics of the S53P4 overwhelms the crystallization kinetics to a certain extent. It has been reported that if the viscous flow is fast enough, surface crystallization does not hinder the densification process [293]. In addition, sintering was estimated to be nearly isotropic by using the approach by Boccaccini and Trusty [294]. The small deviation from the fully isotropic behavior may produce some shear deformation during sintering.

Figure 29 shows the SEM images of the top surfaces with two different magnifications and cross sections of the implants after heat treatment for 1 h at various temperatures in the range 700° to 1000°C. The images of the top surfaces (the first two columns) were obtained using the secondary electrons, while the images of the cross sections (the third column) were obtained using the backscatter electrons. According to the μCT analysis, the total porosity of the implants decreased with increasing sintering temperature (STD ~ 2%): 36%, 30%, and 24% at 650°, 750°, and 900°C, respectively. The total and open porosities of the implants were the same after 1 h of sintering at the three temperatures, which implies that the pores are interconnected. No clear differences were found in the pore size distribution and the cumulative pore size distribution for implants sintered at the three temperatures. The compression strength of the implants was relatively low, but increased with the heat treatment temperature (from 0.7 MPa at 635°C to 10 MPa at 1000°C). To produce implants with greater strength, it will be necessary to optimize the time and temperature conditions. This was, however, outside the scope of this thesis.

It is well known that dissolution depends in part on the surface phase composition and on the surface area of the sample. In partially crystalline porous implants, the surface area depends on the total porosity and on the surface roughness caused by crystallization, both of which are related to the sintering temperature. Dissolution may also be affected by residual tensile stress, which can develop across grain boundaries, or because of the mismatch between different thermal expansion coefficients of the glass and crystalline phases, as discussed by Nychka et al. [174].

The *in vitro* reactivity of the sintered implants was studied by immersing the samples in SBF. The crystal phases which formed affected the dissolution behavior of the implants in SBF. The pH values showed in publication VI suggested slower initial dissolution for the implants sintered at 700°-800°C. The highest values were measured for the implants sintered at 850°C. As the pore distributions of the implants were almost the same, the differences in the pH were assumed to depend on changes in the dissolution behavior due to partial crystallization. While hydroxyapatite formed on all surfaces, the layer structure and thickness differed depending on the heat treatment temperature (Figure 30). There was better hydroxyapatite formation on amorphous and partially crystalline implants containing both primary and secondary crystals than on implants containing only primary crystals.

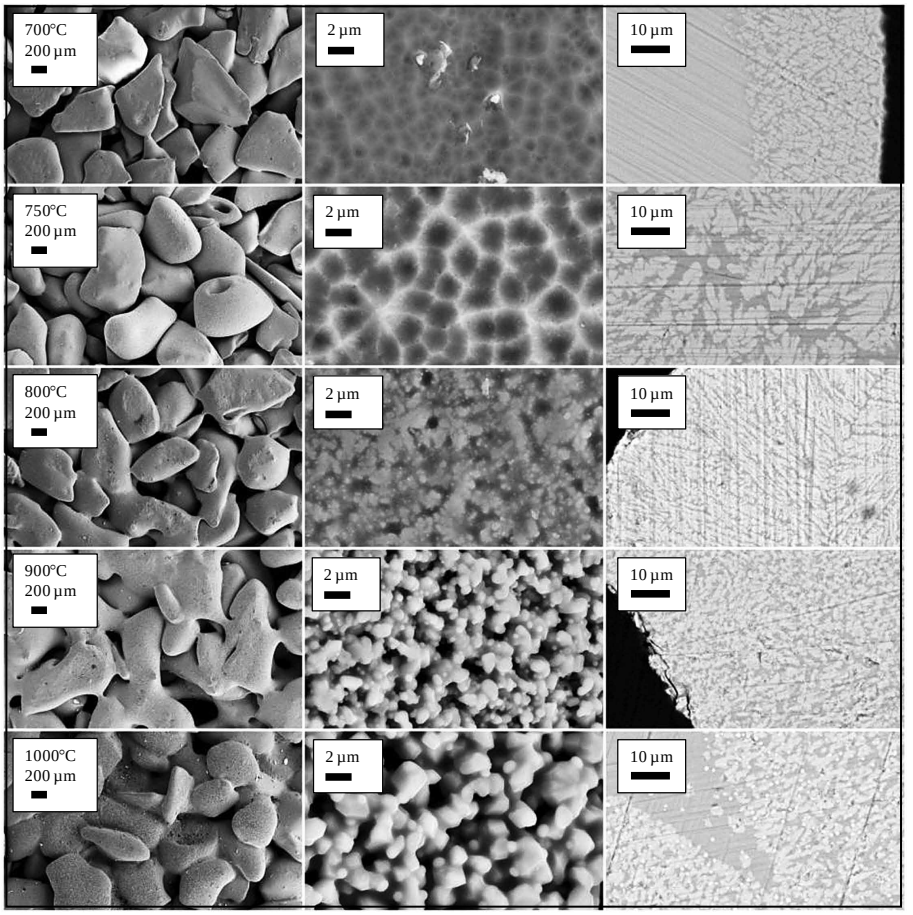

Figure 29. SEM images of S53P4 implants after sintering for 1 h at different temperatures. From the left: implant surface (30x), particle surface (5kx), particle cross section (1.5kx) (publication VI)

All the results suggest that S53P4 can be sintered into porous partly crystalline implants with adequate strength to be utilized as porous bone filler that is easily implantable in non-loadbearing applications. The obtained average pore size (around 200 µm) seemed to be appropriate for tissue ingrowth. However, the obtained pore

morphology and interconnectivity of the pores are likely not optimal for blood vessel formation. The information obtained in this study can be used as guideline when designing sintering conditions for S53P4 for tissue engineering scaffolds manufactured via special methods such as replication technique. Thus, this study opens up new possibilities for using S53P4 to manufacture various structures, while tailoring their bioactivity by controlling the proportions of the different phases.

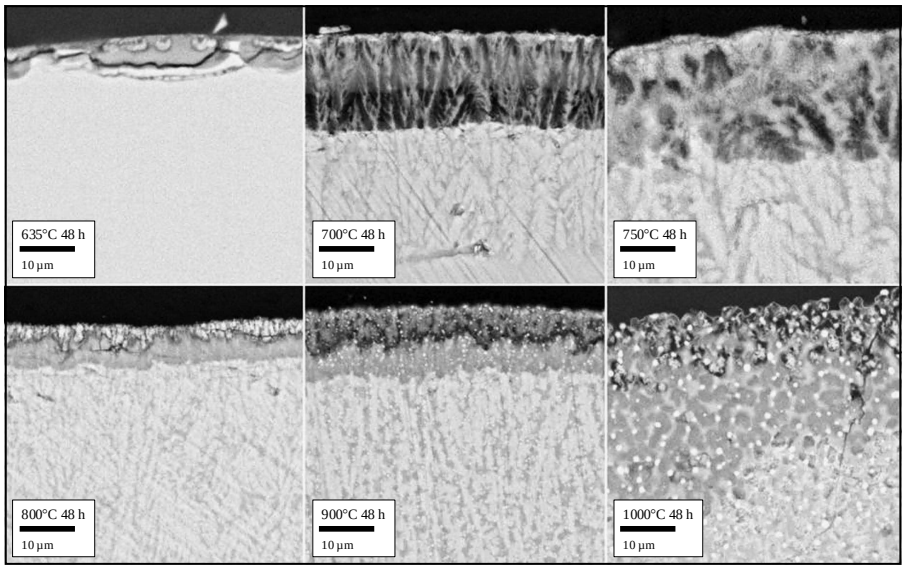

Figure 30. The cross section of the porous implants after immersion for 48 h (publication VI)

5. Conclusions and outlook

By combining information from various experimental conditions, a better knowledge of glass dissolution and the suitability of the glasses for different medical applications can be obtained. Chemical durability of silicate glasses were tested in water and TRIS-buffered solution at static and dynamic conditions at different temperatures. It is noteworthy that in all experimental conditions, the relative dissolution order of the glasses was the same.

It was also verified that the choice of immersion solution and immersion conditions are highly important. Furthermore, it was verified that TRIS is suitable for studying the dissolution behavior of glasses in a continuous flow environment. The traditional *in vitro* testing with a TRIS-buffered solution under static conditions works well with bioactive or with readily dissolving glasses and it is easy to follow the ion dissolution reactions. However, in the buffered solution no marked differences between the more durable glasses were observed.

The hydrolytic resistance of the glasses was studied using ISO 719. The relative scale given by the standard failed to provide any relevant information when bioactive glasses were studied. However, the clear differences in the hydrolytic resistance values imply that the method could be used as a rapid test to get an overall idea of the biodegradability of the glasses. The standard combined with the ion concentration and pH measurement gives a better estimate of the hydrolytic resistance because of the high silicon amount released from a glass. The released silicon decreases the volume needed in the titrations. Furthermore, the standard procedure performed at different temperatures could be used to evaluate the dissolution mechanism of the glasses.

A sensitive on-line analysis method utilizing inductively coupled plasma optical emission spectrometer and a flow-through micro volume pH electrode was developed to study the initial dissolution of bioactive glasses. This approach was found suitable for compositions within a large range of chemical durability. With this approach, the initial dissolution of all ions could be measured simultaneously and quantitatively, which gave a good overall idea of the initial dissolution rates for the individual ions and the dissolution mechanism. These types of results with glass dissolution were presented for the first time during the course of writing this thesis. Furthermore, the experimental parameters could be easily adjusted for various types of dissolution measurements. The method was shown to be sensitive for rapid screening of the dissolution mechanism of glasses in highly different experimental conditions. The experimental conditions clearly affected the initial dissolution rate of glasses, and in some cases the mechanism was changed.

Based on the initial dissolution patterns obtained with the novel approach using TRIS, the glasses could be divided into four distinct categories. The initial dissolution patterns of glasses correlated well with the anticipated bioactivity. Moreover, the normalized surface-specific mass loss rates and the different *in vivo* models and the

actual *in vivo* data correlated well. The results suggest that this type of approach can be used for pre-screening the suitability of novel glass compositions for future clinical applications, and furthermore shed light on possible bioactivity.

To further strengthen the implications given by the novel approach, information about surface property changes would be relevant. Consequently, sensitive analysis methods applied to the surface during and after the dissolution test would be of interest. Furthermore, the method should be tested with known bioactive materials to verify whether the observed trend fits other materials as well. The initial dissolution data could also benefit modeling work in the future. However, parameters like initial density and surface area need to be more accurately defined. As the method also gave implications regarding the glass structure, this path would be interesting to elaborate further by combining information from MAS-NMR studies. The next step for testing the dissolution of materials would be to test the influence of surface area and morphology. In addition, it would be of interest to evaluate how the initial dissolution of putty applications varies with the gel and glass matrix and how different pretreatments affect the initial dissolution.

Engineering type T-T-T curves for glasses 1-98 and 13-93 were established. A good correlation between the values reported for crystallization of the particles and the obtained T-T-T curve for 1-98 was observed. The information gained is essential in manufacturing amorphous porous implants or for drawing of continuous fibers of the glasses. Although both glasses can be hot worked to amorphous products at carefully controlled conditions, 1-98 showed one magnitude greater nucleation and crystal growth rate than 13-93. Thus, 13-93 is better suited than 1-98 for working processes which require long residence times at high temperatures.

It was also shown that amorphous and partially crystalline porous implants can be sintered from bioactive glass S53P4. Surface crystallization of S53P4, forming $Na_2O{\cdot}CaO{\cdot}2SiO_2$, was observed to start at 650°C, and secondary crystals of $Na_2Ca_4(PO_4)2SiO_4$ were detected at higher temperatures, from 850°C to 1000°C. The crystal phases which formed affected the dissolution behavior of the implants in simulated body fluid. This study opens up new possibilities for using S53P4 to manufacture various structures, while tailoring their bioactivity by controlling the proportions of the different phases.

Knowledge of both the dissolution behavior and hot-working properties is of utmost importance when glasses are developed for different clinical applications. Understanding the *in vitro* dissolution rate of glasses provides a preliminary approximation of the behavior of the glasses *in vivo*. The results obtained in this thesis give valuable additional information and tools to the state-of-the-art for designing glasses with respect to future clinical applications. In addition, the novel on-line analysis approach provides an excellent opportunity to further enhance our knowledge of glass behavior in simulated body conditions.

6. References

[1] Bange K. Roadmapping: A tool to look in the FUTURE (new applications & new requirements, Course: Glass Structure-Property Relationsships Montpellier, France, 4-5.5.2008.

[2] Brow RK, Schmitt ML. A survey of energy and environmental applications of glass. J. Eur. Ceram. soc. 2009; 29, 7: 1193-201.

[3] Eugen A. Glasses as engineering materials: A review. Mater. Des. 2011; 32, 4: 1717-32.

[4] Morey GW. The properties of glass, New York: Reinhold Publishing Corporation; 1938.

[5] Shelby JE. Introduction to glass science and technology, Cambridge, UK: The Royal Society of Chemistry; 1997.

[6] Carter CB, Norton MG. Ceramic Materials Science and engineering, New York: Springer Science+Business Media, LLC; 2007.

[7] Bange K, Weissenberger-Eibl M. Making glass better An ICG roadmap with a 25 year Glass R&D horizon, Madrid: International Commission on Glass (ICG); 2010.

[8] Hench L. The story of Bioglass®. J.Mater.Sci.Mater.Med. 2006; 17, 11: 967-78.

[9] Williams DF. On the mechanisms of biocompatibility. Biomaterials 2008; 29, 20: 2941-53.

[10] Williams D. The essential materials paradigms for regenerative medicine. JOM 2011; 63, 4: 51-5.

[11] Ducheyne P. Biomaterials. In Comprehensive Biomaterials Vol 1, ed. P. Ducheyne, K. Healy, D. Hutmacher, D. Grainger and C. Kirkpatrick James. Elsevier, Amsterdam, 2011, pp. 1-4.

[12] Lindgren S., Pänkäläinen T., Lucchesi J. & Ollila F. Regulatory aspects of bioactive glass. In Bioactive glasses Materials, properties and applications ed. H. Ylänen. Woodhead publishing in Materials, Cambridge, 2011, pp. 85-103.

[13] Heikkilä J. Use of bioactive glasses as bone substitutes in orthopaedics and traumatology. In Bioactive glasses Materials, properties and applications ed. H. Ylänen. Woodhead publishing in Materials, Cambridge, 2011, pp. 189-208.

[14] Chevalier J, Gremillard L. Ceramics for medical applications: A picture for the next 20 years. J. Eur. Ceram. Soc. 2009; 29, 7: 1245-55.

[15] Kokubo T, Kim H, Kawashita M. Novel bioactive materials with different mechanical properties. Biomaterials 2003; 24, 13: 2161-75.

[16] El-Ghannam A. Bone reconstruction: from bioceramics to tissue engineering. Expert Rev.Med.Devices 2005; 2, 1: 87-101.

[17] Giannoudis PV, Dinopoulos H, Tsiridis E. Bone substitutes: An update. Injury 2005; 36, 3, Supplement: S20-7.

[18] Desai BM. Osteobiologics. Am. J. Orthop. 2007; 36, 8-11.

[19] Cormack AN, Tilocca A. Structure and biological activity of glasses and ceramics. Phil. Trans. R. Soc. A 2012; 370, 1963: 1271-80.

[20] Lindfors N. Bioactive glass: Performance in experimental cancellous cavitary bone defects and spinal fusion, and interactions with polymorphonuclear leukocytes, PhD thesis, Medical Faculty of the University of Helsinki, Helsinki, 2002.

[21] Aspenberg P. Bank bone, infections and HIV. Acta Orthop. 1998; 69, 6: 557-8.

[22] Virolainen P, Heikkilä J, Hirn M, Aro HT, Aho AJ. 30 years of bone banking at Turku bone bank. Cell Tissue Banking 2003; 4, 1: 43-8.

[23] Aho AJ, Hirn M, Aro HT, Heikkilä JT, Meurman O. Bone bank service in Finland: Experience of bacteriologic, serologic and clinical results of the Turku Bone Bank 1972-1995. Acta Orthop. 1998; 69, 6: 559-65.

[24] Ohtsuki C, Kamitakahara M, Miyazaki T. Bioactive ceramic-based materials with designed reactivity for bone tissue regeneration. J. R. Soc. Interface 2009; 6, Suppl 3: S349-60.

[25] Peltola M. J., Aitasalo K. M. J. Bioactive glass for maxillofacial and dental repair. In Bioactive glasses Materials, properties, applications, ed. H. Ylänen. Woodhead publishing in Materials, Cambridge, 2011, pp. 217-226.

[26] Hench LL. Bioceramics: From Concept to Clinic. J. Am. Ceram. Soc. 1991; 74, 7: 1487-510.

[27] Katri Syvärinen. http://interface.tut.fi/articles/2010/2/Bioactive_glass_heals_-_and_disappears, updated 2010, accessed 2012.

[28] Lindfors NC, Koski I, Heikkilä JT, Mattila K, Aho HJ. A prospective randomized 14-year follow-up study of bioactive glass and autogenous bone as bone graft substitutes in benign bone tumors. J. Biomed. Mater. Res. B: Appl. Mater. 2010; 94, 1: 157-64.

[29] Cao W, Hench LL. Bioactive Materials. Ceram. Int. 1996; 22: 493-507.

[30] Brink M. The Influence of Alkali and Alkaline Earths on the Working Range for Bioactive Glasses. J. Biomed. Mater. Res. 1997; 36, 109-17.

[31] Blaker JJ, Nazhat SN, Boccaccini AR. Development and characterisation of silver-doped bioactive glass-coated sutures for tissue engineering and wound healing applications. Biomaterials 2004; 25, 7–8: 1319-29.

[32] Vernè E, Nunzio SD, Bosetti M, Appendino P, Vitale Brovarone C, Maina G, et al. Surface characterization of silver-doped bioactive glass. Biomaterials 2005; 26, 25: 5111-9.

[33] Bellantone M, Coleman NJ, Hench LL. Bacteriostatic action of a novel four-component bioactive glass. J. Biomed. Mater. Res. 2000; 51, 3: 484-90.

[34] Andersson ÖH, Liu G, Karlsson KH, Niemi L, Miettinen J, Juhanoja J. In vivo behaviour of glasses in the SiO2-Na2O-CaO-P2O5-Al2O3-B2O3 system. J. Mater. Sci.: Mater. Med. 1990; 1, 4: 219-27.

[35] Erol MM, Mouriño V, Newby P, Chatzistavrou X, Roether JA, Hupa L, et al. Copper-releasing, boron-containing bioactive glass-based scaffolds coated with alginate for bone tissue engineering. Acta Biomater. 2012; 8, 2: 792-801.

[36] O'Donnell MD, Hill RG. Influence of strontium and the importance of glass chemistry and structure when designing bioactive glasses for bone regeneration. Acta Biomater. 2010; 6, 7: 2382-5.

[37] Du J, Xiang Y. Effect of strontium substitution on the structure, ionic diffusion and dynamic properties of 45S5 Bioactive glasses. J.Non Cryst.Solids 2012; 358, 8: 1059-71.

[38] Aina V, Malavasi G, Fiorio Pla A, Munaron L, Morterra C. Zinc-containing bioactive glasses: Surface reactivity and behaviour towards endothelial cells. Acta Biomater. 2009; 5, 4: 1211-22.

[39] Hoppe A, Güldal NS, Boccaccini AR. A review of the biological response to ionic dissolution products from bioactive glasses and glass-ceramics. Biomaterials 2011; 32, 2757-74.

[40] Rahaman MN, Day DE, Sonny Bal B, Fu Q, Jung SB, Bonewald LF, et al. Bioactive glass in tissue engineering. Acta Biomater. 2011; 7, 6: 2355-73.

[41] Ylänen H. Bone Ingrowth into Porous Bodies Made by Sintering Bioactive Glass Microspheres, PhD thesis,

Combustion and Materials Chemistry, Åbo Akademi, 2000.

[42] Molin C. Electrospinning of Bioactive Glass Nanofibers, Master of Science Thesis, Laboratory of Inorganic Chemistry, Turku, 2012.

[43] Zhang D, Jain H, Hupa M, Hupa L. In-vitro Degradation and Bioactivity of Tailored Amorphous Multi Porous Scaffold Structure. J. Am. Ceram. Soc. 2012; 95, 9: 2687-94.

[44] Arstila H. Crystallization characteristics of bioactive glasses, PhD thesis, Inorganic Chemistry, Åbo Akademi, Turku, 2008.

[45] Wallenberger FT, Smrcek A. The Liquidus Temperature; Its Critical Role in Glass Manufacturing. Int. J. Appl. Glass Sci. 2010; 1, 2: 151-63.

[46] Brink M, Turunen T, Happonen R, Yli-Urpo A. Compositional dependence of bioactivity of glasses in the system Na2O-K2O-MgO-CaO-B2O3-P2O5-SiO2. J. Biomed. Mater. Res. 1997; 37, 114-21.

[47] Itälä A, Koort J, Ylänen H, Hupa M, Aro H. Biologic significance of surface microroughing in bone incorporation of porous bioactive glass implants. J. Biomed. Mater. Res. 2003; 67A, 2: 496-503.

[48] Zhao D., Moritz N., Vedel E., Ylänen H., Hupa L., Hupa M., et al. Large-scale in vivo validation of bioactivity of silica-based glasses in the SiO2-P2O5-B2O3-Na2O-K2O-CaO-MgO system produced by a new phenomenological model. Manuscript in preparation.

[49] Arstila H, Tukiainen M, Taipale S, Kellomäki M, Hupa L. Liquidus temperatures of bioactive glasses. Adv. Mater. Res. 2008; 39-40, 287-92.

[50] Moritz N, Rossi S, Vedel E, Tirri T, Ylanen H, Aro H, et al. Implants coated with bioactive glass by CO2-laser, an in vivo study. J.Mater.Sci.Mater.Med. 2004; 15, 7: 795-802.

[51] Moritz N, Vedel E, Ylänen H, Jokinen M, Hupa M, Yli-Urpo A. Characterisation of bioactive glass coatings on titanium substrates produced using a CO2 laser. J.Mater.Sci.Mater.Med. 2004; 15, 7: 787-94.

[52] Varila L, Lehtonen T, Tuominen J, Hupa M, Hupa L. In vitro behaviour of three biocompatible glasses in composite implants. J.Mater.Sci.Mater.Med. 1-11.

[53] Andersson Ö. H. Bioaktiva glaskeramer för medicinsk användning, Licentiatavhandling (in Swedish), Licentiate thesis, Oorganisk kemi vid Åbo Akademi, 1989.

[54] Andersson Ö. The bioactivity of silicate glass, PhD thesis, Inorganic Chemistry, Åbo Akademi, Turku, 1990.

[55] Brink M. Bioactive glasses with a large working range, PhD thesis, Åbo Akademi, 1997.

[56] Vedel E. Predicting the Properties of Bioactive Glasses, PhD thesis, Inorganic Chemistry, Åbo Akademi, Turku, 2008.

[57] Zhang D. In vitro Characterization of Bioactive Glass, PhD thesis, Inorganic Chemistry, Åbo Akademi, 2008.

[58] Varila L., Hupa L., Mäkinen M., Skrifvars B. & Werkelin J. Fyrtio år oorganisk kemi vid Åbo Akademi (in Swedish), "Green Report", Inorganic Chemistry, Åbo Akademi, Turku, 2011.

[59] Müller C. From components to systems - Process optimization by means of advanced technical concepts (Clyde Bergemann GmbH). 25.1.2012; Oral presentation at Åbo Akademi University.

[60] BonAlive Biomaterials Ltd. http://www.bonalive.com/, updated 2011, accessed 2011.

[61] RepRegen. http://www.repregen.com/, updated 2011, accessed 2012.

[62] Hench LL. Genetic design of bioactive glass. J. Eur. Ceram. Soc. 2009; 29, 7: 1257-65.

[63] Hench L. Bioactive Glasses: From Concept to Clinic a 45th Year Celebration (oral presentation in 11th ESG Conference), 2012.

[64] Hench LL, Day DE, Höland W, Rheinberger VM. Glass and Medicine. Int. J. Appl. Glass Sci. 2010; 1, 1: 104-17.

[65] Jones JR. Review of bioactive glass – from Hench to hybrids. Acta Biomater. in press.

[66] Thomas MV, Puleo DA, Al-Sabbagh M. Bioactive glass three decades on. J.Long.Term.Eff.Med.Implants 2005; 15, 6: 585-97.

[67] Tuominen J., Lehtonen T. & Ollila F. Implantable paste and its use. WO2011058134 (A1)2011

[68] DePaula C. Ceramic Composition for filling bone defects. US 2008/02266882008

[69] Nypelö T., Harlin A., Hupa L., Ollila F., Vedel E. & Widerholm R. A system and method for manufacturing fibres. WO2008099058 (A1)2008

[70] Pirhonen E, Niiranen H, Niemelä T, Brink M, Törmälä P. Manufacturing, mechanical characterization, and in vitro performance of bioactive glass 13-93 fibers. J. Biomed. Mater. Res. B: Appl. Mater. 2006; 77B, 2: 227-33.

[71] Pirhonen E, Moimas L, Brink M. Mechanical properties of bioactive glass 9-93 fibres. Acta Biomater. 2006; 2, 1: 103-7.

[72] Moimas L, Biasotto M, Lenarda RD, Olivo A, Schmid C. Rabbit pilot study on the resorbability of three-dimensional bioactive glass fibre scaffolds. Acta Biomater. 2006; 2, 2: 191-9.

[73] Fu Q, Saiz E, Rahaman MN, Tomsia AP. Bioactive glass scaffolds for bone tissue engineering: state of the art and future perspectives. Mater. Sci 2011; 31, 7: 1245-56.

[74] Rohanová D, Boccaccini AR, Yunos DM, Horkavcová D, Březovská I, Helebrant A. TRIS buffer in simulated body fluid distorts the assessment of glass–ceramic scaffold bioactivity. Acta Biomater. 2011; 7, 6: 2623-30.

[75] Yue S, Lee PD, Poologasundarampillai G, Jones JR. Evaluation of 3-D bioactive glass scaffolds dissolution in a perfusion flow system with X-ray microtomography. Acta Biomater. 2011; 7, 6: 2637-43.

[76] Gerhardt L, Boccaccini AR. Bioactive Glass and Glass-Ceramic Scaffolds for Bone Tissue Engineering. Materials 2010; 3, 7: 3867-910.

[77] Chen QZ, Thompson ID, Boccaccini AR. 45S5 Bioglass®-derived glass–ceramic scaffolds for bone tissue engineering. Biomaterials 2006; 27, 11: 2414-25.

[78] Niemelä T., Kellomäki M. Bioactive glass and biodegradable polymer composites. In Bioactive glasses Materials, properties and applications ed. H. Ylänen. Woodhead publishing in Materials, Cambridge, 2011, pp. 227-245.

[79] Lehtonen T., Tuominen J. Biocompatible composites and its use. EP 2 243 500 A12010

[80] Lehtonen T., Tuominen J. & Ollila F. Resorbable and biocompatible fibre glass compositions and their uses WO 2010122019A12010

[81] Jones J, Ehrenfried L, Saravanapavan P, Hench L. Controlling ion release from bioactive glass foam scaffolds with antibacterial properties. J.Mater.Sci.Mater.Med. 2006; 17, 11: 989-96.

[82] Greenspan D., West J., Meyers J., Lee S. & Diamond M. Anti-inflammatory and antimicrobial uses for bioactive glass. WO0015167 (A1)2011

[83] Hu S, Chang J, Liu M, Ning C. Study on antibacterial effect of 45S5 Bioglass®. J.Mater.Sci.Mater.Med. 2009; 20, 1: 281-6.

[84] Zhang D, Leppäranta O, Munukka E, Ylänen H, Viljanen MK, Eerola E, et al. Antibacterial effects and dissolution behavior of six bioactive glasses. J. Biomed. Mater. Res. A 2010; 93A, 2: 475-83.

[85] Munukka E, Leppäranta O, Korkeamäki M, Vaahtio M, Peltola T, Zhang D, et al. Bactericidal effects of bioactive glasses on clinically important aerobic bacteria. J.Mater.Sci.Mater.Med. 2008; 19, 1: 27-32.

[86] Leppäranta O, Vaahtio M, Peltola T, Zhang D, Hupa L, Hupa M, et al. Antibacterial effect of bioactive glasses on clinically important anaerobic bacteria in vitro. J.Mater.Sci.Mater.Med. 2008; 19, 2: 547-51.

[87] Tooley FV, Parmelee CW. Powder method for measurement of chemical durability of glass. J. Am. Ceram. Soc. 1940; 23, 304-14.

[88] Ramakrishna S, Mayer J, Wintermantel E, Leong KW. Biomedical applications of polymer-composite materials: a review. Composites Sci.Technol. 2001; 61, 9: 1189-224.

[89] Park JB, Lakes RS. Biomaterials : an introduction, New York: Springer; 2007. pp. 561.

[90] Williams DF. Definitions in biomaterials: Proceedings of a consensus conference of European Society for Biomaterials. Chester, England 3-5.1986. Elsevier, Amsterdam. 1987.

[91] David F. W. On the nature of biomaterials. Biomaterials 2009; 30, 30: 5897-909.

[92] Oxford English Dictionary. http://www.oed.com/, updated March 2012, accessed 2012.

[93] Walker PMB. Larousse dictionary of science and technology, New York: Larousse Press; 2006.

[94] Blair HC, Zaidi M, Schlesinger PH. Mechanisms balancing skeletal matrix synthesis and degradation. Biochem.J. 2002; 364, Pt 2: 329-41.

[95] Shea JE, Miller SC. Skeletal function and structure: Implications for tissue-targeted therapeutics. Adv.Drug Deliv.Rev. 2005; 57, 7: 945-57.

[96] Hertz A, Bruce IJ. Inorganic materials for bone repair or replacement applications. Nanomedicine (Lond) 2007; 2, 6: 899-918.

[97] Kanczler JM, Oreffo RO. Osteogenesis and angiogenesis: the potential for engineering bone. Eur.Cell.Mater. 2008; 15, 100-14.

[98] Jack E. L. Ceramics: Past, present, and future. Bone 1996; 19, 1, Supplement 1: S121-8.

[99] Vallet-Regí M, Ruiz-Hernández E. Bioceramics: From Bone Regeneration to Cancer Nanomedicine. Adv. Mater. 2011; 23, 44: 5177-218.

[100] Cooke, F. W. et al. Materials for reconstructive surgery: sixth international biomaterials symposium; April 20-24, 1974; Clemson University, Clemson, SC. NewYork: Wiley; 1975. 274 pages (Biomed. Mater. Symp. 6). In: FW Cooke, et al, editors. New York: Wiley; 1974.

[101] Hill R. G. Bioactive Glass-Ceramics. In Comprehensive Biomaterials Vol 1, ed. P. Ducheyne, K. Healy, D. Hutmacher, D. Grainger and C. Kirkpatrick James. Elsevier, Amsterdam, 2011, pp. 181-186.

[102] Rey C., Combes C., Drouet C. & Grossin D. Bioactive Ceramics: Physical Chemistry. In Comprehensive Biomaterials Vol 1, ed. P. Ducheyne, K. Healy, D. Hutmacher, D. Grainger and C. Kirkpatrick James. Elsevier, Amsterdam, 2011, pp. 187-222.

[103] Williams DF, Black J, Doherty PJ. Second consensus conference on definitions in biomaterials. Biomaterial-Tissue Interfaces. Eds Doherty P.J., William R.L., Williams D.F., Lee A.J.S. 1992; 525.

[104] Scholz M-, Blanchfield JP, Bloom LD, Coburn BH, Elkington M, Fuller JD, et al. The use of composite materials in modern orthopaedic medicine and prosthetic devices: A review. Composites Sci.Technol. 2011; 71, 16: 1791-803.

[105] Boccaccini AR, Erol M, Stark WJ, Mohn D, Hong Z, Mano JF. Polymer/bioactive glass nanocomposites for biomedical applications: A review. Composites Sci.Technol. 2010; 70, 13: 1764-76.

[106] Curtis AR, West NX, Su B. Synthesis of nanobioglass and formation of apatite rods to occlude exposed dentine tubules and eliminate hypersensitivity. Acta Biomater. 2010; 6, 9: 3740-6.

[107] Ulrich-Vinther M. Gene therapy methods in bone and joint disorders. Evaluation of the adeno-associated virus vector in experimental models of articular cartilage disorders, periprosthetic osteolysis and bone healing. Acta Orthop.Suppl. 2007; 78, 325: 1-64.

[108] Phillips JE, Gersbach CA, Garcia AJ. Virus-based gene therapy strategies for bone regeneration. Biomaterials 2007; 28, 2: 211-29.

[109] Nasu T, Ito H, Tsutsumi R, Kitaori T, Takemoto M, Schwarz EM, et al. Biological activation of bone-related biomaterials by recombinant adeno-associated virus vector. J. Orthop. Res. 2009; 27, 9: 1162-8.

[110] Hench LL, Splinter RJ, Allen WC, Greenlee TK. Bonding mechanisms at the interface of ceramic prosthetic materials. J. Biomed. Mater. Res. 1971; 5, 6: 117-41.

[111] Arcos D, Izquierdo-Barba I, Vallet-Regi M. Promising trends of bioceramics in the biomaterials field. J.Mater.Sci.Mater.Med. 2009; 20, 2: 447-55.

[112] Anderson J. The future of biomedical materials. J.Mater.Sci.Mater.Med. 2006; 17, 11: 1025-8.

[113] Hench LL, Polak JM. Third-Generation Biomedical Materials. Science 2002; 295, 5557: 1014-7.

[114] Novak BM. Hybrid Nanocomposite Materials?between inorganic glasses and organic polymers. Adv. Mater. 1993; 5, 6: 422-33.

[115] Mansur HS, Costa HS, Mansur AAP, Pereira M. 3D-macroporous hybrid scaffolds for tissue engineering: Network design and mathematical modeling of the degradation kinetics. Mater. Sci. Eng., C 2012; 32, 3: 404-15.

[116] De Bartolo L, Leindlein A, Hofmann D, Bader A, de Grey A, Curcio E, et al. Bio-hybrid organs and tissues for patient therapy: A future vision for 2030. Chemical Engineering and Processing: Process Intensification 2012; 51, 0: 79-87.

[117] Vallittu PK. Comparison of the In Vitro Fatigue Resistance of an Acrylic Resin Removable Partial Denture Reinforced With Continuous Glass Fibers or Metal Wires. J. Prosthond. 1996; 5, 2: 115-21.

[118] Vallittu PK. Flexural properties of acrylic resin polymers reinforced with unidirectional and woven glass fibers, J.Prosthet.Dent. 1999; 81, 3: 318-26.

[119] Tanner J, Vallittu PK, Söderling E. Effect of water storage of E-glass fiber-reinforced composite on adhesion of Streptococcus mutans. Biomaterials 2001; 22, 12: 1613-8.

[120] Hench LL, Polak JM, Xynos ID, Buttery LDK. Bioactive materials to control cell cycle. Mater. Res. Innovations 2000; 3, 313-23.

[121] Xynos ID, Hukkanen MVJ, Batten JJ, Buttery LD, Hench LL, Polak JM. Bioglass ®45S5 Stimulates Osteoblast Turnover and Enhances Bone Formation In Vitro: Implications and Applications for Bone Tissue Engineering. Calcif. Tissue Int. 2000; 67, 4: 321-9.

[122] Xynos ID, Edgar AJ, Buttery LD, Hench LL, Polak JM. Ionic products

of bioactive glass dissolution increase proliferation of human osteoblasts and induce insulin-like growth factor II mRNA expression and protein synthesis. Biochem.Biophys.Res.Commun. 2000; 276, 2: 461-5.

[123] Xynos ID, Edgar AJ, Buttery LDK, Hench LL, Polak JM. Gene-expression profiling of human osteoblasts following treatment with the ionic products of Bioglass® 45S5 dissolution. J. Biomed. Mater. Res. 2001; 55, 2: 151-7.

[124] Hench LL. Bioceramics. J. Am. Ceram. Soc. 1998; 81, 7: 1705-27.

[125] Braun S, Rappoport S, Zusman R, Avnir D, Ottolenghi M. Biochemically active sol-gel glasses: the trapping of enzymes. Mater. Lett. 1990; 10, 1–2: 1-5.

[126] Hupa L. Melt-derived bioactive glasses. In Bioactive glasses Materials, properties and applications ed. H. Ylänen. Woodhead publishing in Materials, Cambridge, 2011, pp. 1-28.

[127] Hatakka L. Natural aluminous raw materials in glass melting, PhD thesis, Inorganic Chemistry, Åbo Akademi, Turku, 1987.

[128] Vedel E, Arstila H, Ylänen H, Hupa L, Hupa M. Predicting Physical and Chemical Properties of Bioactive Glasses from Chemical composition, Part I: Viscosity characteristics. Glass technol. - Part A 2008; 49, 6: 251-9.

[129] Arstila H, Vedel E, Hupa L, Hupa M. Predicting physical and chemical properties of bioactive glasses from chemical composition II) Devitrification characteristics. Glass technol. - Part A 2008; 49, 6: 260-5.

[130] Zhang D, Vedel E, Hupa L, Aro H, Hupa M. Predicting Physical and Chemical Properties of Bioactive Glasses from Chemical Composition. Part III. Chemical Composition and In vitro Reactivity of Glasses. Glass technol. - Part A 2009; 50, 1: 1-8.

[131] Vedel E, Zhang D, Arstila H, Hupa L, Hupa M. Predicting physical and chemical properties of bioactive glasses fromchemical composition. Part IV: Tailoring compositions with desiredproperties. Glass technol. - Part A 2009; 50, 1: 9-16.

[132] Alexander Fluegel. http://glassproperties.com/databases, updated 2007, accessed 2012.

[133] Lakatos T, Simmingsköld B. Glaskomponenters inverkan på glasets vattenresistens (in Swedish). Glasteknisk tidskrift 1972; 27, 77-80.

[134] Lakatos T, Johansson L-, Simmingsköld B. Viscosity temperature relations in the glass system SiO2-Al2O3-Na2O-K2O-CaO-MgO in the compositional range of technical glassses. Glass technology 1971; 13, 3: 88-95.

[135] Aertsens M, Ghaleb D. New techniques for modelling glass dissolution. J.Nucl.Mater. 2001; 298, 1–2: 37-46.

[136] Varshneya A, K. Fundamentals of Inorganic Glasses, Sheffield: The Society of Glass Technology; 2006.

[137] Paul A. Chemistry of glasses, London: Chapman and Hall; 1982.

[138] Elgayar I, Aliev AE, Boccaccini AR, Hill RG. Structural analysis of bioactive glasses. J.Non Cryst.Solids 2005; 351, 2: 173-83.

[139] Malfait WJ, Halter WE, Verel R. 29Si NMR spectroscopy of silica glass: T1 relaxation and constraints on the Si–O–Si bond angle distribution. Chem.Geol. 2008; 256, 3–4: 269-77.

[140] McMillan P. Structural studies of silicate glasses and melts; applications and limitations of Raman spectroscopy. Amer. Mineral. 1984; 69, 622-44.

[141] Tilocca A, Cormack AN. Surface Signatures of Bioactivity: MD Simulations of 45S and 65S Silicate Glasses. Langmuir 2010; 26, 1: 545-51.

[142] Tilocca A, Cormack AN. Structural Effects of Phosphorus Inclusion in Bioactive Silicate Glasses. J. Phys. Chem. B 2007; 111, 51: 14256-64.

[143] Gunawidjaja PN, Mathew R, Lo AYH, Izquierdo-Barba I, García A, Arcos D, et al. Local structures of mesoporous bioactive glasses and their surface alterations in vitro: inferences from solid-state nuclear magnetic resonance. Phil. Trans. R. Soc. A 2012; 370, 1963: 1376-99.

[144] Brauer DS, Karpukhina N, O'Donnell MD, Law RV, Hill RG. Fluoride-containing bioactive glasses: Effect of glass design and structure on degradation, pH and apatite formation in simulated body fluid. Acta Biomater. 2010; 6, 8: 3275-82.

[145] Pedone A, Charpentier T, Malavasi G, Menziani MC. New Insights into the Atomic Structure of 45S5 Bioglass by Means of Solid-State NMR Spectroscopy and Accurate First-Principles Simulations. Chem. Mater. 2010; 22, 19: 5644-52.

[146] Watts SJ, Hill RG, O'Donnell MD, Law RV. Influence of magnesia on the structure and properties of bioactive glasses. J.Non Cryst.Solids 2010; 356, 9-10: 517-24.

[147] O'Donnell MD, Watts SJ, Law RV, Hill RG. Effect of P2O5 content in two series of soda lime phosphosilicate glasses on structure and properties – Part I: NMR. J.Non Cryst.Solids 2008; 354, 30: 3554-60.

[148] Lin C, Huang L, Shen P. Na2CaSi2O6–P2O5 based bioactive glasses. Part 1: Elasticity and structure. J.Non Cryst.Solids 2005; 351, 40-42: 3195-203.

[149] Laurence PR, Hillier IH. Towards modelling bioactive glasses: Quantum chemistry studies of the hydrolysis of some silicate structures. Comp. Mater. Sci. 2003; 28, 1: 63-75.

[150] Lockyer MWG, Holland D, Dupree R. NMR investigation of the structure of some bioactive and related glasses. J.Non Cryst.Solids 1995; 188, 3: 207-19.

[151] Greaves GN, Fontaine A, Lagarde P, Raoux D, Gurman SJ. Local structure of silicate glasses. Nature 1981; 293, 5834: 611-6.

[152] Iler RK. The chemistry of silica: solubility, polymerization, colloid and surface properties, and biochemistry, Wiley; 1979.

[153] Pedone A, Charpentier T, Menziani MC. The structure of fluoride-containing bioactive glasses: new insights from first-principle calculations and solid state NMR spectroscopy. J. Mater. Chem. 2012; 22, 19: 12599-608.

[154] Brow RK. Review: the structure of simple phosphate glasses. J.Non Cryst.Solids 2000; 263–264, 0: 1-28.

[155] Kirkpatrick RJ, Brow RK. Nuclear magnetic resonance investigation of the structures of phosphate and phosphate-containing glasses: a review. Solid State Nucl.Magn.Reson. 1995; 5, 1: 9-21.

[156] Hannon AC, Grimley DI, Hulme RA, Wright AC, Sinclair RN. Boroxol groups in vitreous boron oxide: new evidence from neutron diffraction and inelastic neutron scattering studies. J.Non Cryst.Solids 1994; 177, 0: 299-316.

[157] Krogh-Moe J. The structure of vitreous and liquid boron oxide. J.Non Cryst.Solids 1969; 1, 4: 269-84.

[158] Vedishcheva NM, Shakhmatkin BA, Wright AC. The structure of sodium borosilicate glasses: thermodynamic modelling vs. experiment. J.Non Cryst.Solids 2004; 345–346, 0: 39-44.

[159] Kurkjian CR, Gupta PK, Brow RK. The Strength of Silicate Glasses: What Do We Know, What Do We Need to Know? Int. J. Appl. Glass Sci. 2010; 1, 1: 27-37.

[160] Inaba S, Fujino S, Morinaga K. Young's Modulus and Compositional Parameters of Oxide Glasses. J. Am. Ceram. Soc. 1999; 82, 12: 3501-7.

[161] Ylänen H, Karlsson KH, Itälä A, Aro HT. Effect of immersion in SBF on porous bioactive bodies made by sintering bioactive glass microspheres. J. Non Cryst. Solids 2000; 275, 1-2: 107-15.

[162] Rahaman MN, Brown RF, Bal BS, Day DE. Bioactive Glasses for Nonbearing Applications in Total Joint Replacement. Semin.Arthroplasty 2006; 17, 3-4: 102-12.

[163] Arstila H, Fröberg L, Hupa L, Vedel E, Ylänen H, Hupa M. The sintering range of porous bioactive glasses. Glass technol. - Part A 2005; 46, 2: 138-41.

[164] Prado MO, Zanotto ED. Glass sintering with concurrent crystallization. Comptes Rendus Chimie 2002; 5, 11: 773-86.

[165] Höland W, Apel E, van 't Hoen C, Rheinberger V. Studies of crystal phase formations in high-strength lithium disilicate glass–ceramics. J.Non Cryst.Solids 2006; 352, 38–39: 4041-50.

[166] Höland W. Glass-ceramic technology, Westerville : American Ceramic Society; 2001.

[167] Vogel W, Höland W, Naumann K, Gummel J. Development of machineable bioactive glass ceramics for medical uses. J.Non Cryst.Solids 1986; 80, 1–3: 34-51.

[168] Zanotto ED. A bright future for glass-ceramics. Am. Ceram. Soc. Bull. 2010; 89, 19-27.

[169] Höland W. Biocompatible and bioactive glass-ceramics — state of the art and new directions. J.Non Cryst.Solids 1997; 219, 0: 192-7.

[170] Höland W, Rheinberger V, Apel E, van't Hoen C. Principles and phenomena of bioengineering with glass-ceramics for dental restoration. Journal of the European Ceramic Society 2007; 27, 2–3: 1521-6.

[171] Pannhorst W. Glass ceramics: State-of-the-art. J.Non Cryst.Solids 1997; 219, 0: 198-204.

[172] Dittmer M, Rüssel C. Colorless and high strength MgO/Al2O3/SiO2 glass-ceramic dental material using zirconia as nucleating agent. J. Biomed. Mater. Res. B: Appl. Mater. 2012; 100B, 2: 463-70.

[173] Ochoa I, Sanz-Herrera JA, García-Aznar JM, Doblaré M, Yunos DM, Boccaccini AR. Permeability evaluation of 45S5 Bioglass®-based scaffolds for bone tissue engineering. J. Biomech. 2009; 42, 3: 257-60.

[174] Nychka J., Mazur S., Kashyap S., Li D. , Yang F. Dissolution of bioactive glasses: The effects of crystallinity coupled with stress. JOM 2009; 61, 9: 45-51.

[175] Adams P. Predicting corrosion. In Corrosion of glass, ceramics and ceramic superconductors, ed. D. E. Clark and B. K. Zoitos. Noyes Publications, 1991, pp. 29-50.

[176] Grambow B. Geochemical Approach To Glass Dissolution. In Corrosion of glass, ceramics and ceramic superconductors, ed. D. E. Clark and B. K. Zoitos. Noyes Publications, 1991, pp. 124-152.

[177] Jantzen M., Carol. Thermodynamic Approach to Glass Corrosion. In Corrosion of glass, ceramics and ceramic superconductors, ed. D. E. Clark and B. K. Zoitos. Noyes Publications, 1991, pp. 153-217.

[178] Conradt R. A proposition for an improved theoretical treatment of the corrosion of multi-component glasses. J.Nucl.Mater. 2001; 298, 1–2: 19-26.

[179] Paul A. Chemical durability of glasses; a thermodynamic approach. J. Mater. Sci. 1977; 12, 11: 2246-68.

[180] Jiricka A, Heide G, Helebrant A, Hamackova J, Frischat GH. Corrosion modeling of simple glasses from the systems SiO2-Na2O-CaO and SiO2-Na2O-MgO. Glass Sci.Tech. 2003; 76, 298-308.

[181] Helebrant A., Jiřička A. Modelling of glass corrosion under dynamic conditions. ed. S. Persson. Glafo, Växjö, 1997, pp. 80-87.

[182] Helebrant A, Tošnerová B. A mathematical model used to compare glass durability tests under different flow conditions. Glass Technology 1989; 30, 220-3.

[183] Trethewey K,R., Chamberlain J. Corrosion for Science and Engineering, 2nd. Essex, England: Longman Scientific & Technical; 1995.

[184] Cailleteau C, Weigel C, Ledieu A, Barboux P, Devreux F. On the effect of glass composition in the dissolution of glasses by water. J.Non Cryst.Solids 2008; 354, 2-9: 117-23.

[185] Scholze H. Glass-water interactions. J.Non Cryst.Solids 1988; 102, 1–3: 1-10.

[186] Casey WH. Glass and mineral corrosion: Dynamics and durability. Nat. Mater. 2008; 7, 12: 930-2.

[187] Conradt R. Chemical Durability of Oxide Glasses in Aqueous Solutions: A Review. J. Am. Ceram. Soc. 2008; 91, 3: 728-35.

[188] Hench LL, Clark DE. Physical chemistry of glass surfaces. J.Non Cryst.Solids 1978; 28, 1: 83-105.

[189] L.L. H. Characterization of glass corrosion and durability. J.Non Cryst.Solids 1975; 19, 0: 27-39.

[190] White W. B. Theory of corrosion of glass and ceramics. In Corrosion of glass, ceramics and ceramic superconductors, ed. D. E. Clark and B. K. Zoitos. Noyes Publications, 1991, pp. 2-26.

[191] Bunker BC. Molecular mechanisms for corrosion of silica and silicate glasses. J.Non Cryst.Solids 1994; 179, 300-8.

[192] Douglas RW, El-Shamy TMM. Reactions of Glasses with Aqueous Solutions. J. Am. Ceram. Soc. 1967; 50, 1: 1-8.

[193] El-Shamy T, Douglas R. Decomposition of Glasses by Aqueous Solutions. Glass technology 1972; 13, 3: 81-7.

[194] El-Shamy T, Douglas R. Kinetics of the reaction of water with glass. Glass technology 1972A; 13, 3: 77-80.

[195] Bunker BC, Arnold GW, Beauchamp EK, Day DE. Mechanisms for alkali leaching in mixed-Na-K silicate glasses. J.Non Cryst.Solids 1983; 58, 2–3: 295-322.

[196] Baucke F. Glass electrodes: Why and how they function. Ber.Bunsen-Ges.Phys.Chem.Chem.Phys. 1996; 100, 9: 1466-74.

[197] Baucke FGK. The modern understanding of the glass electrode response. Fresenius J.Anal.Chem. 1994; 349, 8: 582-96.

[198] Baucke FGK. The glass electrode — applied electrochemistry of glass surfaces. J.Non Cryst.Solids 1985; 73, 1–3: 215-31.

[199] Dilmore MF, Clark DE, Hench LL. Chemical Durability of Na2O-K2O-CaO-SiO2 Glasses. J. Am. Ceram. Soc. 1978; 61, 9-10: 439-43.

[200] El-Shamy T.M., Lewins J., Douglas R.W. The dependence on the pH of the decomposition of glasses by aqueous solutions. Glass technology 1972; 13, 3: 81-7.

[201] Grambow B, Müller R. First-order dissolution rate law and the role of surface layers in glass performance assessment. J.Nucl.Mater. 2001; 298, 1–2: 112-24.

[202] Varila L. Reactions of bioactive glasses and their composites in aqueous solutions, Master of Science thesis, Laboratory of Inorganic Chemistry, Turku, 2011.

[203] Casey WH, Westrich HR, Banfield JF, Ferruzzi G, Arnold GW. Leaching and reconstruction at the surfaces of dissolving chain-silicate minerals. Nature 1993; 366, 6452: 253-6.

[204] S. P, R. S. Study of alkali silicate glass corrosion using spectroscopic ellipsometry and secondary ion mass spectrometry. Phys. Chem. Glasses 2003; 44, 4: 303-7.

[205] Zhang D, Arstila H, Vedel E, Ylänen H, Hupa L, Hupa M. In Vitro Behavior of Fiber Bundles and Particles of Bioactive Glasses. Key Engineering Materials (Volumes 361-363) 2008; Bioceramics 20, 225-8.

[206] Kokubo T, Kushitani H, Sakka S. Solutions able to reproduce in vivo surface-structure changes in bioactive glass-ceramics A-W. J. Biomed. Mater. Res 1990; 24, 721-34.

[207] Hench L. L., Andersson Ö. H. & LaTorre G. P. The kinetics of bioactive ceramics part III : surface reactions of bioactive glasses compared with an inactive glass. In Bioceramics 4, ed. W. Bonfield, G. W. Hastings and K. Tanner. Pergamon/Elsevier, Oxford, 1991, pp. 156-162.

[208] Hill R. An alternative view of the degradation of bioglass. J. Mater. Sci. Lett. 1996; 15, 13: 1122-5.

[209] Strnad Z. Role of the glass phase in bioactive glass-ceramics. Biomaterials 1992; 13, 5: 317-21.

[210] Rawlings R. D. Composition dependence of the bioactivity of glasses. J. Mater. Sci. Lett. 1992; 11, 20: 1340-3.

[211] Karlsson KH, Ylänen H, Aro H. Porous bone implants. Ceram. Int. 2000; 26, 8: 897-900.

[212] Hill RG, Brauer DS. Predicting the bioactivity of glasses using the network connectivity or split network models. J.Non Cryst.Solids 2011; 357, 24: 3884-7.

[213] Edén M. The split network analysis for exploring composition–structure correlations in multi-component glasses: I. Rationalizing bioactivity-composition trends of bioglasses. J.Non Cryst.Solids 2011; 357, 6: 1595-602.

[214] Brauer DS, Rüssel C, Kraft J. Solubility of glasses in the system P2O5–CaO–MgO–Na2O–TiO2: Experimental and modeling using artificial neural networks. J.Non Cryst.Solids 2007; 353, 3: 263-70.

[215] Haimi S, Gorianc G, Moimas L, Lindroos B, Huhtala H, Räty S, et al. Characterization of zinc-releasing three-dimensional bioactive glass scaffolds and their effect on human adipose stem cell proliferation and osteogenic differentiation. Acta Biomater. 2009; 5, 8: 3122-31.

[216] Lusvardi G, Malavasi G, Menabue L, Aina V, Morterra C. Fluoride-containing bioactive glasses: Surface reactivity in simulated body fluids solutions. Acta Biomater. 2009; 5, 9: 3548-62.

[217] Massera J, Hupa L, Hupa M. Influence of partial substitution of CaO with MgO on the thermal properties and in vitro reactivity of the bioactive glass S53P4. J. Non Cryst. Solids 2012; 358, 18-19: 2701-7.

[218] Bellucci D, Bolelli G, Cannillo V, Cattini A, Sola A. In situ Raman spectroscopy investigation of bioactive glass reactivity: Simulated body fluid solution vs TRIS-buffered solution. Mater. Charact. 2011; 62, 10: 1021-8.

[219] Alm JJ, Frantzén JPA, Moritz N, Lankinen P, Tukiainen M, Kellomäki M, et al. In vivo testing of a biodegradable woven fabric made of bioactive glass fibers and PLGA80 - A pilot study in the rabbit. J. Biomed. Mater. Res. B: Appl. Mater. 2010; 93B, 2: 573-80.

[220] Itälä A, Ylänen HO, Yrjans J, Heino T, Hentunen T, Hupa M, et al. Characterization of microrough bioactive glass surface: Surface reactions and osteoblast responses in vitro. J. Biomed. Mater. Res. 2002; 62, 3: 404-11.

[221] Bergman S. A., Litkowski L. J. Bone In-Fill of Non-Healing Calvarial Defects Using Particulate Bioglass®

and Autogenous Bone. In Bioceramics Volume 8, ed. J. Wilson, L. L. Hench and D. Greenspan. Elsevier Science, Ltd., Oxford, 1995, pp. 17-21.

[222] Kin D, Lee K, Kim J, Chang J, Kim Y. The Influence of Bioactive Glass Particles on Osteolysis. Key Engineering Materials (Volumes 330 - 332) 2007; Bioceramics 19, 193-6.

[223] Oonishi H, Hench LL, Wilson J, Sugihara F, Tsuji E, Kushitani S, et al. Comparative bone growth behavior in granules of bioceramic materials of various sizes. J. Biomed. Mater. Res. 1999; 44, 1: 31-43.

[224] Oonishi H, Hench LL, Wilson J, Sugihara F, Tsuji E, Matsuura M, et al. Quantitative comparison of bone growth behavior in granules of Bioglass®, A-W glass-ceramic, and hydroxyapatite. J. Biomed. Mater. Res. 2000; 51, 1: 37-46.

[225] MacNeill SR, Cobb CM, Rapley JW, Glaros AG, Spencer P. In vivo comparison of synthetic osseous graft materials. A preliminary study. J.Clin.Periodontol. 1999; 26, 4: 239-45.

[226] Wheeler DL, Stokes KE, Hoellrich RG, Chamberland DL, McLoughlin SW. Effect of bioactive glass particle size on osseous regeneration of cancellous defects. J. Biomed. Mater. Res. 1998; 41, 4: 527-33.

[227] Lindfors NC, Aho AJ. Granule size and composition of bioactive glasses affect osteoconduction in rabbit. J.Mater.Sci.Mater.Med. 2003; 14, 4: 365-72.

[228] Labbaf S, Tsigkou O, Müller KH, Stevens MM, Porter AE, Jones JR. Spherical bioactive glass particles and their interaction with human mesenchymal stem cells in vitro. Biomaterials 2011; 32, 4: 1010-8.

[229] Jones JR, Sepulveda P, Hench LL. Dose-dependent behavior of bioactive glass dissolution. J. Biomed. Mater. Res. 2001; 58, 6: 720-6.

[230] Serra J, González P, Liste S, Serra C, Chiussi S, León B, et al. FTIR and XPS studies of bioactive silica based glasses. J.Non Cryst.Solids 2003; 332, 1-3: 20-7.

[231] Aina V, Bertinetti L, Cerrato G, Cerruti M, Lusvardi G, Malavasi G, et al. On the dissolution/reaction of small-grain Bioglass® 45S5 and F-modified bioactive glasses in artificial saliva (AS). Appl.Surf.Sci. 2011; 257, 9: 4185-95.

[232] Aguiar H, Solla EL, Serra J, González P, León B, Malz F, et al. Raman and NMR study of bioactive Na2O–MgO–CaO–P2O5–SiO2 glasses. J.Non Cryst.Solids 2008; 354, 45–46: 5004-8.

[233] Yli-Urpo H, Närhi M, Närhi T. Compound changes and tooth mineralization effects of glass ionomer cements containing bioactive glass (S53P4), an in vivo study. Biomaterials 2005; 26, 30: 5934-41.

[234] Hupa L, Karlsson KH, Hupa M, Aro HT. Comparison of bioactive glasses in vitro and in vivo. Glass technol. - Part A 2010; 51, 2: 89-92.

[235] Cerruti M, Greenspan D, Powers K. Effect of pH and ionic strength on the reactivity of Bioglass® 45S5. Biomaterials 2005; 26, 14: 1665-74.

[236] Jedlicka AB, Clare AG. Chemical durability of commercial silicate glasses. I. Material characterization. J.Non Cryst.Solids 2001; 281, 1–3: 6-24.

[237] Xiu T, Liu Q, Wang J. Comparisons between surfactant-templated mesoporous and conventional sol–gel-derived CaO–B2O3–SiO2 glasses: Compositional, textural and in vitro bioactive properties. J. Solid State Chem. 2008; 181, 4: 863-70.

[238] Clark D. E., Zoitos B. K. Corrosion testing and characterization. In Corrosion of glass, ceramics and ceramic superconductors, ed. D. E. Clark and B. K. Zoitos. Noyes Publications, 1991, pp. 51-102.

[239] Zhang D, Hupa M, Hupa L. In situ pH within particle beds of bioactive

glasses. Acta Biomater. 2008; 4, 5: 1498-505.

[240] Hench LL, Clark DE, Harker AB. Nuclear waste solids. J.Mater.Sci. 1986; 21, 5: 1457-78.

[241] Pierce EM, Rodriguez EA, Calligan LJ, Shaw WJ, Pete McGrail B. An experimental study of the dissolution rates of simulated aluminoborosilicate waste glasses as a function of pH and temperature under dilute conditions. Appl.Geochem. 2008; 23, 9: 2559-73.

[242] Jiricka A., Helebrant A. Dissolution of soda-lime, silica, and high-level waste glass by static and single-pass flow through tests. ed. G. T. Chandler and X. Feng. ACers Westerville, 2000, pp. 309-316.

[243] International Organization for Standardization. ISO 719-1985 (E) Glass -- Hydrolytic resistance of glass grains at 98 degrees C -- Method of test and classification. 1985.

[244] Andersson OH, Karlsson KH, Kangasniemi H, Yli- Urpo A. Models for physical properties and bioactivity of phosphate opal glasses. Glastechn. Berichte 1988; 61, 300-5.

[245] Lindfors NC, Klockars M, Ylänen H. Bioactive glasses induce chemiluminescence by human polymorphonuclear leukocytes. J. Biomed. Mater. Res. 1999; 47, 1: 91-4.

[246] Kokubo T, Takadama H. How useful is SBF in predicting in vivo bone bioactivity? Biomaterials 2005; 27, 15: 2907-15.

[247] Jones JR, Hench LL. Factors affecting the structure and properties of bioactive foam scaffolds for tissue engineering. J. Biomed. Mater. Res. B: Appl. Mater. 2004; 68B, 1: 36-44.

[248] Durst RA, Staples BR. Tris/Tris HCl: A Standard Buffer for Use in the Physiologic pH Range. Clin.Chem. 1972; 18, 3: 206-8.

[249] Andersson Ö. H., Karlsson K. H. Corrosion of bioactive glass under various in vitro conditions. In Clinical implant materials, advances in biomaterials, ed. G. Heimke, U. Soltesz and A. :. Lee. Elsevier, Amsterdam, 1990, pp. 259-264.

[250] Huang W., Day D., Kittiratanapiboon K. , Rahaman M. Kinetics and mechanisms of the conversion of silicate (45S5), borate, and borosilicate glasses to hydroxyapatite in dilute phosphate solutions. Journal of Materials Science: Materials in Medicine 2006; 17, 7: 583-96.

[251] Yun H, Kim S, Hyun Y. Preparation of bioactive glass ceramic beads with hierarchical pore structure using polymer self-assembly technique. Mater.Chem.Phys. 2009; 115, 2-3: 670-6.

[252] Kellomäki M, Niiranen H, Puumanen K, Ashammakhi N, Waris T, Törmälä P. Bioabsorbable scaffolds for guided bone regeneration and generation. Biomaterials 2000; 21, 24: 2495-505.

[253] Niemelä T, Niiranen H, Kellomäki M, Törmälä P. Self-reinforced composites of bioabsorbable polymer and bioactive glass with different bioactive glass contents. Part I: Initial mechanical properties and bioactivity. Acta Biomater. 2005; 1, 2: 235-42.

[254] Niemelä T, Niiranen H, Kellomäki M. Self-reinforced composites of bioabsorbable polymer and bioactive glass with different bioactive glass contents. Part II: In vitro degradation. Acta Biomater. 2008; 4, 1: 156-64.

[255] Wang Q, Huang W, Wang D, Darvell B, Day D, Rahaman M. Preparation of hollow hydroxyapatite microspheres. J.Mater.Sci.Mater.Med. 2006; 17, 7: 641-6.

[256] Hlavac J, Rohanova D, Helebrant A. The effect of TRIS-buffer on the leaching behaviour of bioactive glass-ceramics. Ceramics - Silikáty 1994; 38, 3-4: 119-22.

[257] Bastos IN, Platt GM, Andrade MC, Soares GD. Theoretical study of Tris and Bistris effects on simulated body fluids. J .Mol. Liq. 2008; 139, 1-3: 121-30.

[258] Lu X, Leng Y. Theoretical analysis of calcium phosphate precipitation in simulated body fluid. Biomaterials 2005; 26, 10: 1097-108.

[259] Bohner M, Lemaitre J. Can bioactivity be tested in vitro with SBF solution? Biomaterials 2009; 30, 12: 2175-9.

[260] Cannillo V, Sola A. Potassium-based composition for a bioactive glass. Ceram. Int. 2009; 35, 8: 3389-93.

[261] Abraitis PK, McGrail BP, Trivedi DP, Livens FR, Vaughan DJ. Single-pass flow-through experiments on a simulated waste glass in alkaline media at 40°C.: II. Experiments conducted with buffer solutions containing controlled quantities of Si and Al. J.Nucl.Mater. 2000; 280, 2: 206-15.

[262] Icenhower JP, Strachan DM, McGrail BP, Scheele RD, Rodriguez EA, Steele JL, et al. Dissolution kinetics of pyrochlore ceramics for the disposition of plutonium. Amer. Mineral. 2006; 91, 1: 39-53.

[263] McGrail BP, Ebert WL, Bakel AJ, Peeler DK. Measurement of kinetic rate law parameters on a Na-Ca-Al borosilicate glass for low-activity waste. J.Nucl.Mater. 1997; 249, 2-3: 175-89.

[264] Rámila A, Vallet-Regí M. Static and dynamic in vitro study of a sol–gel glass bioactivity. Biomaterials 2001; 22, 16: 2301-6.

[265] Strnad J, Protivínský J, Mazur D, Veltruská K, Strnad Z, Helebrant A, et al. Interaction of acid and alkali treated titanium with dynamic simulated body environment. J. Therm. Anal. Cal. 2004; 76, 1: 17-31.

[266] Zhang D, Hupa M, Aro HT, Hupa L. Influence of fluid circulation on in vitro reactivity of bioactive glass particles. Mater.Chem.Phys. 2008; 111, 2-3: 497-502.

[267] Zhang X, Tanaka J, Yu,Yaoting, Tabata,Yasuhiko. Influence of Dynamic Flow Speed on Bonelike Apatite Formation in Porous Calcium Phosphate Ceramic in RSBF. Key Engineering Materials 2005; Advanced Biomaterials VI, 273-6.

[268] Cross M. B.Sc. Thesis, Department of Technology, University of Sheffield. 1959.

[269] Mermet J. M. Is it still possible, necessary and beneficial to perform research in ICP-atomic emission spectrometry? J. Anal. At. Spectrom. 2005; 20, - 1: 11-6.

[270] Dean JR. Practical inductively coupled plasma spectroscopy, Hoboken, NJ: Wiley; 2005. pp. 184.

[271] Boonjob W., Zevenhoven M., Ek P., Hupa M., Ivaska A. , Miro M. Automatic dynamic chemical fractionation method with detection by plasma spectrometry for advanced characterization of solid biofuels. J. Anal. At. Spectrom. 2012; 27, - 5: 841-9.

[272] Judprasong K., Ornthai M., Siripinyanond A. , Shiowatana J. A continuous-flow dialysis system with inductively coupled plasma optical emission spectrometry for in vitro estimation of bioavailability. J. Anal. At. Spectrom. 2005; 20, - 11: 1191-6.

[273] Madanat R, Moritz N, Vedel E, Svedström E, Aro HT. Radio-opaque bioactive glass markers for radiostereometric analysis. Acta Biomater. 2009; 5, 9: 3497-505.

[274] Zhao D, Moritz N, Vedel E, Hupa L, Aro HT. Mechanical verification of soft-tissue attachment on bioactive glasses and titanium implants. Acta Biomater. 2008; 4, 4: 1118-22.

[275] Hüttentechnische Vereinigung der Deutschen Glasindustrie (HVG). Standardglas I der DGG (Kalk-Natron-Glas).

[276] Arstila H, Tukiainen M, Hupa L, Ylänen H, Kellomäki M, Hupa M. In vitro reactivity of bioactive glass fibers. Adv. Sci. Tech. 2006; 49, 246.

[277] Tilton J. Fluid and Particle Dynamics. In Perry's Chemical Engineers' Handbook 8, ed. D. Green and R.

Perry. McGraw-Hill Professional, 2007.

[278] Taipale S. Egenskaper hos bioaktivt glas för fiberframställning (in Swedish), Master of Science Thesis, Laboratory of Inorganic Chemistry, Turku, 2007.

[279] Hägg G. Kemisk Reaktionslära (in Swedish), Uppsala: Almqvist & Wiksell-Geber; 1954.

[280] Sillén L. G. In Treatise on Analytical Chemistry Part 1: Theory and Practice (Chapter 8). In Vol. I, Interscience Encyclopedia, ed. E. G. Kolthoff. Wiley, New York, 1959, pp. 277-317.

[281] Urbansky ET, Schock MR. Understanding, Deriving, and Computing Buffer Capacity. J.Chem.Educ. 2000; 77, 12: 1640.

[282] Ringbom A. Konstantsamling (in Swedish, special ÅA edition), attachment to A. Ringbom: Complexation in Anaytical Chemistry", New York: Wiley-Interscience; 1963.

[283] Sigma-Aldrich. http://www.sigmaaldrich.com/etc/medialib/docs/Sigma/General_Information/trizma_base_spec.Par.0001.File.tmp/trizma_base_spec.pdf, updated 2008, accessed 2012.

[284] Taipale S, Ek P, Hupa M, Hupa L. Continuous Measurement of the Dissolution Rate of Ions from Glasses. Advanced Materials Research 2008; Glass – The Challenge for the 21st Century 39-40, 341-6.

[285] Fagerlund S., Hupa L. , Hupa M. Initial dissolutin rate of sixteen glasses with potential for medical applications (oral presentation in the 11th ESC Conference Maastricht) 2012.

[286] Carmona N, Villegas MA, Fernández Navarro JM. Corrosion behaviour of R2O–CaO–SiO2 glasses submitted to accelerated weathering. J. Eur. Ceram. Soc. 2005; 25, 6: 903-10.

[287] Barbieri L, Corradi A, Lancellotti I. Thermal and chemical behaviour of different glasses containing steel fly ash and their transformation into glass-ceramics. J. Eur. Ceram. Soc. 2002; 22, 11: 1759-65.

[288] Zevenhoven-Onderwater M. F. J., Rosenqvist J. & Karlsson K. -. Complexation of calcium, magnesium and aluminum ions on silica gel. In Bioceramics Vol 8, ed. J. Wilson, L. L. Hench and D. Greenspan. Pergamon, 1995, pp. 497-500.

[289] Kerisit S, Pierce EM. Monte Carlo simulations of the dissolution of borosilicate glasses in near-equilibrium conditions. J.Non Cryst.Solids 2012; 358, 10: 1324-32.

[290] Arstila H, Hupa L, Karlsson KH, Hupa M. Influence of heat treatment on crystallization of bioactive glasses. J. Non Cryst. Solids 2008; 354, 2-9: 722-8.

[291] Massera J, Fagerlund S, Hupa L, Hupa M. Crystallization Mechanism of the Bioactive Glasses, 45S5 and S53P4. J. Am. Ceram. Soc. 2012; 95, 2: 607-13.

[292] Lefebvre L, Chevalier J, Gremillard L, Zenati R, Thollet G, Bernache-Assolant D, et al. Structural transformations of bioactive glass 45S5 with thermal treatments. Acta Biomater. 2007; 55, 10: 3305-13.

[293] Huang R, Pan J, Boccaccini AR, Chen QZ. A two-scale model for simultaneous sintering and crystallization of glass–ceramic scaffolds for tissue engineering. Acta Biomater. 2008; 4, 4: 1095-103.

[294] Boccaccini AR, Trusty PA. In Situ Characterization of the Shrinkage Behavior of Ceramic Powder Compacts during Sintering by Using Heating Microscopy. Mater. Charact. 1998; 41, 4: 109-21.

[295] Williams D, F. The Williams dictionary of biomaterials / compiled by D. F. Williams, Liverpool: Liverpool U.P.; 1999.

7. Appendix

Definitions

(compiled from [89, 246, 295])

allograft	Tissue that is taken from one person's body and grafted to another person.
amorphous	having no definite form
angiogenesis	The process of developing new blood vessels
autograft	A tissue or an organ grafted into a new position in or on the body of the same individual
bio-	life; living (prefix)
bioactive	pertaining to a material that displays bioactivity
bioactive glass	any glass or glass ceramic that display characteristics of bioactivity amorphous solid that is not intrinsically adhesive and that is capable of forming a cohesive bond with both hard and soft tissue when exposed to appropriate *in vivo* or *in vitro* environments, such as simulated body fluid or tris-hydroxymethylaminomethane buffer, by developing a surface layer of hydroxycarbonate apatite by release of ionic species from the bulk material (ASTM)
bioactive material	material which has been designed to induce specific biological activity biomaterial that is designed to elicit or modulate biological activity
bioactivity	phenomena by which a biomaterial elicits or modulates biological activity
bioadsorbable	capable of being degraded or dissolved and subsequently metabolized within an organism
bioceramic	any ceramic; glass or glass ceramic that is used as biomaterial ceramic that upon implantation is transformed into less soluble minerals
biocompatibility	See chapter 2.1
Bioglass	45S5 (wt %) 24.5 Na_2O, 24.5 CaO, 6.0 P_2O_5, and 45.0 SiO_2, (registered trademark University of Florida, Gainesville)
bioinert	term used loosely to characterize materials that are considered inert in a biological environment
biomaterial	See Table 1
bone bonding	the establishment, by physico-chemical processes, of continuity between an implant and bone matrix
cancelleous bone	any bone having a lattice-like, spongy structure
clinical	relating to the observation and treatment of disease in patient, as opposed to theoretical and experimental investigations
composite material	structural material made of two or more distinctly different materials, where each component contributes positively to the final properties
corrosion	see 2.2.3
cortical bone	thin outer layer of compact bone, made up of lamellated rings of collagen fibers
craniofacial	relating to the cranium and the face
cytotoxic	able to kill or damage cells
degradation product	product of a material, either particulate or molecular, that is generated by degradation of that material
devitrification	crystallization of an amorphous substance
diffusion	spontaneous movement of molecules or other particles in the solution, owing to their random thermal motion, to reach uniform concentration throughout the solvent, the process requiring no addition of energy to the system
glass durability	see 2.2.2
hydrolytic resistance	see 2.2.2
implant	1.medical device made from one or more biomaterials that is intentionally placed within the body either totally or partially buried beneath an epithelial surface 2.medical device that is placed into a surgically or naturally formed cavity of the human body it is intended to remain there of a period of 30 days or more 3.to insert any object into a surgically or naturally formed site in the body, with the intention of leaving it there after the procedure is complete

in vitro	literally "in glass" or "test tube"; used to refer to processes that are carried out outside the living body, usually in the laboratory, as distinguished from *in vivo*
in vivo	within a living body
ion exchange	exchange of ions of the same charge between a solution (usually aqueous) and a solid in contact with it
ion release	term used to describe the process in which a material interacts with its environment by means of evolution of ions into that environment
isotropy	the ability of materials to display similar mechanical properties in all directions regardless of directions of applied stress, applicable also for other material properties
laminar flow	streamline flow of a fluid in which the fluid moves in layers without fluctuations or turbulence so that successive particles passing the same point have the same velocity
leaching	extraction of soluble components of a solid material or mixture by immersion in a solvent or by percolating a solvent through it
nucleation	initiation of processes, such as crystallization or fracture of materials
osteoblast	bone-forming cell
osteoclast	large multinuclear cell associated with absorption and removal of bone
osteogenesis	The process of formation of bone
osteoinduction	act or process stimulating osteogenesis
resorbable	capable of being resorbed into the body
scaffold	in tissue-engineering, the porous structure, usually polymeric, which serves as a substrate and guide for tissue-regeneration
simulated body fluid	an acellular simulated body fluid that has inorganic ion concentrations similar to those of human extracellular fluid
sintering	process in which particles of a substance are compressed, usually at elevated temperature, to form a solid object
solid solution	arrangement of atoms or molecules of different species within the same crystal lattice
tissue engineering	1. the persuasion of the body to heal itself, through a delivery to the appropriate sites of molecular signals, cells, and supporting structures 2. application of scientific principles to the design, construction, modification, growth, and maintenance of living tissues 3. the application of the principles and methods of engineering and life sciences towards fundamental understanding of structure/function relationships in normal and pathological mammalian tissues and the development of biological substitutes to restore, maintain, or improve functions. 4. an emerging discipline that applies engineering principles to create devices for the study, restoration, modification, and assembly of functional tissues from native or synthetic sources 5. Generation of new tissue using living cells, optimally patient's own cells, as building blocks, coupled with degradable materials as scaffolds
weathering	see 2.2.2
xenograft	Tissue that is transplanted from one species to another (for example from pigs to humans)

RECENT REPORTS FROM THE COMBUSTION AND MATERIALS CHEMISTRY GROUP OF THE ÅBO AKADEMI PROCESS CHEMISTRY CENTRE:

06-01	Edgardo Coda Zabetta	Gas-Phase Detailed Chemistry Kinetic Mechanism "ÅA". A Mechanism for Simulating Biomass Conversion Including Methanol and Nitrogen Pollutants -Validation, Verification and Parametric Tests
06-02	Mischa Theis	Interaction of Biomass Fly Ashes with Different Fouling Tendencies
06-03	Michal Glazer	TGA-Investigation of KCl-Kaolinite Interaction
07-01	Vesna Barišić	Catalytic Reactions of N_2O and NO over Bed Materials from Multi-fuel Circulating Fluidized Bed Combustion
07-02	Andrius Gudzinskas Johan Lindholm Patrik Yrjas	Sulfation of Solid KCl
07-03	Daniel Lindberg	Thermochemistry and Melting Properties of Alkali Salt Mixtures in Black Liquor Conversion Processes
07-04	Linda Fröberg	Factors Affecting Raw Glaze Properties
07-05	Tor Laurén	Methods and Instruments for Characterizing Deposit Buildup on Heat Exchangers in Combustion Plants
08-01	Erik Vedel	Predicting the Properties of Bioactive Glasses
08-02	Tarja Talonen	Chemical Equilibria of Heavy Metals in Waste Incineration -Comparison of Thermodynamic Databases-
08-03	Micaela Westén-Karlsson	Assessment of a Laboratory Method for Studying High Temperature Corrosion Caused by Alkali Salts
08-04	Zhang Di	*In vitro* Characterization of Bioactive Glass
08-05	Maria Zevenhoven, Mikko Hupa	The Environmental Impact and Cost Efficiency of Combustible Waste Utilization - The Potential and Difficulties of On-going Technology Developments-
08-06	Johan Werkelin	Ash-forming Elements and their Chemical Forms in Woody Biomass Fuels
08-07	Hanna Arstila	Crystallization Characteristics of Bioactive Glasses
10-01	Markus Engblom	Modeling and Field Observations of Char Bed Processes in Black Liquor Recovery Boilers

RECENT REPORTS FROM THE COMBUSTION AND MATERIALS CHEMISTRY GROUP OF THE ÅBO AKADEMI PROCESS CHEMISTRY CENTRE:

11-01	Leena Varila *et al.*	Fyrtio år oorganisk kemi vid Åbo Akademi
11-02	Johan Lindholm	On Experimental Techniques for Testing Flame Retardants in Polymers
11-03	Minna Piispanen	Characterization of Functional Coatings on Ceramic Surfaces
11-04	Sonja Enestam	Corrosivity of hot flue gases in the fluidized bed combustion of recovered waste wood
12-01	Xiaoju Wang	Enzyme Electrode Configurations: for Application in Biofuel Cells
12-02	Patrycja Piotrowska	Combustion Properties of Biomass Residues Rich in Phosphorus
12-03	Dorota Bankiewicz	Corrosion behavior of boiler tube materials during combustion of fuels containing Zn and Pb
12-04	Mikael Bergelin, Jan-Erik Eriksson, Xiaoju Wang, Max Johansson,et al.	Printed Enzymatic Power Source with embedded capacitor on next generation devices, Tekes-PEPSecond

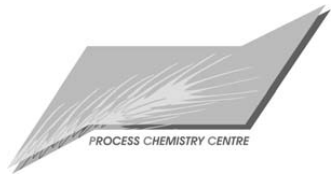

ISSN 159-8205
ISBN 978-952-12-2814-8 (paper version)
ISBN 978-952-12-2815-5 (pdf version)
Åbo, Finland, 2012